Structure and relaxation dynamics of comb-like polymers with rigid backbone

DISSERTATION

zur Erlangung des akademischen Grades

doctor rerum naturalium (Dr. rer. nat.)
genehmigt durch

die Naturwissenschaftliche Fakultät II
Institut für Physik
der Martin-Luther-Universität
Halle-Wittenberg

vorgelegt von
MSc. **Tamoor Babur**
geboren am 17.03.1987 in Lahore, Pakistan

Gutachter:

1. Prof. Dr. Mario Beiner

2. Prof. Dr. Martin Steinhart

3. Prof. Dr. Jörg Kressler

Halle (Saale), am 16.08.2017

This thesis is dedicated to my Mentor, my Parents and my wife Rabia

for their continue support, sacrifice and endless love

Contents

Chapter 1

Introduction

Comb-like polymers with rigid backbone are an important class of polymers consisting usually of a stiff main chain and grafted side chains with varying lengths [1–3]. Comb-like polymers with long (flexible) alkyl side groups have attracted great interest in various fields of application based upon their structure and functionality. They are used as organic semi-conductors in thin-film transistors [4, 5], organic photovoltaic cells [6] or light emitting diodes [7] and they are potential candidates for the use as high performance materials with excellent mechanical properties [8]. Alkyl side groups are commonly introduced in these comb-like polymers in order to improve their solubility and processibility which otherwise are difficult to attain at desired conditions [9–11]. These side chains act practically like a solvent (internal plasticizer [12]) which mainly reduces the steric interactions between the rigid main chains [13] and thus lower the processing temperature of the polymers [8, 9].

A common feature of comb-like polymers with rigid backbone is the formation of layered structures with typical spacings in the 10-30 Å range [14–16]. This layered structure formation is due to the affinity of side chains to aggregate at nanoscopic level and the tendency of rigid main chains to form stacks. The resulting morphology has also a strong influence on the properties of such polymers [17–19]. The underlying self-assembling phenomenon, also known as nanophase separation, [15, 20, 21] is found in various comb-like polymers such as regio-regular poly(3-alkyl thiophenes) [rreg P3ATs], [21–25] alkoxylated polyesters [PPAOTs] [8, 11, 14, 26] and alkoxylated polyphenylenevinylenes [AOPPVs] [18, 27, 28]. The overall layered morphology allows to study the packing behavior of side chains within their alkyl nanodomains as well as the packing of rigid main chains independently. The main chains are commonly long range ordered and packed on a crystalline lattice. The state of alkyl side chain varies

from amorphous to crystalline depending upon the side chain length and main chain architecture. However, the side chain packing in comb-like polymers is often controversially debated and various structure models are proposed based on the crystallographic analysis [22,23]. In case of rreg poly(3-hexyl thiophene), it is frequently discussed that the side chains are packed in such a manner that they are either tilted or non-tilted as well as intercalated or non-intercalated. In all these cases it is a priori assumed that they exist in all-trans conformation (Section 2.1.2). Alternative approaches where the side chains are considered to be disordered, do also exist [24]. In alkoxylated polyesters, an interdigtation is usually considered for the side chains. Their arrangement relative to the main chains varies, however, depending on the considered state. 'Positional disorder' (modification A) as well as 'crystalline order' (modification B) are reported for different modifications of alkoxylated polyesters (Section 2.1.1). Whether or not all these models and assumptions are really applicable seems to be open and is broadly discussed for the above mentioned systems. In many cases it is a priori assumed that all subunits have to sit on the same lattice excluding the opportunity that a certain degree of disorder is possible within the main and side chain domains like in case of liquid-crystalline systems. This is a shortcoming which has to be studied in more depth in order to understand the overall packing state.

Another interesting aspect of these stiff main chain polymers with comb-like architecture is that they provide a platform to study the confined dynamics of methylene sequences in alkyl nanodomains with tunable dimensions and well defined interfaces. This touches fundamental questions in the field of glass transition research since there is an ongoing discussion about the influence of domain size [29–33], interactions at interfaces [34–37] and average density effects on the softening behavior of glass forming materials (Section 2.2.3). These topics have been in particular attacked by studies done on glass forming liquids confined in nanoporous host systems like controlled porous glasses [29,31,38], self-assembled polymers [15,39] and broadly investigated in ultra-thin polymer films [37,40–43]. However, there are still many open questions which are controversially discussed despite of the fact that some progress with the interpretation of the partly contradicting results has been made in the recent years [37,41,44]. One of the most fundamental questions of such studies is to what extent simple geometrical confinement on the nanometer scale results in a significant change of the cooperative α dynamics. This is related to the question whether or not dynamic heterogeneities [45–48] in glass forming materials do really exist and which length scale is relevant in this case [49]. A basic limitation of most of the experiments is that interac-

tions at interfaces can influence the situation and small changes in the average density cannot be excluded. It is known that both effects are important for the cooperative α dynamics but it is in most of the cases practically impossible to quantify their influence experimentally. At that point the well defined structure at the interface of the alkyl nanodomains in self-assembled comb-like polymers is offering new opportunities.

The above mentioned structure-property relations in comb-like polymer with rigid main chains are the starting point of experimental studies in this work focusing on two main objectives:

1. A deeper understanding of the packing state of alkyl side groups within their alkyl nanodomains in comb-like polymers with layered morphology as well as interrelations to the packing of the rigid main chains in their direct neighborhood.

2. Additional insights regarding the cooperative dynamics of methylene (CH$_2$) units confined in alkyl nanodoamins based on a quantification of influencing factors like nanodomain size, interfacial effects and average density.

An experimental approach is chosen to make progress with these topics. A detailed crystallographic analysis based on X-ray diffraction measurements is performed for two series of comb-like polymers (PPAOTs and alkoxylated polyphenylenevinylene [AOP-PVs]) with different side chain length (Section 4.1). Different relaxation spectroscopy methods (dynamic mechanical analysis and dielectric spectroscopy) are combined in order to study the influence of confinement effects on the cooperative dynamics of methylene units in self-assembled alkyl nanodomains seen as α_{PE} process in PPAOTs (Section 4.2).

Chapter 2

Basic concepts

2.1 Side chain packing in stiff main chain comb-like polymers

A common feature of stiff main chain comb-like polymers is the formation of layered structures with typical spacings in the 1-3 nm range where main and side chain domains alternate. Interestingly, the packing within these domains can vary depending on the microstructure of the rigid backbones as well as the conditions under which structure formation occurs [1, 2, 8, 21]. The rigid backbones contain in many cases ring-like units which tend to form stacks. The resulting long range order within the main chain domains is often determining the performance if comb-like polymers are used as functional materials. However, of major importance for the overall structure is the packing of the methylene sequences within alkyl nanodomains. Many research groups have performed the crystallographic analysis of such comb-like polymers and on the basis of it various models are proposed considering the interdigitation and tilting of alkyl side groups while assuming a totally stretched all trans state [11, 22–25].

2.1.1 Models for aromatic polyesters

Among the family of rigid rod comb-like polymers, thermotropic stiff main chain polymers with flexible side chains have been extensively investigated over the decades due to their unique mechanical and thermal properties. One of the early works on such polymers was performed by Majnusz et al [9]. They studied stiff main chain polyester obtained from terephthalic acid and 2-n-alkylhydroquinone in which an alkyl side chain was attached to hydroquinone moiety as shown in Figure 2.1.a. They determined the
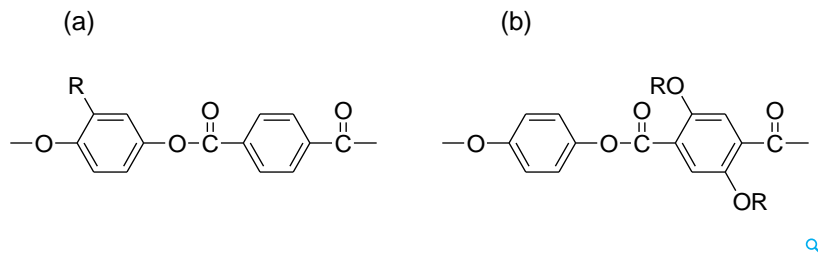
Figure 2.1: (a) Thermotropic poly(2-n-alkyl-l,4-phenylene terephthalate)s as synthesized by Majnusz et al. [9], and (b) thermotropic poly(1,4-phenylene-2,5-n-dialkoxy terephthalate)s as synthesized by Ballauff et al. [14].

melting point variation of these polymers via DSC and observed that the melting point shifted from 277°C for hexyl member ($n = 6$) to 217°C for the dodecyl member ($n = 12$) which mainly highlighted the change of melting point with the side chain length variation. A similar study in this context was also done by Krigbaum et al. [10]. They reported that the attachment of alkyl substitutes to the stiff aromatic main chains facilitate the lowering of transition temperature as well as the melting point.

Further studies on thermotropic polyester were carried out by Ballauff et al. [11,14]. They synthesized a series of poly (1,4-phenylene 2,5-n-dialkyloxyterephthalate)s (Figure 2.1.b), with different CH_2 per side chain length ($n = 2$ - 16), from melt condensation of diethyl dihydroxy terephthalate and hydroquinone, and characterized their melting temperatures by DSC. A reduction of melting temperature (> 350°C to 205°C) was observed with increasing side chain length ($2 \leq n \leq 12$) [14] which was further confirmed by Rodriguez-Parada et al. [50]. They also performed comparable experiments on the series of rigid chain polyesters with n-alkyl groups ($n = 6$ - 12) and highlighted the effect of side chains on the melting temperatures in their work [50].

Besides, lowering of the processing temperatures, another interesting feature of comb-lke polymers with rigid backbone is the formation of mesophases. This can be a nematic mesophase for short side chain or a layered mesophase if the alkyl side groups are long [11,51]. Due to the general interest in the packing state of comb-like polymers, the layered mesophase is studied extensively by various research groups [11,50–53].

The initial studies of the molecular packing in aromatic polyesters having layered meso-phases was carried out by Ballauff et al. [8,11,52]. They conducted their work on poly(1,4-phenylene-2,5-n-dialkoxy terephthalate)s (PPAOTs) (Figure 2.1.b). Through the structural analysis of this aromatic polyester, three different modifications namely
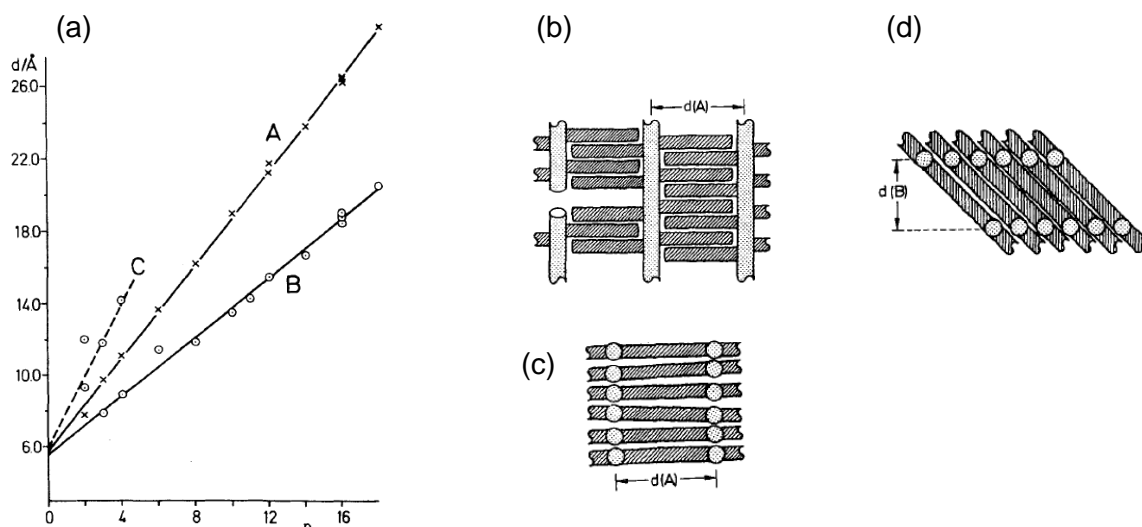
Figure 2.2: (a) Layer spacings *vs.* number of carbons in the side chains (n). 'C' represents the larger layer spacings with 'no intercalating side chains', 'A' corresponds to the 'layered mesophase' where the side chains are perpendicular to the main chain and 'B' indicates a packed structure where side chains tilted relative to the main chains. (b,c) Packing model of modification A (side and top view) and (d) packing model of modification B (top view) with the main chains (light gray rods) and alkoxy side chains (dark gray rods). Figures taken from Ref. [11].

A, B and C are observed based on the side chain lengths and thermal program. According to Ballauff et al. [11], the polymer with alkyl side chains less than $n < 7$ forms a nematic mesophase (mainly modification C) whereas those with side chains more than $n > 6$ tends to form a layered mesophase (modification A and B). Furthermore, based on the X-ray diffraction data and corresponding spacings of modification A and B, a packing model was proposed by Ballauff et al. [11] (Figure 2.2). According to this packing model, modification A is a layered mesophase consisting of main chains and side chain nanolayers, where side chains intercalate as well as protrude perpendicularly to the main chain direction (Figure 2.2.a-c). The perpendicular fashion of side chains in modification A is suggested from the slope of the curve which is 1.25 Å per methylene unit and is in close proximity of slope expected for fully interdigitated and extended methylene sequences in all trans conformation (1.27 Å/CH$_2$ unit) [52]. Similar layered and interdigitating structure is also suggested for modification B but with a tilt of 50° due to smaller layer spacings (Figure 2.2.a and 2.2.d). This tilting theorizes for the efficient packing of side chains and assumes implicitly their crystalline state.

Further studies on the packing of side chains within the layers of stiff main chain
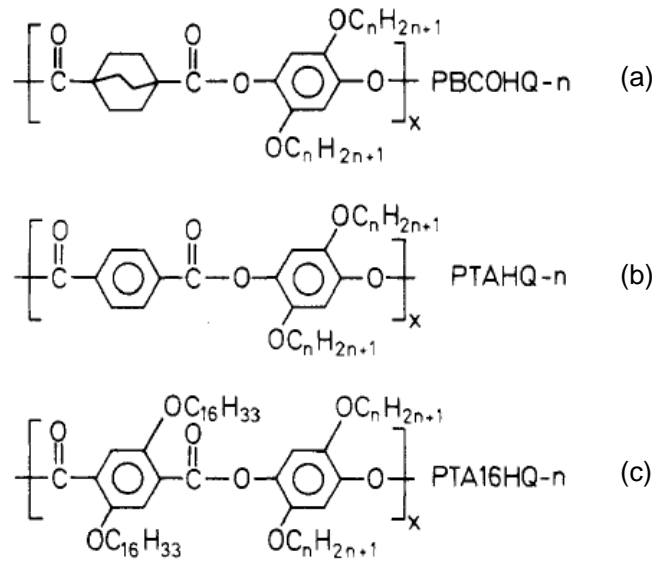
7

Figure 2.3: Rigid rod polyesters with flexible side chains (a) PBCOHQ-n, (b) PTAHQ-n and (c) PTA16HQ-n as synthesized by Rodriguez-Parada et al. Figure taken from Ref. [50].

polyesters were conducted by Rodriguez-Parada et al. [50]. They performed a comparative study on a series of three different aromatic polyesters namely PBCOHQ-n, PTAHQ-n and PTA16HQ-n (Figure 2.3), and proposed various models for the side chain packing in all three systems (Figure 2.4). In case of first two series, PBCOHQ-n and PTAHQ-n, a layered structure is observed on the basis of their x-ray diffraction data which also leads to the speculation of two different models for the packing of side chains in both systems. In the first case, a simplistic packing model is considered (similar as for modification A by Ballauff et al. [11]) where side chains are fully extended and in perpendicular direction with respect to the main chain and also intercalating into each other (Figure 2.4.b). However, this model does not fit with the corresponding x-ray data of PBCOHQ-n and PTAHQ-n because the obtained layer spacings in both cases are smaller than what is predicted by the above model. The second case proposed by Rodriguez-Parada et al is similar as for modification B by Ballauff et al. [11] in which the side chains are tilted with respect to main chains and also interdigitating into each other (Figure 2.4.c). This model fits comparatively well for both systems where tilting is present and predicted inter-layer spacings is in an agreement with the actual data. Furthermore, a comparison is also made between PTAHQ-n ($n = 16$) and PPAOTs ($n = 16$) to understand the influence of position of side chain attachment to main chain on the packing behavior of alkyl groups. Although the length of side chains is equal in

both cases, however, in PTAHQ-n ($n = 16$), the side chain is attached to hydroquinone moiety whereas in PPAOTs ($n = 16$) it is appended to the terephthalic acid residue. It is observed that both polymers formed layered structure. However, in PPAOTs ($n = 16$) the obtained layer spacing is 25.8 Å (Figure 2.2.a) whereas in PTAHQ-n ($n = 16$) it is 19.1 Å (Figure 2.4.a). In the former case, the corresponding spacing was explained by a packing model in which the side chains are arranged in a perpendicular fashion to the backbone axes with extended side chains interdigitating into each other (Figure 2.2.b). In the latter case, the layer spacing has been related to a packing model with side chains staggered with respect to its main chain (Figure 2.4.c). Beside the study on PBCOHQ-n and PTAHQ-n, the work carried out by Rodriguez-Parada et al on PTA16HQ-n gives more insight on the alkyl side groups' effect on the packing behavior in cases where four side chains are attached to each monomeric unit in the polymer chain. In one case, all side chains are of equal length (PTA16HQ16) whereas in other case, it is unequal (PTA16HQ6). The x-ray results of PTA16HQ16, where all alkyl groups contain n=16 carbons (Figure 2.4.d), revealed a well-defined layered morphology with layer spacing (d_{100}) of 32.5 Å, which is almost twice as compared to layer spacings of PBCOHQ16 and PTAHQ16. Such layer spacing cannot fit to the models used for PBCOHQ-n and PTAHQ-n as it is much larger than the interdigitated structure. Therefore, a non-interdigitating but titled model is predicted for PTA16HQ16 as shown in Figure 2.4.d. On the other hand, the x-ray diffraction data of PTA16HQ6, containing alkyl groups with $n = 16$ and $n = 6$ carbons, shows a situation where a *'mesophase with layered structure'*is suggested because of the unequal side chain length attached to the backbone. The proposed packing model of such system is shown in Figure 2.4.e where side chains are disordered resulting in a smaller layer spacing as compared to layer spacing of PTA16HQ16. However, based on the above models, it seems to be very much open to what extent such packing models are really conclusive. In particular, there are no clear experimental evidences provided for the proposed difference in the side chain packing comparing PTA16HQ16 and PTA16HQ6. Evidences for differences in side chain packing will be in the focus of the discussion in this PhD thesis.

Beside aromatic polyesters, several research groups have worked on other rigid rod polymers with flexible side chains like aromatic polyamides [8, 52–54] and aromatic polyimides [8, 53, 54]. Among all, the work of Clauss et al. [54] on aromatic polyester (PPTE-16), aromatic polyamide (PPTA-16) and aromatic polyimide (PPPI-16) (Figure 2.5.a), via 2D solid state NMR spectroscopy, provides a different approach for
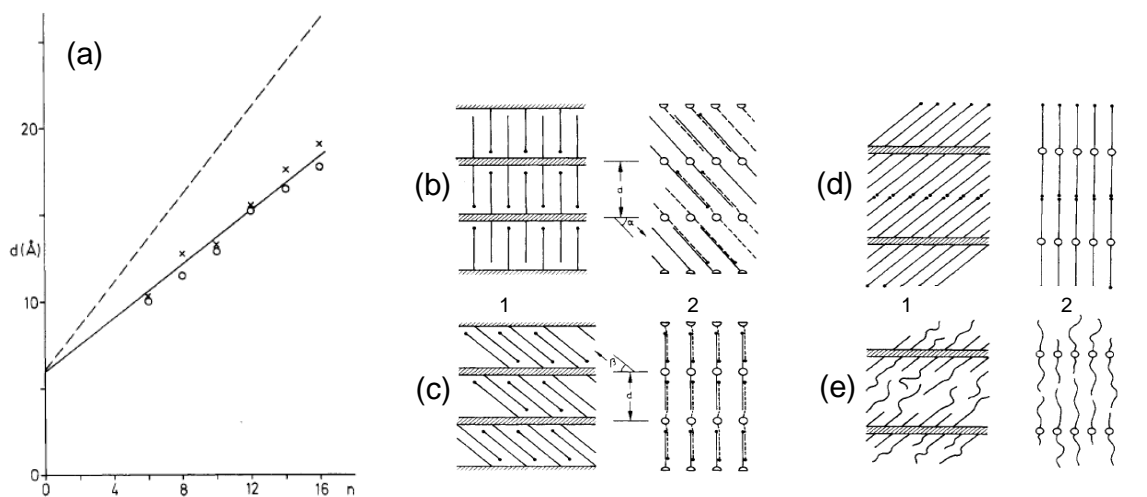
Figure 2.4: (a) Layer spacings *vs.* number of carbons in the side chains (*n*). Actual data of PBCOHQ-*n* (open circles) and PTAHQ-*n* (crosses) are compared with PPAOTs from melt cooled [11] (dashed line) and solvent precipitated [11] (solid line). Packing model of PBCOHQ-*n* and PTAHQ-*n* with (b) side chains perpendicular to main chains and (c) side chains staggered with respect to main chains. Packing model of (d) PTA16HQ16 with equal but non-interdigitating side chains and (e) PTA16HQ6 with unequal but non-interdigitating side chains. In each model (1) and (2) corresponds to side view and top view respectively. Figures taken from Ref. [50].

determining the packing as well as nature of alkyl side groups. In their study, the packing behavior of side chains within the stiff main chains is based on the side chains' molecular mobility and conformational order. Their ^{1}H-^{13}C NMR (2D WISE-NMR) spectroscopy findings revealed different types of modifications in aromatic polyester, polyimide and polyamide based on the packing of alkyl side chains. The ^{13}C spectrum of aromatic polyester (PPTE-16B) and polyimide (PPPI-16), as compared to the low-density polyethylene (LDPE), exhibited a highly ordered trans conformation for modification B indicating a highly crystalline region with a small amount of amorphous region. In case of modification A (both for PPTE-16A and PPTA-16), a trans confirmation is observed but a broader ^{13}C signal line width with respect to LDPE, highlight a lower conformational order of side chains which is attributed to the presence of gauche content in the trans segments. Furthermore, the studies on the arrangement of main chains and their close connection to the packing of side chains are also pointed out by Clauss et al. [54]. It is observed through the ^{13}C MAS-NMR spectra of modification B aromatic polymers (polyester (PPTE-16B) and polyimide (PPPI-16)) that main chains of these polymers are regularly pack (a trans-trans conformation) thus allowing the alkyl side chains to sit on a regular lattice which than lead to a highly
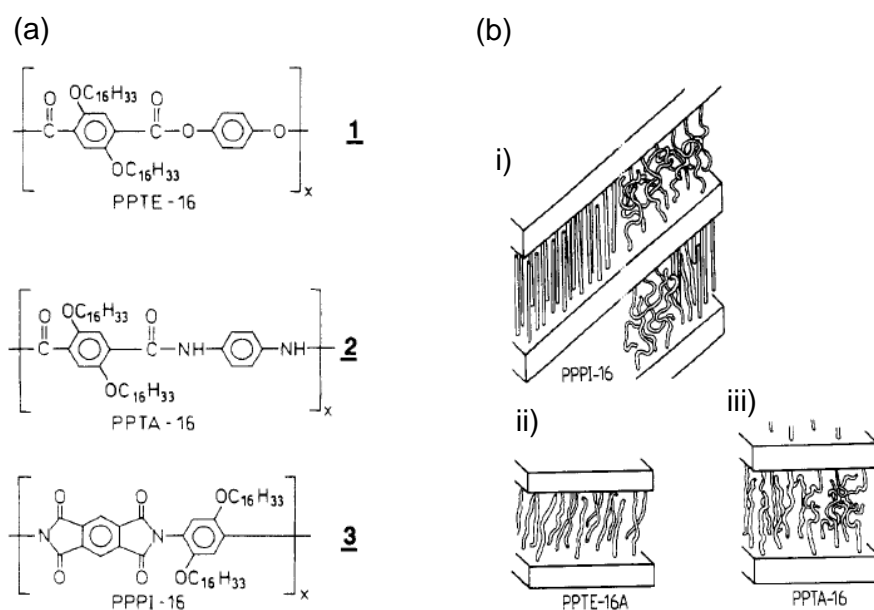
10

Figure 2.5: (a) Chemical structure of rigid rod aromatic polyester (1), polyamide (2) and (3) polyimide with alkyl side chains ($C_{16}H_{33}$). (b) Packing model proposed for (i) aromatic polyimide and polyester modification B, (ii) aromatic polyester modification A and (iii) aromatic polyamide modification A. Figures taken from Ref. [54].

crystalline system with low amorphous regions (Figure 2.5.b). On the other hand, a staggered main chain arrangement is observed for modification A aromatic polyamide (PPTA-16) and polyester (PPTE-16A) which does not facilitate the crystallization of side chains within the main chain domains (Figure 2.5.b).

2.1.2 Models for poly(3-alkyl thiophenes)

Another class of comb-like polymers which has been widely studied over the years is poly(3-alkyl thiophene)s (P3ATs) [21, 22, 24, 25, 55, 56]. Alkylated polythiophenes are important conjugated polymers which are considered as potential candidates for various electronic and optoelectronic applications due to their high conductivity and thermal stability [23, 57, 58]. As compared to its parent polymer, poly(3-alkyl thiophene)s are easily soluble and processable due to the alkyl side groups attached to the thiophene rings [57]. It has to be noted that both the properties varies with the variation of methylene units in the alkyl side groups [59]. Beside the enhancement in the solubility and processability of poly(3-alkyl thiophene)s, the side chains strongly effects the properties of polymer both at molecular level and macroscopic level [24, 59]. Partic-
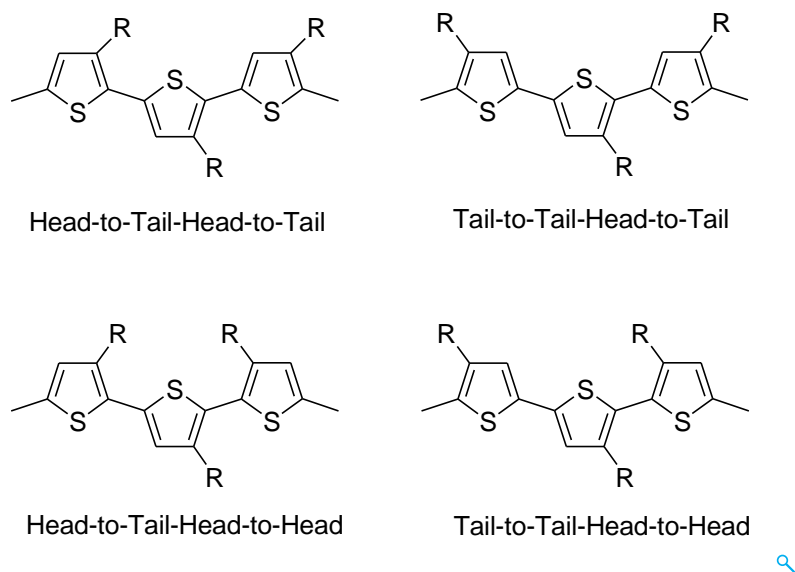
Figure 2.6: Schematic illustration of head-tail arrangements in poly(3-alkyl thiophenes).

ularly, the regio-regularity, which arises due to the arrangement of alkyl side chains attached to the backbone connected with the head to tail coupling of thiophene rings along the main chain, plays a prominent role in defining the crystallographic structure of the polymer. In poly(3-alkyl thiophene)s, this regio-regularity results the division of polymer into two major classes, (a) regio-regular P(3AT)s and (b) regio-random P(3AT)s. The regio-regular P(3AT)s contain a higher fraction ($> 97\%$) of head-tail-head-tail (HT-HT) sequences where the head is on the position 2 of the thiophene ring and tail is attached on position 5 of thiophene ring (Figure 2.6) [60]. On the other hand, in the regio-random P(3AT)s, the attachment of monomers to the main chain during polymerization is random which can result either head-tail, head-head or tail-tail arrangement as shown in Figure 2.6 [61]. Furthermore, the regio-regularity, in both regio-regular and regio-random P(3AT)s, influences significantly the conducting properties of these polymers. In regio-regular P(3AT)s, the polymer has high conductivity due to the crystalline backbone which facilitates the efficient charge transport. Whereas, the HT arrangement in regio-random P(3AT)s results in an absence of long range order with no $\pi - \pi$ orbital overlap in case of the thiophen rings in the main chains. This causes hindrance in the charge transport and leads to a strongly reduced conductivity as compared to regio-regular P(3AT)s [21].

The very regular attachment of side chains onto the main chains in rreg poly(3-alkyl-thiophene)s results into a lamellar morphology with separated main and side

chain nanolayers as already discussed above for other series of comb-like polymers with rigid backbones and long alkyl groups as side chain. This is obviously a common feature of this class of materials where main and side chain subunits tend to nanophase separate [21,25]. The crystalline structure of regio-regular P(3AT)s has been researched in very much detail by various groups [22–25, 55, 56, 59] since Heeger et al. explored the conductivity of P(3AT)s [62] in 1980s. Among other, the work of Kawai et al. [56] provide a detailed insight on the structural changes in regio-regular P(3AT)s due to the change in the alkyl side chain length. They studied a complete series of regio-regular P(3AT)s and proposed an orthorhombic unit cell for these polymers [56]. The theorized scheme of the unit cell is shown in Figure 2.7 along with its lattice parameters: **a** the main chain to main chain distance ($h00$), **b** the $\pi - \pi$ stacking ($0k0$) and **c** the side chain to side chain distance along the backbone ($00l$). According to this scheme, a stacked lamellar structure is observed in all regio-regular P(3AT)s along with alternating regions of main and side chain domains. The orthogonal unit cell parameters determined by Kawai et al for $n = 4$ to 12 are **a** = 12.7 Å to 26.43 Å, **b** = 7.5 Å and **c** = 7.77 Å [56]. The difference of the a-axis length with the increase in the carbon atoms per side chain implies that the alkyl side groups are directed on the a-axis [55]. Also, the minute difference between **b** and **c** corresponds to a combined peak with a ($0k0$) reflection dominance [55]. Beside the work of Kawai et al., similar packing models were also suggested by other research groups for regio-regular P(3AT)s but with slight variations in the lattice parameters [22,55].
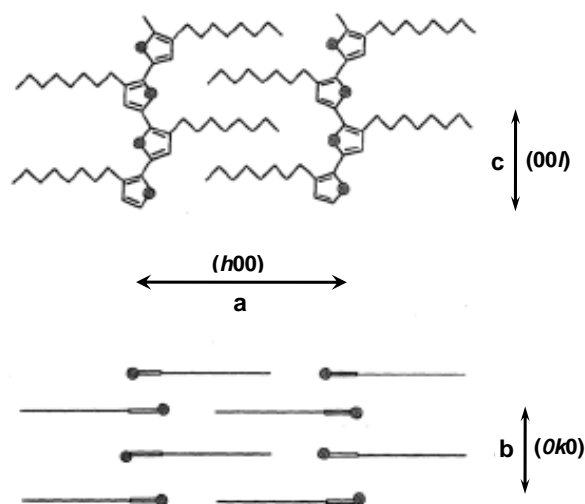
Figure 2.7: Schematic representation of the orthorhombic unit cell of P(3AT)s. Figure adapted from Ref. [56].
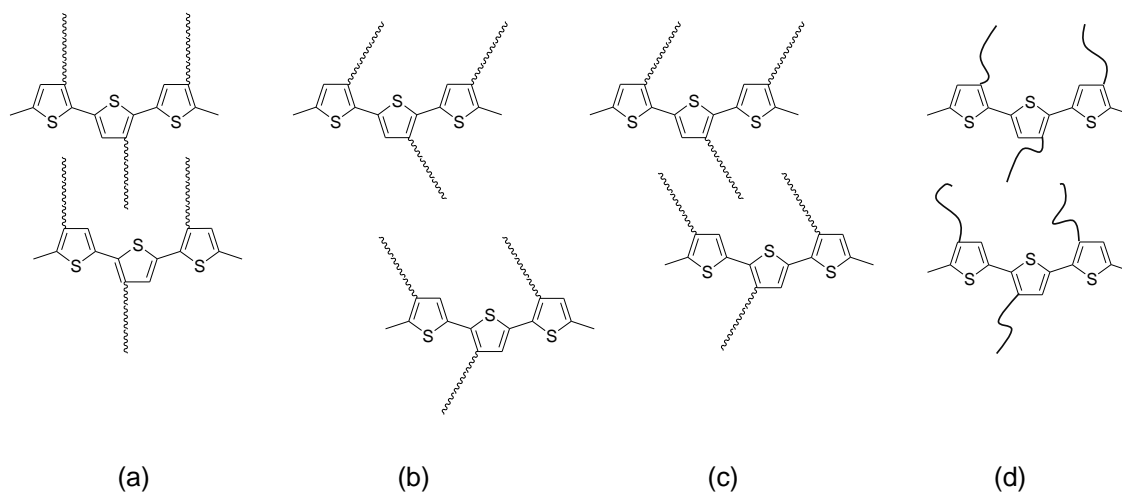
Figure 2.8: Schemes for packing of side chains in regio-regular P(3AT)s i.e., (a) interdigitation with non-tilted side chains, (b) non-interdigitation with tilted side chains, (c) interdigitattion with tilted side chains and (d) liquid like disordered side chains.

Despite of this general consensus about the unit cell, which is applicable for P(3AT)s, the packing of the side chains within the unit cell has been often discussed controversially. In case of regio-regular P(3AT)s, it is frequently debated that the side chains are packed in such a manner that they are either tilted or non-tilted, intercalated or non-

intercalated, exist in all-trans conformation or are entirely disordered. Summarizing the literature, mainly four possible schemes are discussed for side chains packing in regio-regular P(3AT)s with their structural models as shown in Figure 2.8. One of the early work on the packing of alkyl groups was carried out by Tashiro et al. [55]. Although, they mainly studied the structure and phase transition in poly(3-alkylthiophene)s, they also predicted the side chain packing model based on the x-ray scattering results. An all-*trans* conformation was suggested for the side chains in the lateral direction with the packing structure of alkyl chains having one chain interdigitating into the other. This trans conformation arises due to a large difference of the main chain to main chain distance between P3HT and P3DT based on the orthogonal unit-cell parameters determined by Tashiro et al. [55]. Though, the proposed structural model highlights interdigitating side chains without tilting (Figure 2.8.a), no clear evidence is available in their work which supports tilting or non-tilting behavior of side chains within the main chain domains. The same structural model was also used by Mena-Osteritz et al. [58] for the interpretation of results from high resolution imaging of the packing state of low molecular weight P(3AT)s on the surface of substrates by scanning tunneling microscopy (STM) technique. However, in this work, it is also mentioned that the penetration of side chains into each other is possibly maximized due to the substrate's epitaxial effect on the sample which could lead to a slightly different packing of side chains as compared to bulk samples or sample on substrates with non-epitaxial effects [57].

Beside the above scheme, various groups have given an illustrative image of another model where crystalline side chains are non-intercalated but tilted with respect to each other (Figure 2.8.b) [25, 63, 64]. Based on the x-ray scattering measurements by Prosa et al. [63], the obtained layer spacings of polymer suggest a tilting in side chains along with no intercalation for the efficient packing of alkyl groups. Their structural model was further sustained by structure factor calculations; according to which all-*trans* conformation was assumed for side chains along with the 'dihedral' and 'bond angle'. These factors cause, according to Prosa et al. [63], the non-interdigitation of side chain from one stack into other attached to the neighboring layer. Similar packing behavior of alkyl side groups was also considered by another work group explaining scattering results along with computer simulations [64] by a packing model with non-interdigitated but tilted side chains. According to this work, a layered morphology exist in polymer where side chains are tilted to 50°. This angle is taken from the slope of the d_{100} *vs.* n curve which is 1.62 Å per methylene unit; more than the slope of

extended polyethylene conformation (1.27 Å/CH$_2$ unit). This difference is explained by tilting assuming that the side chains are in an all-*trans* conformation in lateral direction. Furthermore, a computer simulation is reported suggesting that only those packing models are energetically stable in which side chains are titled with no intercalation. Although, these theoretical models provide good insight for the side chain packing, the comparison between the calculated and experimentally obtained results are mostly semi-quantitative because the "*structural variables to be determined are too many compared with the observed number of reflections*" [64].

Along side with the other structural models, the side chains packing where alkyl groups are titled and interdigitated (Figure 2.8.c) is also described in literature [23]. This packing behavior is mostly used in cases where the synthesis resulted into two different crystalline modifications of poly(3-alkylthiophene)s: type I and type II. Among both types, type II represents the model where side chains are assumed to be not only interdigitated but also tilted. However, when type II samples were heated, they transformed to type I where side chains are titled but with minimal to no interdigitation at all. Contrary to the other studies [65], this work suggest that type II polymer could be thermodynamically more stable at room temperature than common type I sample. To what extent - this difference can be mostly related to the adopted synthetic routes resulting in slightly different mirostructures or more due to different thermal treatment during sample preparation - is an interesting question which cannot be finally answered based on the information given in the relevant papers.

Besides the discussed models assuming an all-*trans* state of the alkyl groups within their alkyl nanodomains, there are also various approaches considering liquid-like disordered alkyl side groups (Figure 2.8.d) has also been discussed in various works [22,24]. An example for such a packing model is proposed by Kline et al. [24]. The argumentation is based on the areal density of side chains and its relation to the areal density of crystalline polyethylene [24]. According to their areal density calculations, the attachment density of regio-regular P(3HT) is less than that of crystalline PE which is interpreted as a reason for the disordering of side chains. This disordering of side chains was further confirmed by their spectroscopy experiments. Furthermore, it is argued that the side chains in P(3HT) cannot interdigitate because the areal density required for penetration of side chains into each other would be >50% higher than that in polyethylene, which is assumed to be unphysical. However, the question arises whether or not the areal density can be really understood as major criterion for the packing state of the methylene units. Areal density can vary with tilting angle and

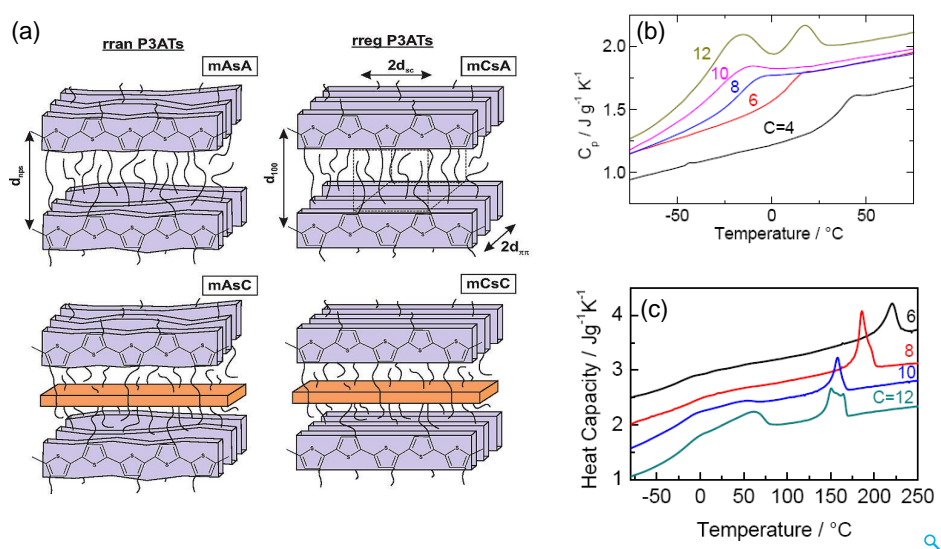volume data might be more useful for a final judgment of the situation.

Figure 2.9: (a) Packing scheme of main chains and side chains in regio-random P(3AT)s and regio-regular P(3AT)s. DSC heating scans of (b) regio-random P(3AT)s and (c) regio-regular P(3AT)s. Figures taken from Ref. [21, 66].

State of side chains in alkylated polythiophenes. Regarding the state of side chains, amorphous to crystalline packing is considered by different researchers. However, although of major importance for the packing, this was often not explicitly stated but can be concluded only from the chosen context or special sentences. In work by Prosa et al., [22] it is commonly assumed that the side chains are in disordered state despite of the long range ordered arrangement of main and side chains in nanolayers (d_{100}), similar to the situation that is called mesophase in the comb-like polymers described above (cf. Section 2.1.1). Many other researchers make implicitly or explicitly use of the assumption that the alkyl groups in P(3AT)s are in a all-trans state and sit on a regular lattice defined by the orthorhombic unit cell. A more focused study dealing with this question was performed by Pankaj et al. on poly(3-alkylthiophene)s [21]. They have argued based on a comparison of rreg and rran P(3AT)s with different side chain length that the side chains in P(3AT)s $6 \leq n \leq 10$ alkly carbons are basically amorphous [21]. Their calorimetric measurements shows no prominent melting peak of the alkyl groups with $n = 6$ to 10 per side chain while for the higher member (n=12) a weak additional melting peak related to side chain melting seems to occur at low temperatures (20°C to 60°C) (Figure 2.9.b and 2.9.c). Furthermore, it is observed from their work that the main chain state (crystalline stacks or disordered arrangements)

does not have major influence on the state of alkyl side groups, as in both cases (rreg and rran P(3AT)s) the side chains show their amorphous or semi-crystalline state independent of the backbone packing only depending on side chain lengths. Pankaj et al. [21] attributed the amorphicity in alkyl groups to the frustration effects mainly arising due to the thiophene rings which causes the side chains unable to sit on their 'native crystal lattice'. Four scenarios with differences regarding the packing within the main and side chain domains have been proposed (Figure 2.9.a). Contrary to the work of Pankaj et al. [21], the study carried out by Wu et al. [25] provides a different scenario of nature of side chains. According to their work on the n = 6 member, regio-regular P(3HT), the alkyl side groups are part of a 3D-crystal structure having ordered main and side chains at room temperature. With the increase in temperature, this 3D-crystal transformed into a 2D structure where backbone is packed on the lattice and side chains are in disordered state. Further heating, according to this study, leads to an isotropic liquid where both the main and side chains are disordered [25]. Pankaj et al. [21] highlight, however, that main and side chains are still nanophase-separated in rran P(3AT)s and rreg P(3AT)s in the molten state indicated by a broad "prepeak" in the XRD pattern close to the (100) reflection observed for the long range ordered rreg P(3AT)s below melting. Beside the above two examples, similar situations are also likely to be observed in other works [24, 67]. Possibly the reported differences in the packing state of the side chains occur to certain extent also due to differences in the molecular architecture of the investigated systems and the way the samples have been treated. Note that the samples used by Wu et al. [25] have a relatively low molecular weight and have been prepared by slow solution casting while the samples studies by Pankaj et al. [21] had much higher molecular weights and ordered states have been achieved by cooling of bulk samples. From this point of view more energetically optimized states observed in the paper by Wu et al. [25] might not be achieved in many other cases where high molecular weight sample (possible also containing more head-tail defects) have been investigated. Relations to the existence of different modifications in other comb-like polymers like PPAOTs seem to be very likely.

Summarizing this literature review, one can conclude (i) that there are common structural features, which are characteristic for comb-like polymers with rigid backbone and (ii) that there are standard concepts, which are frequently used to model such systems. Most common structural feature is a self-assembled layered morphology with alternating main and side chain nanodomains observed in practically all cases if alkyl groups contain more than six carbons. Such structures are usually modeled as-

suming that the main chains form stacks in their individually nanolayers. The situation in the alkyl nanodomains is often a bit more unclear. Although many models assume that the alkyl groups are in the all-*trans* state which can be either tilted or interdigitated. This concept is often used to explain differences in periodicity d_{100} depending on microstructure of the backbone or sample treatment. Alternative concepts which are more seldom used assume that the alkyl side groups are in a disordered state. Differences in side chain packing are hard to detected directly but important for a better understanding of the overall packing of comb-like polymers with rigid backbone. This calls for alternative approaches helping to discriminate between different packing states in the alkyl nanolayers and an explanation for the occurrence of different modifications in various series of comb-like polymers.

2.2 Glass transition

Glasses are solids without long-range ordered internal structure which is typical for crystalline solids. When a glass-forming material is cooled from its liquid-like state at high temperatures towards low temperatures its density and viscosity increases enormously in combination with a significant slowing down of the underlying molecular motions. At a certain temperature the relevant molecular motions are so slow that the time needed for the structural rearrangements in the system is not longer available during cooling. Hence, the material 'freezes-in' and falls out of equilibrium. This temperature is called glass temperature T_g and is related to the so-called *thermal glass transition* from the equilibrium liquid state to the non-equilibrium glassy state [68,69]. In contrast, the relaxation process measured in equilibrium above T_g where a transition from liquid-like to solid-like behavior occurs under isothermal conditions depending on time or measurement frequency is often called *dynamic glass transition* or α relaxation [69]. Both phenomena will be discussed in some more detail below.

The thermal glass transition is often investigated either by dilatometry or by differential scanning calorimetry (DSC). In case of dilatometric measurements, the thermal glass transition is seen in specific volume vs. temperature plots by a change of the slope as shown in Figure 2.10.a. The temperature-dependent specific volume v(T) changes above and below a certain transition interval linearly with temperature. At the transition region the slope changes and the thermal expansion coefficients are significantly different above and below. The transition region is related to the thermal glass transition and the glass temperature (T_g) is defined as the temperature at which
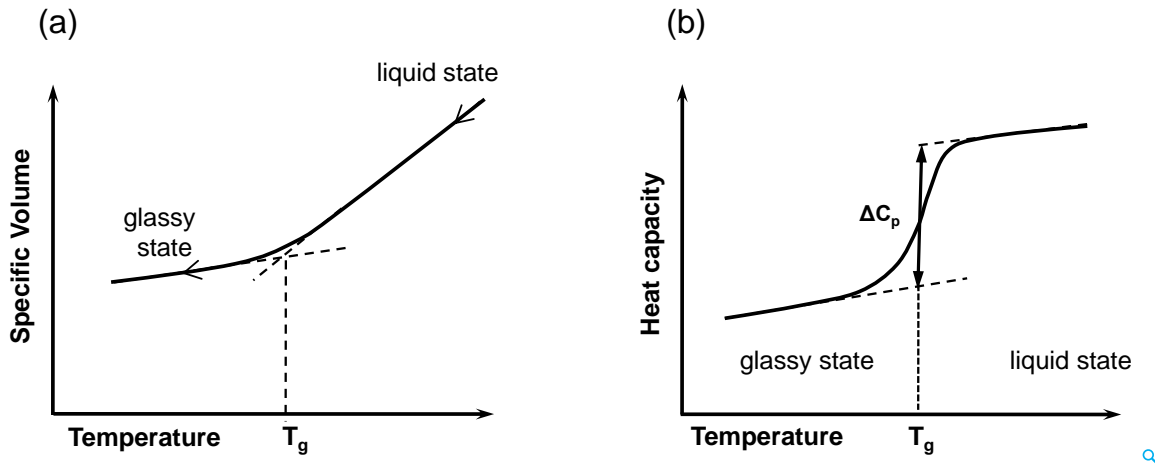
Figure 2.10: A schematic diagram displaying the determination of glass transition temperature (T_g) from plot of (a) specific volume and (b) heat capacity *vs.* temperature.

the two extrapolated lines describing the behavior above and below the transition region intersect [70–72]. Note that the value of T_g depends on the cooling rate since the equilibrium to non-equilibrium transition temperature decreases if the glass-forming system has more time to equilibrate. By definition, T_g is related to the temperature above which a glassy material starts to soften during heating and behaves like liquid (or rubber in case of polymers with high molecular weight). In case of DSC measurements, the thermal glass transition is indicated by a step-like change in the heat capacity $C_p(T)$. The glass temperature (T_g) can be determined from DSC cooling scans performed at fixed cooling rate (e.g. 10 K/min) based on a tangent construction as shown in Figure 2.10.b. T_g is then defined for example as temperature where $C_p(T)$ coincides with the half step height between both tangents (half-step method). Alternative definitions are based on an onset construction or an equal area construction [73]. Further parameters describing the thermal glass transition in $C_p(T)$ are the relaxation strength ΔC_p as well as the width of the transformation interval ΔT of about a few K [69].

Above the glass temperature (T_g), glass-forming materials exit in the equilibrium state. The so-called dynamic glass transition or α relaxation reflecting the cooperative dynamics of molecules or monomeric units in case of polymers occurs then isothermally depending on time or measurement frequency. The fluctuations related to the α dynamics are very slow near T_g ($\tau_\alpha \approx 100$s) but speed up with increasing temperature rapidly. The physical short time limit is $\tau_\alpha \approx 10^{-14}$s at highest temperatures. The term dynamic glass transition is also used for entire trace describing the temperature
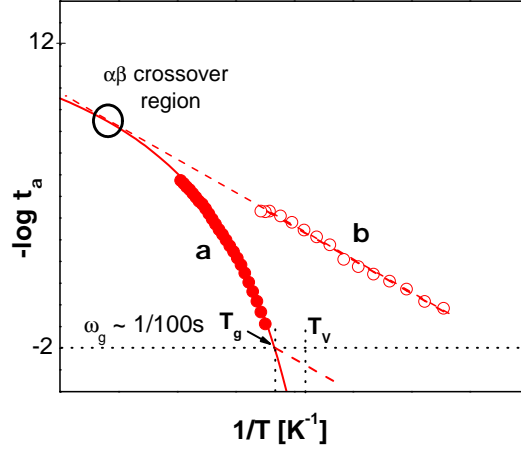
Figure 2.11: Schematic showing an Arrhenius plot (-log τ_α vs $1/T$) for α relaxation process (dynamic glass transition) and β relaxation process (localized dynamics). The black circle corresponds to a crossover region where temperature dependence of α and β approach each other and T_v represents the Vogel temperature. Figure adapted from ref. [75].

dependence of the α relaxation process under isobaric conditions with a strong temperature dependence of its characteristic relaxation time τ_α (or relaxation frequency $\omega_\alpha = 1/\tau_\alpha$). The dynamic glass transition is generally determined by linear response experiments like dynamic mechanical analysis or dielectric spectroscopy. Characteristic is a strong non-Arrhenius-like temperature dependence of the relaxation frequency (ω_α) upon temperature as indicated in the Arrhenius plot shown in Figure 2.11. Besides of the α relaxation process, a secondary β relaxation process occurs in practically all glasses at higher frequencies [74]. It is related to localized motions and shows an Arrhenius-like temperature dependence of its relaxation frequency ω_β according to

$$log(\omega_\beta) = log(\omega_0) - (E_A/RT) \tag{2.1}$$

where E_A is the activation energy, R is the gas constant and ω_0 is the limiting frequency.

The temperature dependence of the α relaxation is commonly well described by the Vogel-Fulcher-Tammann-Hesse (VFTH) equation [69, 76–78]

$$log(\omega_\alpha) = log(\omega_0) - (B/(T - T_v)) \tag{2.2}$$

where (ω_0), B and T_v correspond to limiting frequency, curvature and Vogel temperature, respectively. Generally T_v is found 30-70 K below the glass temperature T_g.

An important concept which is used to classify glass-forming materials based on the temperature dependence of the dynamic glass transitions (α relaxation) is *fragility* [79–81]. Fragility has been defined as measure of the deviation of temperature dependence of α relaxation time from the Arrhenius-like behavior [66, 82]. Polymers with low fragility are more close to Arrhenius-like behavior (β relaxation process) while those having high fragility show pronounced non-Arrhenius behavior (α relaxation process) [82]. Normally, the fragility m - also called steepness index - can be directly calculated based on parameters from the VFTH equation as [80]

$$m \equiv -dlog\omega/d(T_g/T)|_{T=T_g} = (BT/(T_g - T_v)^2) \tag{2.3}$$

Value of m ranging from 20 to 214 are reported [81]. Glass forming materials with lower m values are considered as a strong liquids while those with higher m values are considered as fragile liquid [79, 81, 83]. Note that the lowest possible m value corresponding to Arrhenius-like behavior of the temperature-dependent α relaxation frequency should be about 16 [84].

2.2.1 Traditional glass transition models

Free volume theory. A traditional approach to understand glass transition is based on the assumption that 'free volume' is required for the molecules to move if a glass-forming material (e.g. an amorphous polymer) has to undergo conformational changes. At temperatures well above the glass temperature (T_g), the molecules can move relatively freely due to a large fraction of free volume and low overall density. However, as the temperature decreases the free volume is reduced accompanied by a significantly reduced mobility of molecules. At T_g, the mobility of these molecules becomes so slow that their translational diffusive motions freeze and what remains are more localized relaxations in polymer seen as secondary relaxations (β processes) in the glassy state [74].

Generally, the free volume model postulates that

$$V_f = V - V_0 \tag{2.4}$$

where V is actual volume and V_0 is the theoretical volume of the liquid or Van der Waals volume of the molecules at 0K. A relation between free volume V_f and viscosity has been proposed by Doolittle [85]

$$\eta = A exp[b(V - V_f)/V_f]. \qquad (2.5)$$

Furthermore, a linear dependence of free volume on temperature is assumed according to

$$f = f_g + \Delta\alpha(T - T_g) \qquad (2.6)$$

where f is the fractional free volume which is the total amount of free volume per unit volume of the polymer, f_g is the fractional free volume at T_g and $\Delta\alpha$ is the difference in thermal expansion coefficients above and below T_g. With that, the Doolittle equation (Equation 2.5) is giving a physical reason based on free volume for the Williams-Landel-Ferry (WLF) equation [72] describing the temperature dependence of the α relaxation. The relevant equation is

$$log a_T = -\frac{(B/2.303 f_g)(T - T_g)}{(f_g/\Delta\alpha) + (T - T_g)}. \qquad (2.7)$$

The WLF equation describes the temperature dependence of shift factors a_T for the α relaxation and is mathematically analogous to the VFTH equation 2.2. Note that the temperature dependence taken from shift factors should correspond to that of the α relaxation time for thermorheological simple materials showing no deviations from the time-temperature superposition principle [80]. It is important to mention that the free volume model is a qualitative model and does not involve cooperativity related ideas or any characteristic length scale for the α relaxation process.

2.2.2 Cooperativity based concepts

Another traditional approach to understand the dynamics in glass forming liquids is starting from the idea that more and more molecules have to move in a cooperatively way in order to undergo molecular rearranging motions. Adam and Gibbs formulated a thermodynamic approach to the (dynamic) glass transition and postulated the existence of *cooperatively rearranging regions* (CRRs) [45] in glass forming liquids which can be defined as smallest subsystem which, upon a sufficient thermal fluctuation, can rearrange into another configuration independent from its environment. This concept, according to Donth, can also be defined as the statistical independence of the thermal fluctuations related to the glass transition from that of neighbored subsystems [49,69]. Adam-Gibbs theory proposes that the cooperative rearrangements in a subsystem of

CRR is related to z molecules ($z \equiv N_{CRR}$). The main conclusion of this work is that 'the temperature dependence of the relaxation process is interrelated to the temperature dependence of the size of a CRR', [45] highlighting that the length scale (size) of CRR varies inversely with the change of temperature. This central message of Adam Gibbs work is mathematically expressed as

$$\bar{W}(T) = \bar{A}exp(-\Delta\mu \ s_c^*/kT \ S_c) = \bar{A}exp(-C/TS_c) \tag{2.8}$$

where $\bar{W}(T) \sim 1/\tau(T)$ is the cooperative transition probability which is inversely proportional to the relaxation time $\tau(T)$ and $\bar{A}$ is frequency factor. C is equal to $\Delta\mu \ s_c^*/k$ where $\Delta\mu$ is a 'largely the potential energy hindering the cooperative rearrangement per monomer segment', s_c^* is the the limiting value for configurational entropy related to the a critical size of a CRR and k is the Boltzmann constant. $S_c = Ns_c$ is the configurational entropy of a macroscopic supersystem composed of N subsystems. It is important to mention that the size of CRR at T_g cannot be calculated from the Adam-Gibbs model.

The Adam-Gibbs theory was expanded by Donth [69] based on the Fluctuation-Dissipation Theorem (FDT), in order to quantitatively elucidate the CRR size [46]. According to Donth [86], the von Laue approach, which considers temperature fluctuations, can be used to determine CRR sizes. The determination of the CRR sizes is based then on line response experiments [87] (i.e., calorimetric experiments) where the fluctuations of molecules (monomers) within a CRR can be obtained from experiments. Therefore each cooperatively rearranging region (CRR) can be regarded as a thermodynamic sub-system with fluctuating variables having its own relaxation time and glass transition temperature [88]. Following Donth's approach, the CRR volume (V_{CRR}) or characteristic length of the glass transition ($\xi_\alpha^3 \equiv \xi_{CRR}^3$) can be estimated based on the following equation [69, 89]

$$V_{CRR} = \xi_{CRR}^3 = \frac{k_b T^2 \ \Delta(1/C_p)}{\rho\delta T^2} \tag{2.9}$$

where $\Delta(1/C_p)$ is related to the step height of reciprocal specific heat capacity and is approximately equal to $\Delta(1/C_v)$ at the glass transition, ρ is the average mass density and δT^2 corresponds to the temperature fluctuation which can be obtained from width of the glass transition in $C_p(T)$. Note that, the CRR sizes have been calculated from the calorimetric data for various glass-forming materials according to this model. Typical ξ_{CRR}^3 values are in range of 10-30Å at T_g [89, 90].
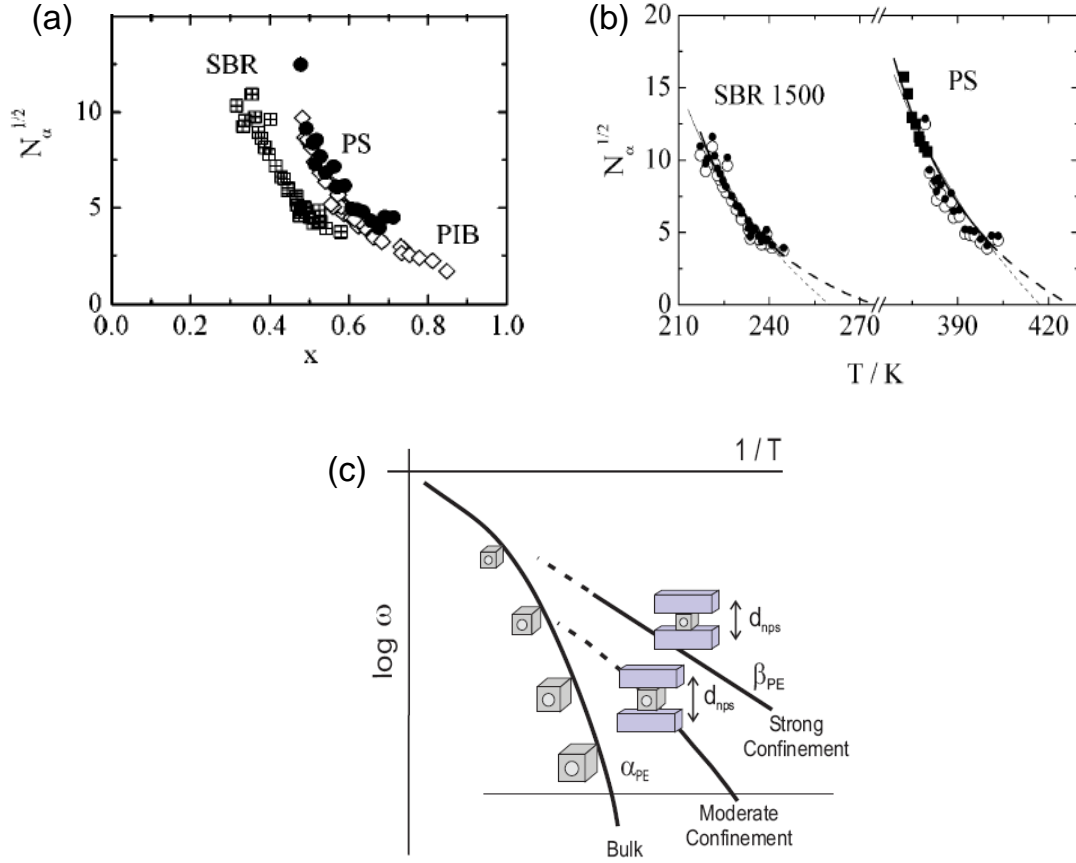
Figure 2.12: (a) Cooperativity (N_α) *vs.* reduced temperature (x) and temperature (T) for different polymers. Figure taken from ref. [49,91]. (b) Schematic depicting the hindered glass transition picture for the cooperative dynamics of confined systems. Figure taken from ref. [69].

From the CRR volume (V_{CRR}), the cooperativity (N_{CRR}) can be determined according to

$$N_{CRR} = V_{CRR} N_A \rho / M_0 \tag{2.10}$$

with M_0 being the molecular weight per molecule (monomer) and N_A being Avogadro's constant. Typically one gets N_{CRR} = 10-300 molecules (monomers) per CRR at T_g.

Temperature dependence of CRR sizes. The experimental findings based on the calorimetric data reveals that the the CRR volume V_{CRR} and cooperativity N_{CRR} do decrease systematically with increasing temperature [47, 49, 87, 90, 91]. It has been also reported that the cooperativity N_{CRR} approaches 1 at a finite temperature T_{on} in the so-called crossover region. An equation predicting the temperature dependence of

cooperativity (N_{CRR}) has been proposed Donth et al. [49,90,91]. $N_{CRR}^{1/2} = A(1-x)/x$ is used to estimate the temperature-dependent CRR size, where $x = (T - T_\infty)/(T_{on} - T_\infty)$ is a reduced temperature and A is a proportionality constant [49,87]. Accordingly, the cooperativity (N_{CRR}) increases strongly with decreasing temperature corresponding to an increase of CRR size V_{CRR} as predicted already by Adam and Gibbs (Figure 2.12.a).

Hindered glass transition. As discussed before, Eq.2.9 predicts that the CRR size increases with decreasing temperature. If glass-forming materials are geometrically confined in nanoscopic domains having sizes comparable to the CRR size ($d_{conf} \approx \xi_\alpha$), the temperature dependence in the CRR size should result then in a change of the temperature dependence of the α relaxation time τ_α. The reason is that the number of molecules within a domain is then smaller than N_{CRR}. Accordingly, the cooperative α dynamics should speed up and the glass temperatures should decrease in very small nanoscopic domains. This physical picture (gedankenexperiment) is proposed by Donth [69, 92] and called 'hindered glass transition'. The schematics shown in Figure 2.12.b [15] illustrates the trends. As smaller the domain size as earlier the deviation from the bulk-like α dynamics should occur during cooling. Apart from the already mentioned changes in relaxation time τ_α and glass temperature T_g, a transition from non-Arrhenius to Arrhenius is expected when the size of the domain size d_{conf} decreases. This hindered glass transition picture has been often used to explain qualitatively decreasing α relaxation time and glass temperatures obtained in nanoconfined glass formers as compared to corresponding bulk systems [15, 21, 29, 93, 94].

2.2.3   Effects of constraints on glass transition

In the literature, various factors have been discussed and studied which influence the glass transition. Three main influencing factors can be highlighted: (i) geometrical confinement effects, (ii) change in density due to confinement and (iii) interfacial effects on glass transition. Extended reviews have been provided by Alcoutlabi et al. [95] as well as Alba-Simionesco et al. [96]. Changes in the α dynamics caused by the three main important influencing factors will be considered in more detail below.

Geometrical confinement effects. Glass forming liquids in nanoporous host systems and thin polymeric films have been extensively investigated in order to understand the impact of geometrical confinement on glass transition temperature and α relaxation time. In case of nanoporous host systems, the effect on T_g is frequently examined in the controlled porous glasses (CPGs) containing small molecules [29,97]

or low molecular weight polymers as glass formers [94]. An early work focusing on T_g of small molecules in CPGs was carried out by Arndt et al. [29]. In this study, phenyl salicylate (salol) was confined in CPGs having three different pore diameters. Dielectric spectroscopy and differential scanning calorimetry (DSC) data for salol in CPGs showed a downwards shift of T_g by 15, 11 to 8 K in 25, 50 and 75Å pores, respectively. These shifts highlight the effect of confinement on T_g. A similar work was conducted by Zheng et al. on propyleneglycol and glycerol confined in nanoporous glass [97]. They observed a T_g shift in range of 3 to 5K in 25Å pores of controlled porous glasses. Moreover, it is reported in work by Schönhals et al. [94] that low molecular weight polymers like poly(propylene glycol) (PPG) and poly(methyl phenyl siloxane) (PMPS) show faster dynamics compared to bulk systems if confined in CPGs (25Å- 200Å). It is noteworthy to mention that all these results are acquired in surface treated (silanized) host systems, as without treatment the surface interaction would strongly affect the result.

Beside the nanoporous host systems, geometrical confinement effects on the glass transition have been also widely studied in thin films [32,40,93,98]. An early study in this regards, has been preformed by Forrest et al. on the free standing films [40,93]. They found a depression in glass transition with reduction of polymer film thickness. For instance, the glass transition measured in their study for a 200Å thick film was decreased by more than 70 K with respect to the 700Å thick film. There are later several other studies where similar finding are reported. Contrary to earlier findings, dielectric spectroscopy experiments on 'carefully prepared' thin films reported no reduction of glass transition for films down to the thickness of ≈100Å [32,98]. More recently, it has been discussed that the methods used for the preparation of thin films along with the experimental techniques used for the determination of their T_g can dramatically affect the result of such investigations [44,95].

Change in average density due to confinement. Several groups have considered and studied changes of glass transition in confined systems with respect to changes in density with the main conclusion that the density of the confined liquid is not same as that of the bulk [38,95,99,100]. McCoy et al. reported the T_g shift in a confined liquid due to the changes in density of that liquid [99]. Commonly, it is predicted that the glass transition temperature should decrease with the decrease in the density. [101,102] Jackson and McKenna [38] observed in their pioneering work on CPGs filled with o-terphenyl and benzyl alcohol a depression of glass transition temperature. This decrease in T_g with decreasing pore diameter was attributed to the

density variation of the confined liquids in CPGs without experimental confirmation for this claim. The neutron scattering study by Morineau et al. [100] on toluene confined in nanoporous hosts (MCM-41 and SBA-15) showed no correlation between T_g and density. Their comparison of confined toluene in nanopores with different diameters (24Å, 35Å, 47Å) with bulk toluene revealed no major density changes at room temperature. Also, no shift of T_g was observed for toluene confined in 35Å and 47Å pores. On the other hand, a reduction in density was observed for toluene in 24Å pores together with an increase in T_g of about 30K. This was in conflict with earlier expectations and shows probably the superposition of different influencing factors in these host-guest systems. Similar to the situation in filled CPGs, relations between T_g and changes in density are also controversially debated in thin films. Dewetting studies by Reiter et al. [103] on thin PS films relate the change of glass transition temperature to a density change in the films. Otherwise, reflectivity experiments conducted by Wallace et al. [104] on similar thin PS films on Si substrates did not show any noteworthy density change depending on film layer thickness. This again shows that different systems, sample preparation methods and experimental techniques give often no clear picture for understanding the factors influencing T_g.

Interfacial constraint effects. Throughout the decades, many research groups have conducted studies on liquids in nanoporous systems (e.g. CPGs) demonstrating that the glass temperature of confined liquids near the walls of nanopores are higher as compared to its centre (core) [33, 105–107]. This difference can be attributed to molecular mobility gradients in liquids confined in nanoporous systems (CPGs) and has been described based on a two phase model for salol confined in CPGs by Arndt et al. [29, 105]. Furthermore, the interfacial effects on the glass transition temperature have also be observed in a study carried out by Richert et al. [108]. They examined an increase of glass transition temperature resulting from a strong interaction of 3-methyl pentane with the pore walls of a CPG with 75Å nanopores. In case of thin films, opposing shifts of T_g have been observed for free surfaces as well as for material close to the substrate due to different types of interactions at the interfaces [109, 110].

In summary, it is observed that all the three effects considered above can significantly influence the glass transition of glass forming materials in nanoscopic compartments and that it is often extremely complicated to clarify the reasons for changes compared to the bulk state. Basically this is due to the fact that it is hard to find model systems and experiments where only one parameter is varied. Thus, it is also risky to draw final conclusions regarding dynamic heterogeneities is glasses and size of

cooperatively rearranging regions (CRRs) only based on the findings for thin polymer films as well as liquids in nanoporous host system. However, a answer to this question is essential for making progress with a deeper understanding of the softening behavior of glass-forming materials which is still not finally understood. Excellent model systems for contributing to this discussion are comb-like polymers with crystalline main chain and amorphous alkyl side chains. The self-assembled nature of these polymers allows to study the cooperative dynamics of methylene units (α_{PE}) in alkyl nanodomains with tunable dimensions (10-20 Å) and well defined interfaces. An example in this regard are poly(3-alkyl thiophenes) P(3AT)s [21] which have been used to study the confined dynamics of CH_2 units in alkyl nanodomains in order to learn more about CRR sizes. These studies will be deepened here using another comb-like polymer with crystalline main chains (PPAOTs) in order to extent the knowledge about different factors influencing the confined dynamics.

Chapter 3

Materials and methods

3.1 Materials

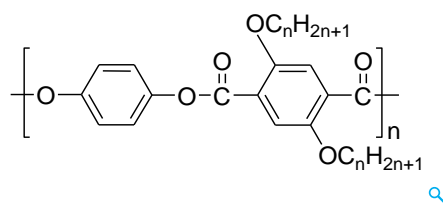### 3.1.1 Poly (1,4-phenylene-2,5-n-dialkyloxy terephthalate)s PPAOTs

Figure 3.1: Repeating unit of poly (1,4-phenylene-2,5-n-dialkyloxy terephthalate)s PPAOTs.

Synthesis. Poly(1,4-phenylene-2,5-n-dialkyloxy terephthalates) (PPAOTs) with $n = 6 - 12$ alkyl carbons per side chain are synthesized by Dr. H. Budde (Fraunhofer PAZ Schkopau) following the route described by Ballauff et al. [13] with four steps. The repeating unit of poly(1,4-phenylene-2,5-n-dialkyloxy terephthalates) is shown in Figure 3.1.

Step 1 - Synthesis of diethyl-2,5-dialkoxyterephthalates. Initially, 0.056 mol 2,5-dihydroxy terephthalic acid diethylester were dissolved in 250 ml cyclohexanone in a 500 ml three-necked flask with magnetic stirrer, dropping funnel, reflux condenser and nitrogen connection. Then, 0.12 mol potassium carbonate powder and 0.01 mol potassium iodide were added to the stirred solution followed by dropwise addition of the respective alkyl bromid (0.18 mol) within one hour. The mixture was refluxed for 20 h or until the yellow color had disappeared. The filter cake was washed with

cyclohexanone after filtering off the hot solution. All cyclohexanone solutions were collected and the solvent removed by using a rotation evaporator. The oily residue crystallized during cooling to room temperature. The product was recrystallized twice from ethanol. In all cases the yields were between $60 - 80\%$ of the theoretical value.

Step 2 - Synthesis of 2,5-dialkoxyterephthalic acid. 0.03 mol of the synthesized esters were refluxed in 250 ml ethanolic KOH (5%) for 4 h. After cooling to room temperature the free acids were precipitated by neutralization with dilute hydrochloric acid. The product was filtered off and recrystallized from ethanol. The yields were nearly quantitative.

Step 3 - Synthesis of 2,5-dialkoxyterphthalic acid chloride. The free acids were converted in the acid chlorides by refluxing with an excess of thionyl chloride for approximately 8 h. The excess of thionyl chloride was removed by distillation in vacuo. The yellow residue was recrystallized twice from dry $n-$pentane.

Step 4 - Melt polymerization. Hydroquinone and the respective 2,5-dialkoxy terephthalicacid chlorides were condensated in a nitrogen atmosphere at 100 °C in a 50 ml flask. The formed hydrogen chloride was removed from the reactor by a continuous stream of nitrogen. Depending on the viscosity, the temperature has been increased to up to 250°C.

Cyclohexanone (for synthesis, Merck), n-alkylbromides (Aldrich) and n-pentane (Aldrich) were dried over molecular sieve 4A and distilled prior to use. Hydroquinone ($> 99\%$, Aldrich) was sublimated in vacuo and stored under nitrogen. Potassium carbonate (for analysis, Merck), potassium iodide (for analysis, Merck), potassium hydroxid (pure, BDH Prolabo), ethanol (technical purity, CVM), thionyl chloride ($> 99\%$, Aldrich) and 2,5-dihydroxyterephthalic acid diethylester (97%, Aldrich) were used without further purification.

Sample characteristics. The average molecular weights and polydispersities of these alkoxylated polyesters as obtained from gel permeation chromatography measurements in chloroform against polystyrene standards are given in Table 3.1.

Table 3.1: Molecular weight parameters of PPAOTs

Label	n	M_n kg/mol	M_w kg/mol	PDI
PPHOT	6	179	183	1.02
PPOOT	8	12.4	78	6.30
PPDOT	10	14.6	95	6.50
PPDDOT	12	2.6	5.2	2.01

3.1.2   Poly (2,5-n-dialkyloxy-1,4-phenylenevinylene)s AOPPVs
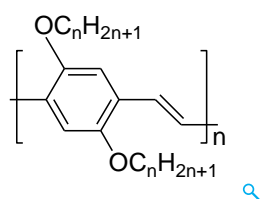
Figure 3.2: Repeating unit of poly (2,5-n-dialkyloxy-1,4-phenylenevinylene)s (AOPPVs).

Synthesis. Poly (2,5-n-dialkyloxy-1,4-phenylenevinylene) (AOPPVs) with $n = 6$ - 12 alkyl carbons per side chain are synthesized by Prof. D. A. M. Egbe (Friedrich-Schiller Universität Jena) following the route described through Horner-Wadsworth-Emmons (HWE) olefination polycondensation reaction of dialdehyde with bisphosphonate [111]. All members of AOPPVs were synthesized according to procedure mentioned below; however, herein the synthesis of DDOPPV ($n = 12$) is described as an example. The repeating unit of poly (2,5-n-dialkyloxy-1,4-phenylenevinylene) is shown in Figure 3.2.

A solution of dialdehydes [1,4-dialdehyde-2,5-didodecyloxybenzne, 2 g, 3.98 mmol] and bisphosphonates [2,5-bis(dodecyloxy)-p-xylylene-bis(diethylphosphonate), 2.97 g, 3.98 mmol] were dissolved in dry toluene (60 ml), stirred vigorously and heated up to 150°C-160°C under nitrogen and reflux for 1 hour (stirring was realized by using a mechanical stirrer). The polycondensation was initiated and supported by the addition of portions of potassium tertbutylate (t-BuOK, 1.122 g, 10 mmol) and the reaction mixture was heated at reflux. After 2 hours the heating was stopped, further toluene (300 ml) was added and the reaction mixture was quenched by the addition of hydrochloric acid (10 %, 150 ml). The phases were separated and the organic phase was washed with deionized water until neutrality. Residues of water were removed by refluxing in a Dean-Stark apparatus, and the still warm solution was filtered. Most

of the solvent was removed under reduced pressure using a rotary evaporator and precipitated in cooled methanol (ice / NaCl bath). After 1 hour stirring the precipitated material was filtered off and transferred into a Soxhlett extractor. Low molecular species were extracted heating a methanol / water mixture (2:1) for 10 hours to reflux. After the purification procedure the polymer was obtained as a red material (2.4 g, 64.08 % yield).

All chemicals and solvents used in the preparation of the intermediates and polymers were purchased from commercial suppliers, such as Sigma Aldrich, Fluka and Merck, and were used as received, if not stated otherwise. The solvents were deaerated with nitrogen for two hours before use. During the reactions a constant flow of nitrogen was provided to prevent any intake of oxygen or moisture. The synthesis of dialdehydes as well as bisphosphonates was performed according to the literature descriptions [111–114].

Sample characteristics. Molecular weights and polydispersities of these alkoxylated polyphenylenevinylenes as obtained from GPC measurements in tetrahydrofuran against polystyrene standards are given in Table 3.2.

Table 3.2: Molecular weight parameters of AOPPVs

Label	n	M_n kg/mol	M_w kg/mol	PDI
HOPPV	6	3.0	5.0	1.69
OOPPV	8	3.5	5.9	1.67
DOPPV	10	3.3	4.5	1.37
DDOPPV	12	2.8	3.6	1.30

3.1.3 Capillary Extrusion

Extrusion is a process widely used to prepare profiles of sheets, pipes or plastic tubing and fibers etc in a continuous or semi-continuous manner with a specific geometry and shape. The basic working principle of this technique includes feeding of material into the feeder which is heated to the desired processing temperature and then a ram is used to push the material through the die. Keeping the above principles intact, a lab scale ram extruder is developed in this work which can process very small amount (200mg) of the material with a controlled shear rate.
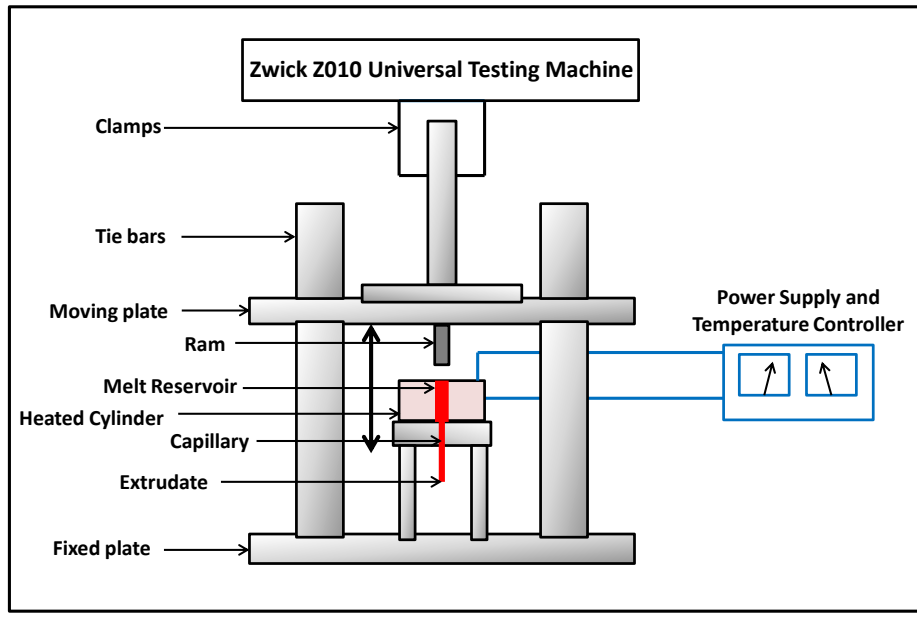
Figure 3.3: Construction and working principle of the lab scale 'mini-extruder'.

Instrumental setup. The scheme of the used lab extruder is shown in Figure 3.3. The home-made ram extruder contains three main parts. 1. The extruder unit which consists of ram and circular die. The ram is connected to a vertically movable plate which is in turn connected to the tensile testing machine. The die, with a cylindrical hole (capillary), though which the material comes out in form of a continuous fiber, is attached at the lower end of the heated cylinder. 2. Power supply and temperature controller which stabilizes and monitors the temperature of the heated cylinder containing the melt in the extruder unit. 3. A universal testing machine which work in compression mode with a defined shear rate. Note that the processing temperature and shear rate (processing speed) are two significant parameters influencing the extrusion process.

The apparent shear rate ($\dot{\gamma}_{aw}$) for a circular capillary at walls can be calculated from the flow rate Q through the capillary [115].

$$\dot{\gamma}_{aw} = \frac{32Q}{\pi D_c^3} \tag{3.1}$$

$$Q = A_p \nu_p \tag{3.2}$$

where A_p is the area of the piston head and ν_p is the velocity of the moving piston. This is a result of the continuity equation of fluid mechanics.
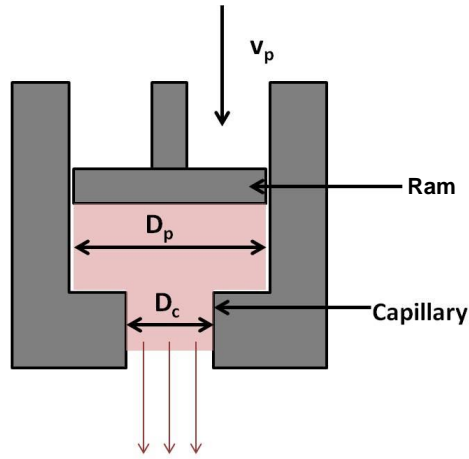
Figure 3.4: Capillary and ram assembly of the extruder. D_p is the diameter of piston, D_c is the diameter of die and ν_p is the velocity of the moving piston.

$$Q = \nu_p \frac{\pi}{4} D_p^2 \qquad (3.3)$$

On replacing the value of Q, the apparent shear rate can be described as:

$$\dot{\gamma}_{aw} = \frac{8 D_p^2 \nu_p}{D_c^3} \qquad (3.4)$$

The equation 3.4 allows calculating the apparent shear rate during processing. Here the polymer melt is assumed as a Newtonian fluid.

Program used. An extruded sample was prepared in order to study the degree of orientation according to the setup shown in Figure 3.3 at 120°C with processing speed of 6 mm/min, 90 mm/min and 180 mm/min with 5 mm piston diameter. The samples were extruded at three different shear rates: $20s^{-1}$, $300s^{-1}$ and $600s^{-1}$ which were calculated from equation 3.4.

3.2 Characterization methods

3.2.1 X-ray diffraction

Basics. X-ray diffraction methods are based on the elastic scattering of x-ray photons by atoms located on well-ordered lattice planes. In the case of elastic scattering, the

wavelength of the incident (primary) beam and the diffracted beam remains constant. A basic description of the constructive interference of waves scattered by different lattice planes is given by Bragg's law (Figure 3.5.a). Consider a set of parallel planes of atoms with an interplanar distance d. When an incident beam of known wavelength λ falls on these atoms, a constructive interference occurs if the waves scattered on different lattice planes are shifted by a multiple of the wavelength $n * \lambda$. For isotropic samples containing a large number of randomly oriented crystals, the scattering angles where constructive interference appears can be therefore expressed as

$$n\lambda = 2dsin\theta_B \tag{3.5}$$

The above equation is Bragg's law and θ_B is the incident angle (Bragg angle) for which constructive interference occurs. The most common concepts to describe diffraction pattern and their relation to real space structures require operating in reciprocal space. According to this concept, every set of crystal lattice planes in real space corresponds to a specific vector in reciprocal space [116]. The transformation equations for the coordinates from real space to reciprocal space are given by

$$\mathbf{a}^* = \frac{2\pi}{V_u} \ (\mathbf{b} \times \mathbf{c}) \tag{3.6}$$

$$\mathbf{b}^* = \frac{2\pi}{V_u} \ (\mathbf{c} \times \mathbf{a}) \tag{3.7}$$

$$\mathbf{c}^* = \frac{2\pi}{V_u} \ (\mathbf{a} \times \mathbf{b}) \tag{3.8}$$

where $\times$ represents the vector product, and V_u is the unit cell volume expressed as

$$V_u = \mathbf{a} \cdot (\mathbf{b} \times \mathbf{c}) = \mathbf{b} \cdot (\mathbf{c} \times \mathbf{a}) = \mathbf{c} \cdot (\mathbf{a} \times \mathbf{b}) \tag{3.9}$$

In general, the reciprocal lattice vector given by

$$\mathbf{G}_{hkl} = h\mathbf{a}^* + k\mathbf{b}^* + l\mathbf{c}^* \tag{3.10}$$

with h, k and l being the Miller indices describes fully the set (hkl) of planes within a crystal. Note that the $\mathbf{G}_{hkl}$ is always perpendicular to the planes (hkl) in the direct lattice. Furthermore, the magnitude of the reciprocal lattice vector $|\mathbf{G}_{hkl}|$ is proportional to the reciprocal of the interplanar spacing (d_{hkl}). The full relation is
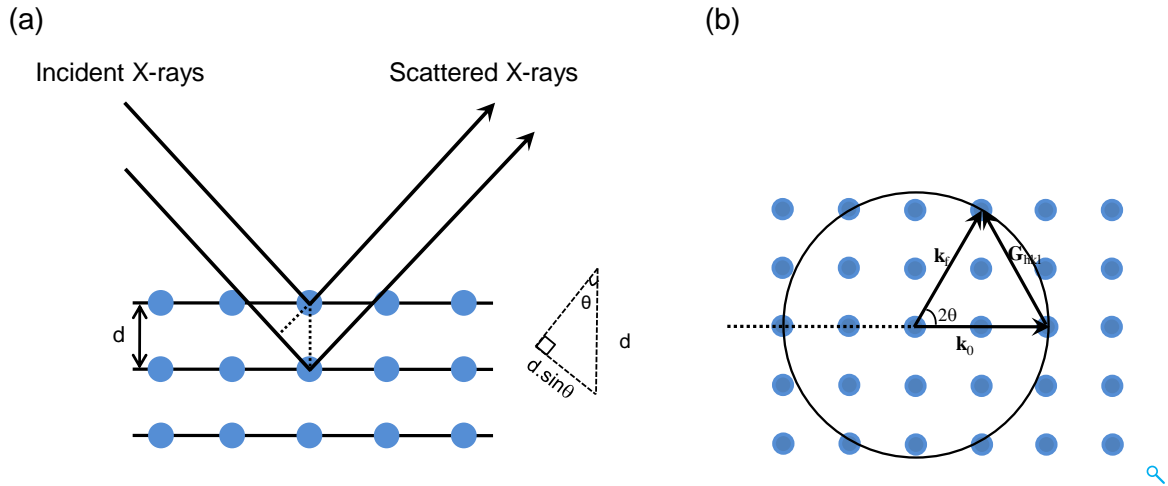
Figure 3.5: (a) Origin of Bragg's law through constructive interference between the two interplaner lanes having spacing d. (b) Ewald's sphere construction and reciprocal lattice.

$$|\mathbf{G}_{hkl}| = \frac{2\pi}{d_{hkl}} \tag{3.11}$$

The conditions for constructive interference in case of anisotropic samples can be explained with the help of Ewald's sphere construction (Figure 3.5.b). Consider an incoming wave characterized by a wave-vector ($\mathbf{k}_0$), which is drawn in the direction of the incident beam, with one end at the origin of the reciprocal lattice. The other end of ($\mathbf{k}_0$) is taken as the center of a sphere of radius $1/\lambda$. Constructive interference can be observed only if any of the reciprocal lattice vectors $\mathbf{G}_{hkl}$ representing a set of lattice planes lies on the Ewald sphere. The direction ($\mathbf{k}_f$) is the direction of the diffracted wave (which also has its origin at the center of the Ewald's sphere). The scattering vector is defined by $q = k_f - k_0$.

$$\mathbf{q} = (k_f - k_0) = 2\pi\mathbf{G}_{hkl} \tag{3.12}$$

$$|\mathbf{q}| = \frac{4\pi}{\lambda}sin\theta_B = \frac{2\pi}{d_{hkl}} \tag{3.13}$$

WAXS setup and program used. Wide angle x-ray scattering (WAXS) measurements in reflection mode were performed on PPAOT and AOPPV samples using an Empyrean diffractometer (PANalytical) equipped with the temperature chamber TTK 450 (Anton Paar). The emitted radiation was parallelized and monochromatized using a parallel beam mirror ($\lambda = 1.54$ Å). The scattered intensity passes a parallel plate

collimator (0.27°) and is detected by a Pixel 3D detector with 19 channels of 0.055 μm size combined to be used as a receiving slit. The scan range was 2 $nm^{-1} \leq q \leq 28$ nm^{-1}, the step size 0.05° and the counting time per step 1 s. Before the start of the experiments, the samples were aligned in two steps. In the first step, the sample stage was moved down so that it was out of the x-ray beam path. A 2θ scan was performed for the beam position calibration and then a zero position was selected based on the center of the resulting beam profile. This method sets the fine calibration offset in 2θ of the primary beam position. The second step corresponds to the adjustment of the sample height which was performed by a z scan. A z shape profile obtained in this scan, from which the half of the direct beam intensity was taken as sample height. Temperature-dependent measurements were carried out for both polymers in two cycles of heating (30°C to 230°C) and cooling from (230°C to 30°C) in steps of 10°C/min. In case of PPAOTs, temperature-dependent measurements were conducted in order to define the thermal programs needed to get specimen containing only modification A for each PPAOT sample (cf. Results section). Pretreated samples containing mainly modification A were further investigated at room temperature. The as-received samples (PPAOTs and AOPPVs) as well as melt-pressed PPAOT samples were placed onto silicon substrates cut from a single crystalline wafer with no Bragg reflections present in the above mentioned scan range. All the measurements were performed in air.

IAXS setup and program used. Intermediate angle x-ray scattering (IAXS) was used to determine the structural orientation resulted from extrusion in the PPDOT (n = 10) and DOPPV ($n = 10$) using a pinhole instrument designed by JJ X-rays with a Rigaku rotating anode as radiation source (CuK_α, λ =1.54Å), an Osmic multilayer optics and a Bruker Hi-star 2D detector. The samples were measured under vacuum at room temperature. The experiments were performed in such a way that the x-ray beam was perpendicular to the extrusion direction.

3.2.2 Dynamic shear measurements

Dynamic mechanical analysis is an important technique widely used to analyze and characterize the viscoelastic properties of polymers as a function of time, temperature and frequency. The basic principle of this method lies in the application of a periodic force and to observe its response on the subjected material [117].

Basic principle. In case of dynamic shear measurements, a sinusoidal shear strain (γ) is applied to a sample and the shear stress (σ) is detected which in general will
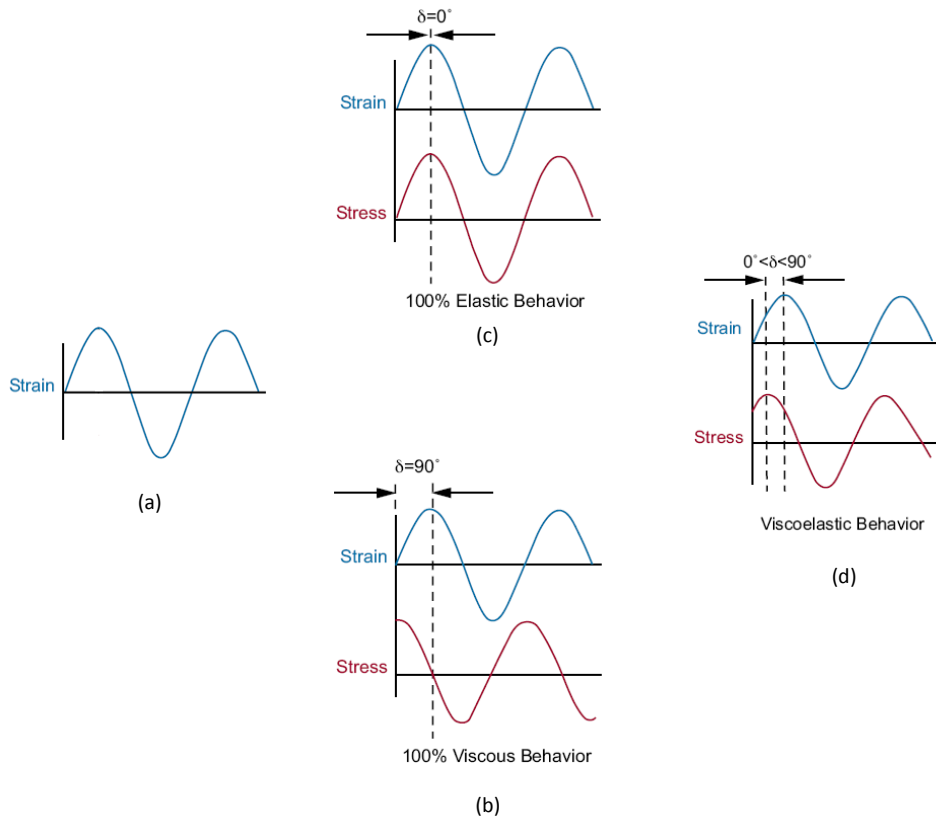
Figure 3.6: (a) Sinusoidal strain applied to the samples (blue). Response to sinusoidal strain as sinusoidal stress (red) for perfectly (b) viscous system , for (c) elastic system and for (d) a polymeric system where it lies in between these two extremes. Figure taken from Ref. [118].

be shifted by a phase angle δ with respect to applied strain. This phase lag is due to viscous contributions in the overall response. The entire phenomenon is depicted in Figure 3.6 and mathematically expressed by following equations

$$\gamma(t) = \gamma_0 sin(\omega t) \qquad (3.14)$$

$$\sigma(t) = \sigma_0 sin(\omega t + \delta) \qquad (3.15)$$

where ω is the angular frequency. Using this notation, stress can be decomposed into two components: one in-phase with the strain ($sin\omega t$) and other 90° out-of-phase with the strain ($cos\omega t$) and thus, the total stress can be described as

$$\sigma(t) = \sigma_0 sin(\omega t)cos\delta + \sigma_0 cos(\omega t)sin\delta \qquad (3.16)$$

Dividing the shear stress by shear strain, a dynamic shear modulus $G^* = G^{'}(\omega) + iG^{''}(\omega)$ can be defined. The storage modulus $G^{'}$ is related to the in-phase part and the loss modulus is then the $G^{''}$ out-of-phase part in the above equation. Both parts can be expressed in terms of shear stress and applied strain amplitude γ_0 as

$$\sigma(t) = \gamma_0 [G^{'}(\omega)sin\omega t + G^{''}(\omega)cos\omega t] \tag{3.17}$$

where $G^{'} = \sigma_0/\gamma_0 \, cos\delta$ and $G^{''} = \sigma_0/\gamma_0 \, sin\delta$.

The storage modulus, $G^{'}$ denotes the real part of the dynamic modulus and describes the ability of the material to store potential energy and release it upon deformation. Whereas, $G^{''}$ represents the imaginary part which is associated with energy dissipation in the form of heat upon deformation.

The loss modulus, $G^{''}$, defines the energy dissipation because of the following calculations of the energy (ΔE) dissipated per cycle

$$\Delta E = \oint \sigma d\gamma = \int_0^{2\pi/\omega} \sigma \frac{d\gamma}{dt} dt \tag{3.18}$$

Substituting for σ and γ values from the Eq 3.14 and 3.15 respectively, yields

$$\Delta E = \omega\gamma_0^2 \int_0^{2\pi/\omega} \sigma(G^{'}sin\omega t cos\omega t + G^{''}cos^2\omega t)dt \tag{3.19}$$

The integral is solved by using $sin\omega t \, cos\omega t = 1/2 \, sin2\omega$ and $cos^2\omega t = 1/2(1 + cos2\omega t)$, resulting in

$$\Delta E = \pi G^{''}\gamma_0^2 \tag{3.20}$$

Instrument used. A G2 rheometer from TA instruments was used for temperature dependent dynamic shear measurements of PPAOTs at discreet frequencies ($\omega = 0.1$, 1, 3, 10, 30, 100 rad/s) in the range between -140 °C to 100 °C with 3°C/step and 60s soak time per step. An oscillatory perturbation with a strain amplitude of 0.1 % was commonly applied. Stripes with a thickness of 1 mm, a width of 6.5 mm and a length of 12 mm were used as samples. Melt-pressed samples were prepared according to the thermal program (Figure 4.2) defined based on the temperature dependent x-ray diffraction experiments to ensure higher fractions of modification A. (c.f. Results section) In each measurement, the sample was first cool down to -140 °C with the help of cold nitrogen gas and equilibrated for 10 min before starting the experiment. Also the normal force was kept zero during the shear measurement.

3.2.3   Broadband dielectric spectroscopy

Broadband dielectric spectroscopy is a powerful tool for determining the dielectric permittivity of materials as the function of frequency and temperature [119]. It is based on the interaction of external electric field with the electric polarization of the material [120], often represented as permittivity (ϵ^*). This permittivity, in periodic electric field, is described as $\epsilon^*(\omega) = \epsilon^{'}(\omega) - i\epsilon^{''}(\omega)$ where $\epsilon^{'}(\omega)$ is the real part associated with energy stored and $\epsilon^{''}(\omega)$ the imaginary part related to the energy dissipation within the medium. The measured polarizability of the materials depends on the mobility of permanent molecular dipoles and therefore strongly temperature- and frequency-dependent. Hence, dielectric spectroscopy is detecting the specific reorientation of molecular dipoles in an external electric field and can give information about relaxation processes in all kind of materials over a wide frequency range (μHz - THz) [120].

Basic principle. In broadband dielectric spectroscopy, a sine wave voltage with an amplitude U_0 of about 1 V is generated from a generator and is used to produce an alternating electric field in the capacitor according to $E^* = U^*/d_c$. This alternating electric field, which act as a input program, is applied to the sample and the response to that program is observed as a polarization current I^*. Both input program and output response are shown in Figure 3.7 and can be mathematically expressed as

$$Program: U^* = U_0 \; . \; exp \; (i\omega t) \tag{3.21}$$

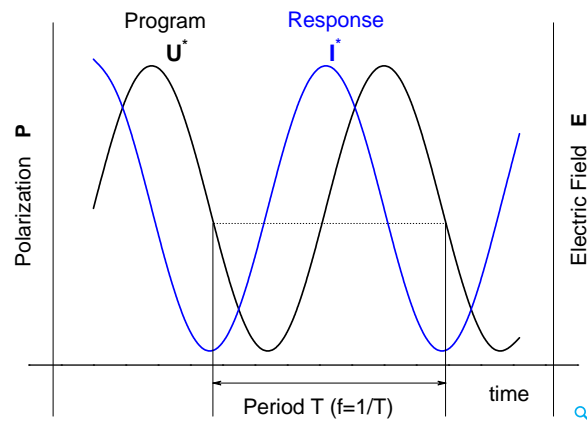$$Response: I^* = I_0 \; . \; exp \; (i\omega t + \pi/2 - \delta) \tag{3.22}$$

Figure 3.7: Sinusoidal voltage U^* (black) applied to the samples as an input program and the polarization current I^* (blue) is obtained as a response.

42

The complex capacitance (C^*) of the sample can be used to calculate the permittivity ϵ^* according to

$$C^* = \frac{I^*}{i\omega U^*} \tag{3.23}$$

$$\epsilon^*(\omega) = \epsilon^{'}(\omega) - i\epsilon^{''}(\omega) = \frac{C^*}{C_0} \tag{3.24}$$

Here $C_0 = \epsilon_0 \, A/d_c$ is the capacitance of the empty cell where ϵ_0 is the vacuum permittivity and A is the face area of the electrode plate.

Dielectric spectra analysis and models. The dielectric relaxation processes, which arise due to the response of a material to an electric field, are characterized by various fitting functions, which are required to determine the peak broadening and asymmetry in the real ($\epsilon^{'}$) and loss part ($\epsilon^{''}$) of the complex dielectric function (ϵ^*). In the ideal cases, these relaxation processes can be described by Debye function, which mainly deals with the noninteracting dipole moment of a sample in an AC external electrical field, and is often given as [121]

$$\epsilon^*(\omega) = \epsilon_\infty + \frac{\Delta\epsilon}{1 + i\omega\tau_D} \tag{3.25}$$

where $\Delta\epsilon = \epsilon_S - \epsilon_\infty$ is dielectric relaxation strength, ϵ_∞ is the permittivity at the high frequency, ϵ_S is the static, low frequency permittivity and τ_D is the characteristic relaxation time of the medium.

However, in real complex systems (e.g., polymers), the Debye equation cannot be used to predict the relaxation behavior of the dielectric processes and thus, empirical modified versions of Debye functions are developed to illustrate the asymmetric nature of imaginary peaks ($\epsilon^{''}$) as well as its broadness.

The broadness of dielectric loss curves, in real systems, can be shown by Cole/Cole function [122]

$$\epsilon_{CC}^*(\omega) = \epsilon_\infty + \frac{\Delta\epsilon}{1 + (i\omega\tau_{CC})^\beta} \tag{3.26}$$

where β ($0 < \beta \leq 1$) corresponds to the symmetric broadening of the loss peak. On the other hand, the Cole/Davidson function [123] is used to explain the asymmetric broadening of imaginary peak in dielectric relaxation process

$$\epsilon_{CD}^*(\omega) = \epsilon_\infty + \frac{\Delta\epsilon}{1 + (i\omega\tau_{CD})^\gamma} \tag{3.27}$$
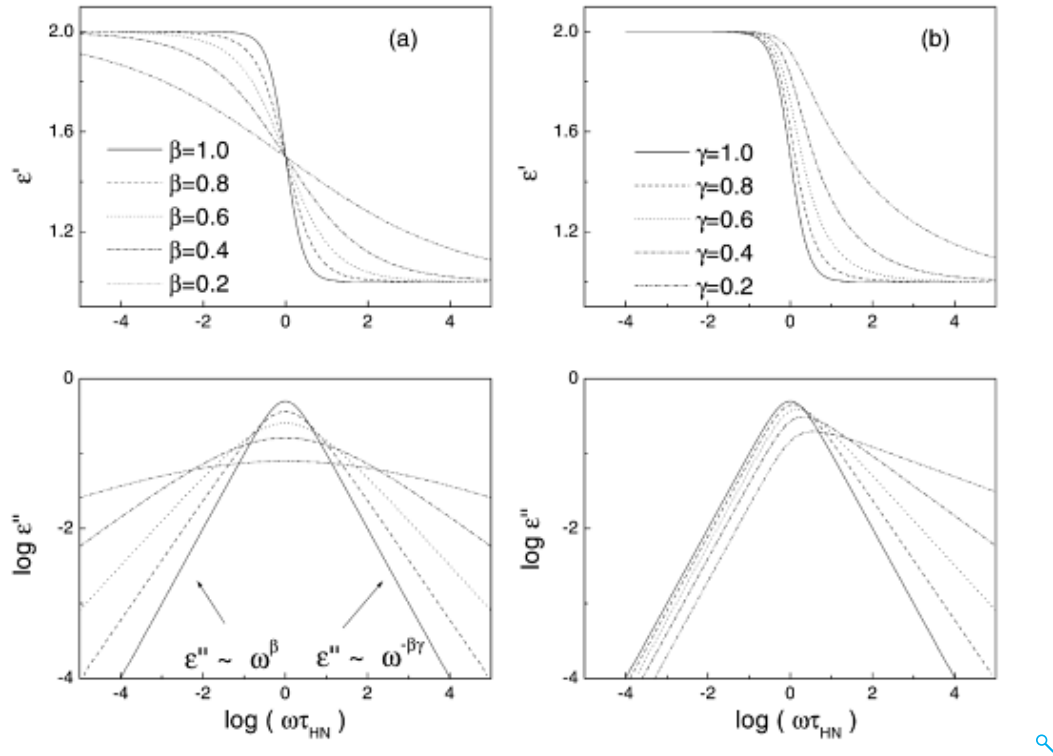
Figure 3.8: Real and loss part of complex dielectric permittivity for the Havriliak-Negami function with fixed: (a) $\gamma = 1$; (b) $\beta = 1$; ($\tau_{HN} = 1$s, $\Delta\epsilon = 1$, $\epsilon_\infty = 1$). Figure taken from Ref. [121].

In this equation, the exponent $0 < \gamma \leq 1$ represents the asymmetric broadening of the dispersion curve.

There is another fitting function (combination of the Cole/Cole and Cole/Davidson equation) which can explain both the broadness and asymmetric nature of dielectric loss peak (ϵ''). This is Havrialiak-Nagami function [124], which can be described as

$$\epsilon^*_{HN}(\omega) = \epsilon_\infty + \frac{\Delta\epsilon}{(1 + (i\omega\tau_{HN})^\beta)^\gamma} \quad (3.28)$$

The two exponent β and γ determine the broadness and asymmetry behavior of the corresponding peak in dielectric spectra ($0 < \beta$, $\beta\gamma \leq 1$), respectively. The exponent β is the slope $dlg\epsilon''/dlg(\omega)$ on the low frequency side far below the relaxation peak maximum and $-\beta\gamma$ is the asymptotic slope $dlg\epsilon''/dlg(\omega)$ at the high frequency side. Both the shape parameters (β and γ) with fixed values showing the asymmetry and broadness of dielectric curves are depicted in Figure 3.8.

Instrument used. A NOVOCONTROL Alpha analyzer equipped with a Quatro temperature controller was used for dielectric spectroscopy experiments of PPAOTs.

The experiments were performed on thin melt-pressed samples with thickness of 100 - 200 μm and $\sim$20 mm diameter. These melt-pressed samples were prepared according to the thermal program (Figure 4.2) defined based on the temperature dependent x-ray diffraction experiments to ensure higher fractions of modification A. All the measurements were conducted using a measuring cell in which the sample was placed between two parallel, disc like, gold plated electrodes. Isothermal frequencies in the range 0.01 Hz < f < 1MHz were performed at temperatures between -140°C and +130°C with a temperature step of +5°C. All the measurements were performed under a controlled nitrogen gas atmosphere.

Chapter 4

Results

4.1 Structural investigations on comb-like polymers

4.1.1 Poly (1,4-phenylene-2,5-n-dialkyloxy terephthalate)s

In this section, the results of structural investigations on poly(1,4-phenylene-2,5-n-dialkyloxy terephthalate)s with different alkyl side chain (n = 6 to 12) length are presented. Temperature dependent x-ray diffraction measurements are performed on non-oriented samples (isotropic) in conjugation with 2D scattering measurements on oriented fibers (obtained by ram extrusion). Main aim of this part of the work is to understand and quantify the packing state of side chains within different polymorphic states of PPAOTs (modifications A and B) as well as interrelations between main and side chain packing in these comb-like polymers.

   Evaluation of modification A. Temperature dependent x-ray diffraction patterns for PPAOTs with different side chain lengths during a stepwise cooling scan (from the melt) are shown in Figure 4.1. Independent of the side chain length, a featureless scattering pattern is observed for all PPAOTs samples at the highest temperatures (T > 200°C) which corresponds to a disordered or amorphous state. A broad 'pre-peak' at $q < 5\ nm^{-1}$ and a conventional amorphous halo around $10\ nm^{-1} < q < 20\ nm^{-1}$ is seen at these temperatures. The 'pre-peak', which is observed at higher temperatures, is also found for many fully amorphous nanophase-separated polymers with comb-like architecture which show a main chain independent polyethylene-like glass transition (α_{PE} process) within alkyl nanodomains [15]. As the temperature decreases, sharp Bragg reflections corresponding to q_{100}^{A} start to emerge in all investigated samples. The existence of this reflection is observed in the range of $3.0\ nm^{-1}$ to $4.5\ nm^{-1}$ along with
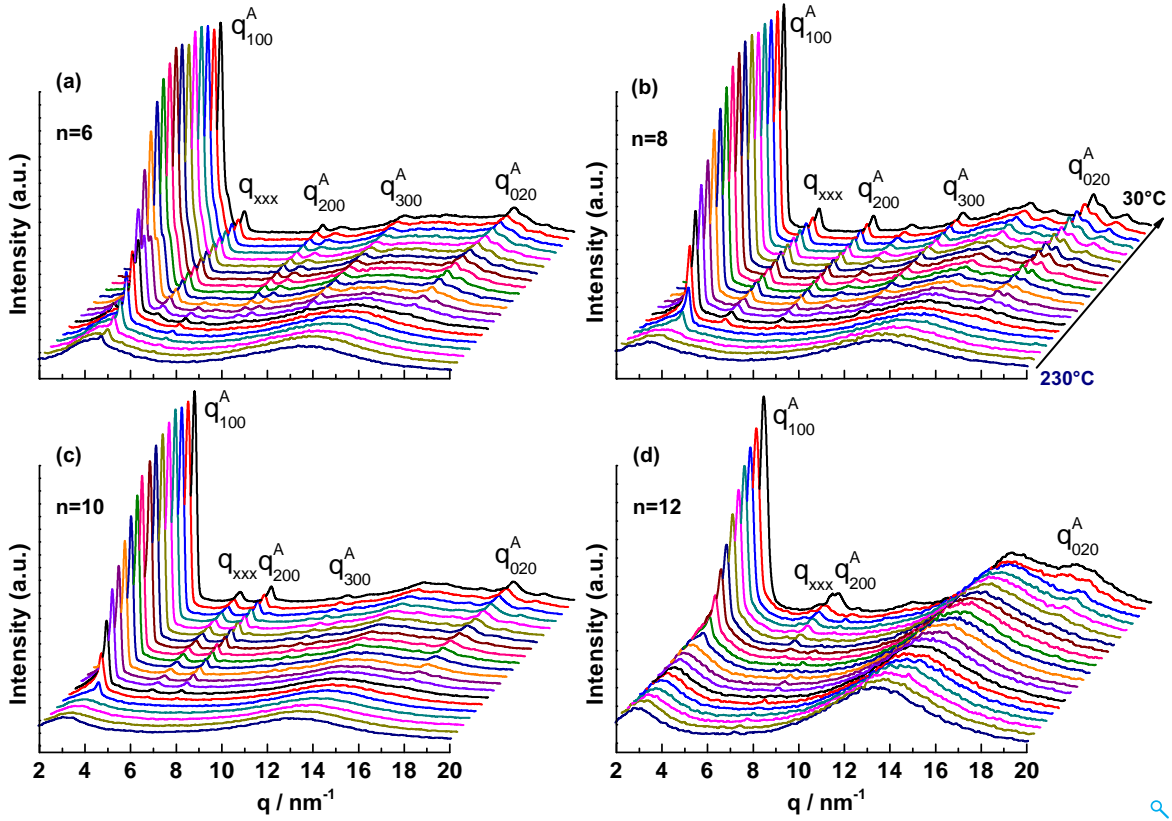
Figure 4.1: Temperature-dependent x-ray diffraction patterns for (a) PPHOT (*n*=6), (b) PPOOT (*n*=8), (c) PPDOT (*n*=10) and (d) PPDDOT (*n*=12) measured during the first cooling scan (230°C to 30°C) in steps of 10°C/min. The labels are the Miller indicies for the most important scattering peaks.

the higher orders, q_{200}^A and q_{300}^A, which confirms the presence of a lamellar morphology originating from alternating main and side chain domains. On the other hand, a prominent q_{020}^A Bragg peak around $q \approx 17.3 \ nm^{-1}$ begins to appear upon cooling from the amorphous halo, which in general seen at 30-60°C lower than the 'pre-peak'. This Bragg reflection (q_{020}^A) is related to the $\pi - \pi$ stacking of the aromatic rings within the main chain domains [11]. The temperature at which these peaks appear upon cooling is known here as onset temperature ($T_{on,100}$ and $T_{on,020}$), and its values varies for $n = 6$ to 12 member of the PPAOTs (Table 4.1). Furthermore, an additional peak, q_{xxx}, is also observed around 5.3 nm^{-1} in all PPAOTs showing its independent appearance in comparison to q_{100}^A and q_{020}^A reflections. The exact nature of this peak will be highlighted in more details in the later part of this work.

As the samples received after the synthesis have an unknown thermal history, one aim of this study was to thermally treat all PPAOT samples in order to obtain spec-
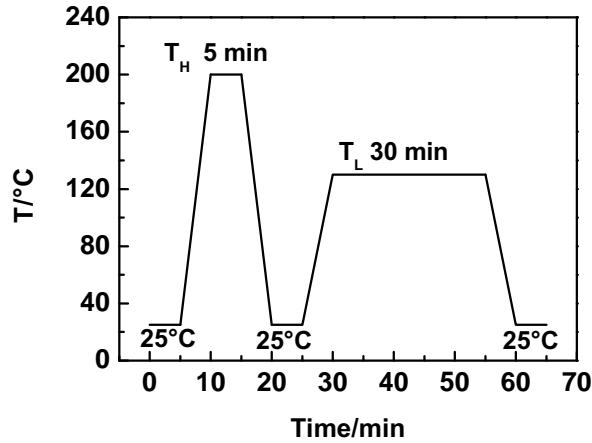
Figure 4.2: Temperature program used for the thermal treatment for preparing higher fraction of modification A in PPAOT samples.

Table 4.1: Temperature program and crystallization temperatures for PPAOT samples (* onset temperatures where (100) and (020) reflection peaks start to develop)

Label	n	T_H	T_L	$T_{on,100*}$	$T_{on,020*}$
		°C	°C	°C	°C
PPHOT	6	185	130	230	170
PPOOT	8	210	160	210	170
PPDOT	10	210	170	200	170
PPDDOT	12	170	150	140	100

imens containing a very high fractions of modification A which will be later used in the relaxation spectroscopic studies. Therefore, a program to obtain modification A of PPAOTs has been defined based on the above mentioned temperature-dependent x-ray diffraction experiments. The chosen program is shown in Figure 4.2.

A two step program is used. The samples are annealed in a first step for 5 min in a hot press under slight pressure at a temperature T_H where the samples are basically molten. Then the samples are cooled down under defined conditions, and afterward annealed for 30 minutes at a lower temperature T_L. The values of T_H and T_L are sample-specific and listed in Table 4.1. Here, the T_H corresponds to the temperature where only a very small portion of modification A with q_{100}^A lattice planes exists and no higher orders are present whereas the T_L relates to the temperature where the layered structure of modification A is nicely indicated by higher order peaks to the q_{100}^A reflection. The structure of samples prepared according to this program is characterized at room temperature by x-ray diffraction experiments. The measured patterns are given
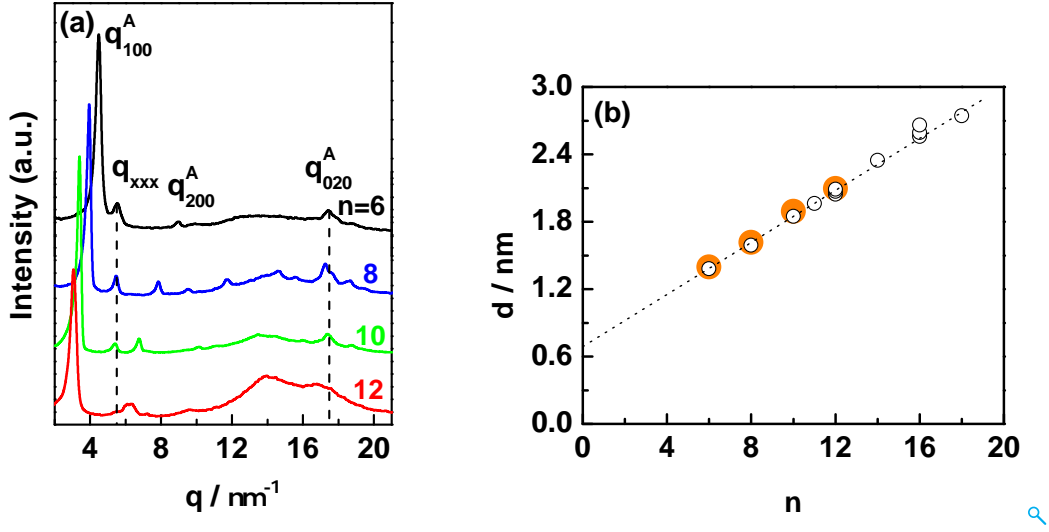
Figure 4.3: (a) X-ray diffraction patterns for PPHOT (n=6), PPOOT (n=8), PPDOT (n=10), and PPDDOT (n=12) measured at room temperature after applying a special two step thermal treatment in order to get high fractions of modification A. The Miller indicies for the most important scattering peaks are labeled. The vertical dotted lines at 5.3 nm^{-1} and 17.3 nm^{-1} indicate the weak dependence of (xxx) and (020) peaks on side chain lengths. (b) Layer spacing d $vs.$ number of carbon atoms per side chain n. d_{100}^A values for modification A (circles - full symbols) of PPAOTs are compared to those reported by Ballauff et al (circles - open symbols) [11]. The intercept (dotted line) with the y-axis (n=0) corresponds to the thickness of the main chain domains (d_{mc}).

in Figure 4.3.

Table 4.2: Unit cell parameters, spacings and crystallographic density for modification A of PPAOTs

Label	n	d_{100}	d_{020}	d_{001}	d_{alkyl}^*	**a**	**b**	**c**	M_o	ρ
		Å	Å	Å	Å	Å	Å	Å	g/mol	g/cm^3
PPHOT	6	13.9	3.54	11.6	7.2	13.9	7.1	11.6	446	1.29
PPOOT	8	16.2	3.65	11.6	9.5	16.2	7.3	11.6	502	1.21
PPDOT	10	18.9	3.63	11.8	12.2	18.9	7.3	11.8	558	1.14
PPDDOT	12	21.0	3.64	11.9	14.3	21.0	7.3	11.9	614	1.12

$$* \ d_{alkyl}^A = d_{100}^A - d_{mc}$$

Lattice model for modification A. A detailed comparison of the scattering patterns of modification A for different PPAOT samples in Figure 4.3.a shows nicely that the main features are qualitatively similar for all the investigated samples independent on side chain length. A lamellar structure on the nanoscale is indicated by q_{100}^A, q_{200}^A and q_{300}^A reflections appearing at low q values. A comparative look at the room temperature x-ray scattering pattern (Figure 4.3.a) reveals that the q_{100}^A reflection

systematically shifts to lower q values, indicating an increased main-chain side-chain distance d_{100}^A. The d_{100}^A values of all the investigated samples are tabulated in Table 4.2. The increase of d_{100}^A indicates an increasing thickness of the alkyl nanodomains with increasing side chain length as commonly found in comb-like polymers showing nanophase separation [15, 20, 21, 125]. The obtained layer spacings d_{100}^A (Table 4.2) are comparable to the experimental values determined by Ballauff et al. [11] for modification A of PPAOTs. This comparison is graphically shown in Figure 4.3.b in which the layer spacings d_{100}^A are plotted together with data from Ballauff et al. [11]for PPAOTs with different number of carbon atoms per alkoxy chain (n). The slope, (1.13 Å per additional carbon atom in the side chain) obtained through linear fitting, is lower to that what is expected for fully interdigitating alkoxy side chains in all trans conformation (1.25 Å per additional carbon atom in the side chain). The extrapolated intercept for PPAOTs corresponding to the space required for the main chain ($d_{mc} = 6.7$ Å) is larger than that given by Ballauff et al. (6.0 Å) [11]. As already mentioned above, the position of the q_{020}^A reflection is basically independent on side chain lengths. The interplanar spacing corresponding to this reflection is about 3.6 Å, which relates to the distance between the aromatic rings within the stacks of main chains ($\pi - \pi$ stacking). Note that an additional peak q_{xxx} at $q \approx 5.3 \ nm^{-1}$ is also clearly seen in the diffraction data for all PPAOTs. Whether or not the related spacing of about 11.9 Å corresponds to the true periodicity in main chain direction remained open but was one possible interpretation of this peak since the difference related to literature values [26, 126] of 12.6 Å is moderate (about 6%). However, further studies on oriented samples are needed to support this interpretation. The results will be discussed in the next part of this subsection.

To ascertain a lattice model for modification A of PPAOTs, it is important to understand whether the (xxx) reflection represents indeed the periodicity between the neighbored alkyl groups along the polymer backbone. For this, extruded fibers were prepared at different shear rates and temperatures for the PPDOT member of the PPAOT series using the ram extrusion setup described in the section 3.1.3. PPDOT fibers having a diameter of about $\approx$1.5 mm are prepared and measured in a 2D x-ray scattering setup at intermediate scattering angles.

The 2D scattering pattern of the PPDOT sample extruded at 120°C and a shear rate of $600s^{-1}$ is shown in Figure 4.4.a. The initial observation from Figure 4.4.a and 4.4.c is that the lamellar morphology (modification A) present prior to the ram extrusion process is preserved with almost constant inter-lamellar spacing. Further-
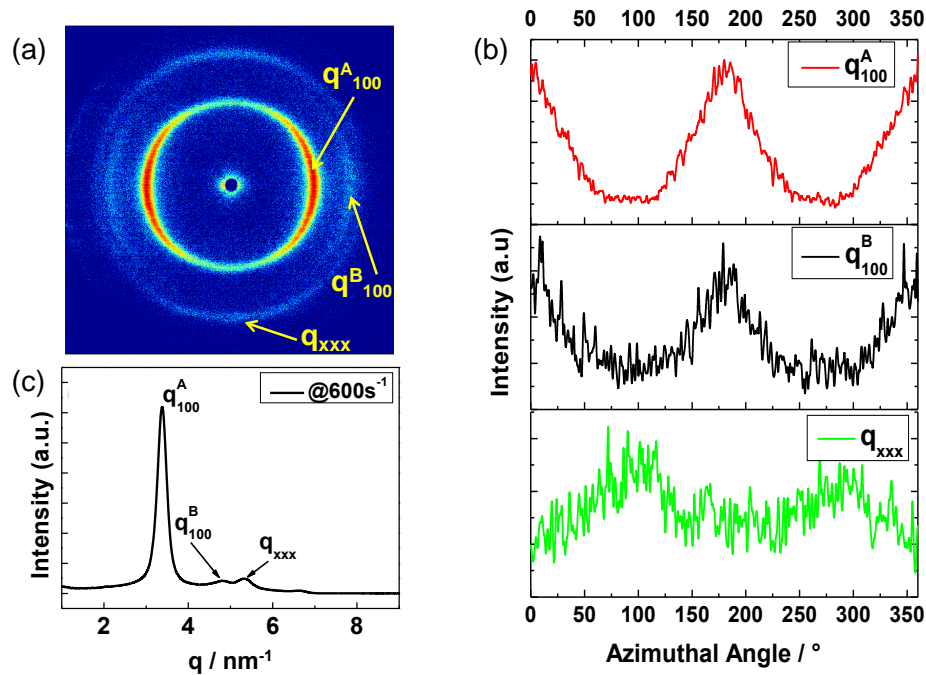
Figure 4.4: (a) 2D scattering pattern of an extruded fiber from PPDOT (n=10) fiber processed at 120°C and $600s^{-1}$. The fiber is placed such that the fiber axis (= extrusion) direction is perpendicular to the direction of incoming x-ray beam and vertical in front of the detector plane as indicated in the 2D pattern. Intensity maximum is observed at the equatorial position for the q_{100}^A reflection for modification A and modification B while meridional scattering is stronger for the q_{xxx} reflection. (b) Corresponding azimuthal plots for the q_{100}^A reflection for modification A and modification B and the q_{xxx} reflection obtained from the 2D image. (c) Integrated intensity profile over the entire q range.

more, anisotropic intensity distribution is observed with intensity maxima along the equatorial position for the q_{100}^A peak corresponding to the lamellar morphology and along the meridional position for the q_{xxx} reflection. Note that the orientation development by shearing was nearly similar irrespective of the chosen processing conditions (temperatures between 120°C, 140°C and 160°C; shear rates between $20s^{-1}$, $300s^{-1}$ and $600s^{-1}$) [127]. Interestingly, an additional weak peak corresponding to the interlamellar spacing for modification B is also observed with an orientation distribution similar to that observed for modification A. The integrated intensities over the entire azimuthal angular range (Figure 4.4.c) reveal that the maximum in the scattered intensity for the q_{100}^A reflection (for both modification A and modification B) and the q_{xxx} reflection are shifted by 90° implying that the surface normals of the respective lattice planes are orthogonal to each other. This strongly supports the interpretation that the q_{xxx} peak corresponds to the side chain to side chain distance along to backbone q_{001}^A being about 11.9 Å. This value is smaller than the spacing of about 12.5 Å reported
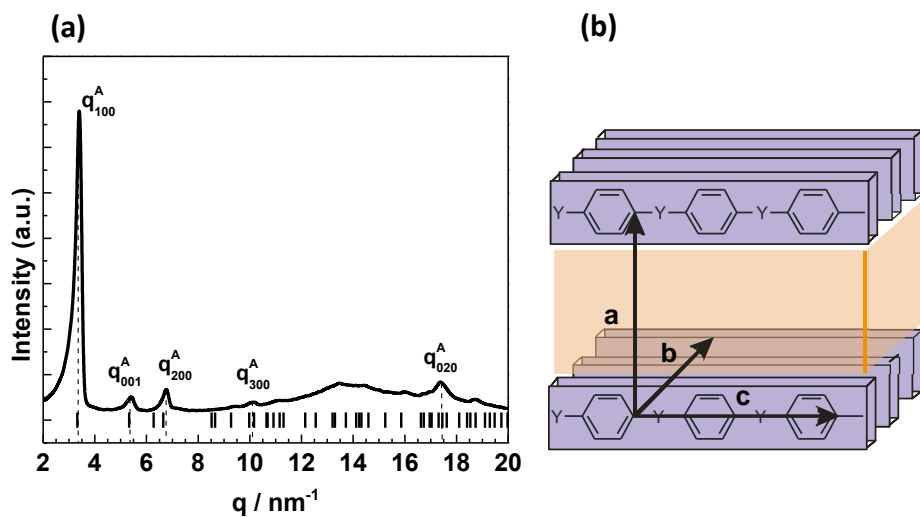
Figure 4.5: (a) Scattering pattern of a PPDOT (n=10) sample exhibiting modification A along with peak indexing based on an orthorhombic unit cell. (b) A schematic of the orthorhombic unit cell. The light orange box denotes the alkyl nanodomain whereas the lattice parameters **a**, **b** and **c** are marked.

by Ballauff et al. based on numerical simulations [26].

Based on the results obtained from the presented scattering measurements on oriented and non-oriented samples, a lattice model is established. The relevant peaks in the scattering pattern for PPDOT can be indexed using an orthorhombic unit cell with lattice parameters **a** = 1.85 nm, **b** = 0.722 nm and **c** =1.16 nm (Figure 4.5.a). The lattice parameters are calculated from the peak positions labelled as q_{100}^A, q_{020}^A and q_{001}^A corresponding to main chain-to-main chain distance, $\pi-\pi$-stacking and side chain to side chain distance along the backbone, respectively. A schematics of the unit cell structure is shown in Figure 4.5.b. The peak positions corresponding to the propsed orthorhombic unit cell are shown as vertical lines and fits well to the experimentally observed peak positions. The crystallographic density as calculated from the monomer mass M_o = 558 g/mol and the unit cell volume is 1.21 g/cm^3 for 2 monomers per unit cell.

An orthorhombic lattice is also describing the scattering pattern for the other PPAOTs quite well (Figure 4.6). Obviously, the lattice is preserved independent on side chain length. The obtained unit cell parameters are given together with the monomer masses and crystallographic densities in Table 4.2. The lattice parameters **b** and **c** are similar for all PPAOTs members whereas the **a** varies accordingly with the change of side chain length (n). Also the crystallographic densities (ρ) decreases with the
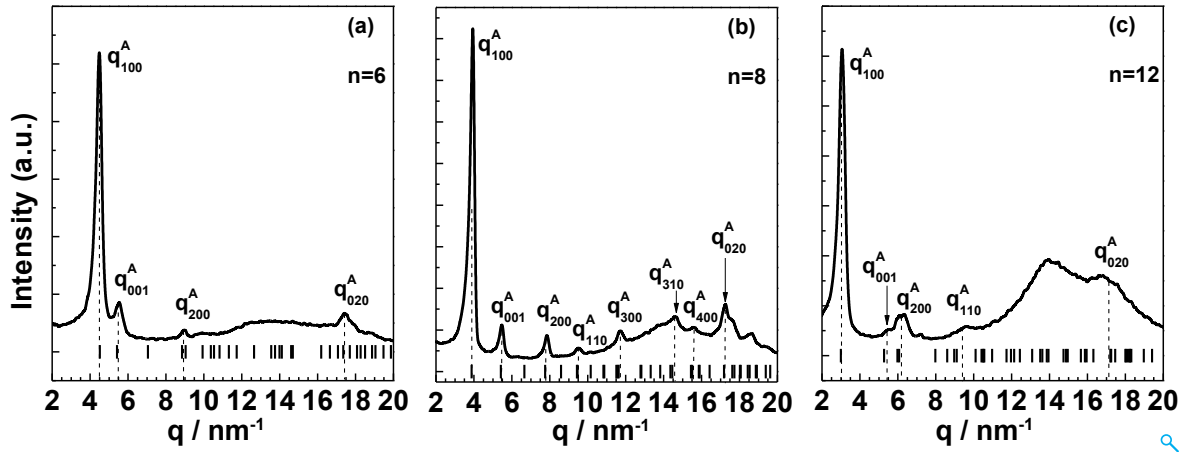
Figure 4.6: Scattering pattern of (a) PPHOT (n=6), (b) PPOOT (n=8) and (c) PPDDOT (n=12) sample exhibiting modification A along with peak indexing based on an orthorhombic unit cell.

increase of side chain length which is an indicative of side chain disordering in alkyl-nanodomains.

Formation of and lattice model for modification B. According to Ballauff et al., [11] higher members of the PPAOT series shows apart from the 'mesophase', i.e. modification A, a different packing state called modification B. This modification corresponds to a different side chain packing as compared to modification A. In this work, the higher members of the PPAOT series ($n = 10$ and 12) shows large fractions of modification B particularly after the synthesis where this modification is probably growing in the presence of solvent (Figure 4.7).

Temperature dependent x-ray scattering pattern measured during a step wise 1st heating run on as-received (as-synthesized) PPDOT and PPDDOT samples are shown in Figure 4.7.c and 4.7.d, respectively. At T = 30°C both PPDOT and PPDDOT exhibit a Bragg reflection at $q \approx 4.6$ nm^{-1} and $q \approx 4.1$ nm^{-1} respectively coming from the q_{100}^B lattice planes along with higher orders indicating a lamellar morphology. At higher temperatures a solid-solid transition is indicated for both samples, PPDOT and PPDDOT, respectively. In case of PPDOT the lamellar structure appearing low temperatures is obviously replaced by another lamellar structure during heating in the temperature interval from 80°C to 100°C. The high temperature modification is characterized by a q_{100}^A peak occurring at lower scattering values ($q \approx 3.3$ nm^{-1}). A similar transition is observed for PPDDOT in the temperature interval from 50°C to 80°C. In this case the high temperature structure is characterized by a q_{100}^A reflection
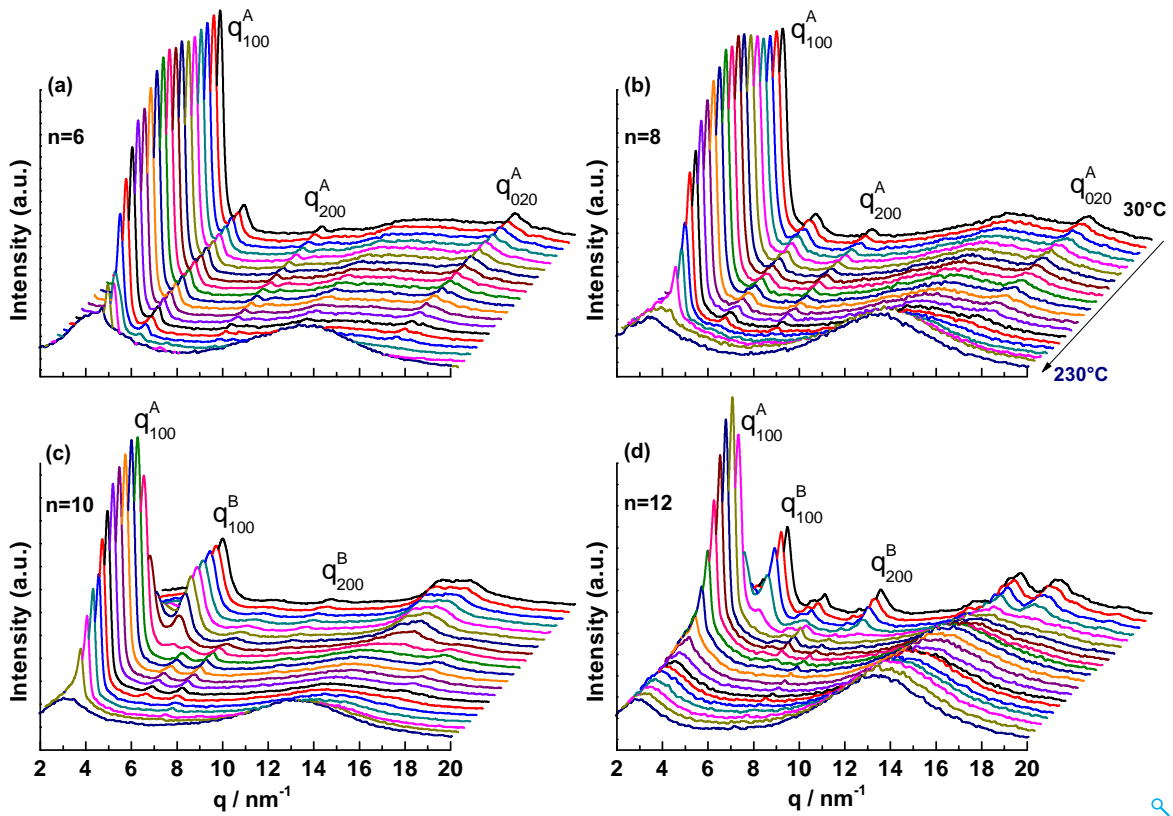
Figure 4.7: Temperature-dependent x-ray diffraction patterns for as synthesized (a) PPHOT (n=6), PPOOT (n=8), (c) PPDOT (n=10) and (d) PPDDOT (n=12) samples measured during the first heating scan (30°C to 230°C) in steps of 10°C/min. The labels are the Miller indicies for the most important scattering peaks.

at $q = 3$ nm^{-1}. Further heating to a temperature of T $= 230$°C results in both the cases in a complete loss of long range order. It should be mentioned that the lower members of the PPAOT series with $n = 6$ and 8 carbons were predominantly found to occur in modification A with no such transition observed during the heating scan (Figure 4.7.a and 4.7.b). Furthermore, the solid-solid transition during the heating run was found to be irreversible during the subsequent cooling scan for both the samples. The structure observed at room temperature after cooling is modification A, as shown before in Figure 4.1.c and 4.1.d.

A closer inspection of the scattering patterns for PPDOT (Figure 4.8) and PPDDOT (Figure 4.9) confirms that the layered structure occurring at low temperatures corresponds to modification B as reported by Ballauff et al. [11] while modification A is occurring at high temperatures. This is evidenced by the Bragg spacings d_{100}. At temperatures above the solid-solid transition, one gets 18.5 Å and 20.95 Å for PPDOT

and PPDDOT, respectively. This values are quite close to those which have been found for modification A previously (c.f. Figure 4.3 and Table 4.2). The d_{100} spacings observed at low temperature (13.6 Å for PPDOT and 15.3 Å for PPDDOT) are in good agreement with those reported for modification B (Figure 4.10) [11]. Considering the reflections in the wide angle range (12 $nm^{-1} \leq q \leq 20\ nm^{-1}$) the typical q_{020}^{A} peak expected for modification A is seen at high temperatures. Interestingly, this peak is missing at low temperatures indicating that the $\pi - \pi$ stacking is significantly changed in case of modification B. What is seen in the WAXS pattern of modification B are two pronounced peaks at 14.3 nm^{-1} and 15.2 nm^{-1} for PPDOT (Figure 4.8.b) as well as 14.3 nm^{-1} and 15.9 nm^{-1} for PPDDOT (Figure 4.9.b), receptively. Further studies by 2D scattering experiment on PPDOT reveal a 2D WAXS pattern which exhibits an intensity maximum along the equatorial position for the reflections at $q \approx 14.3\ nm^{-1}$ and $q \approx 15.2\ nm^{-1}$ with similar intensity distribution as q_{100}^{B}. According to this scattering pattern, the reflection at $q \approx 14.3\ nm^{-1}$ corresponds to stacking of the backbones (q_{020}^{B}). The Bragg spacings for all scattering peaks belonging to modification B are listed in Table 4.3.

Figure 4.8: Temperature-dependent x-ray diffraction patterns for PPDOT (n=10) measured during heating at different temperatures. A solid-solid transition is indicated by intensity changes of the peaks at (a) q_{100}^{B} to q_{100}^{A} and (b) q_{020}^{B} to q_{020}^{A} with increasing temperature.
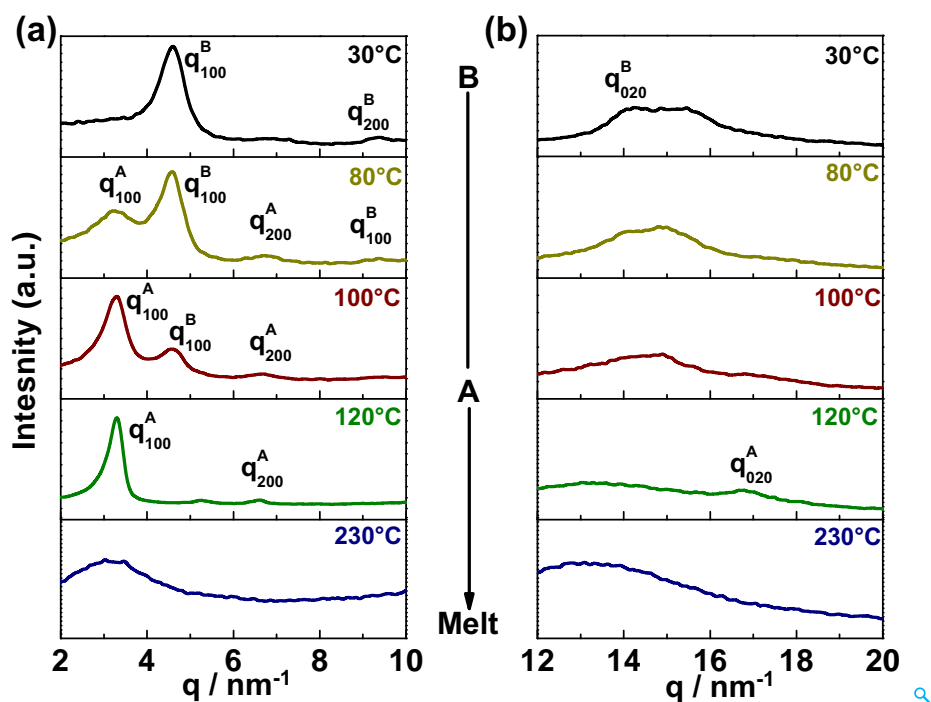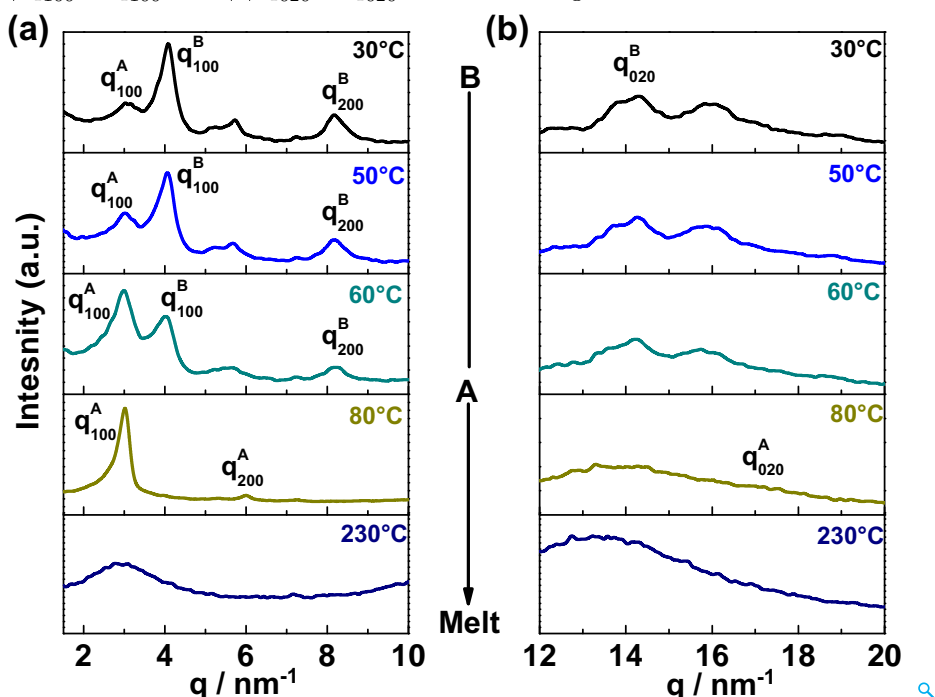

Figure 4.9: Temperature-dependent x-ray diffraction patterns for PPDDOT (n=12) measured during heating at different temperatures. A solid-solid transition is indicated by intensity changes of the peaks at (a) q_{100}^{B} to q_{100}^{A} and (b) q_{020}^{B} to q_{020}^{A} with increasing temperature.
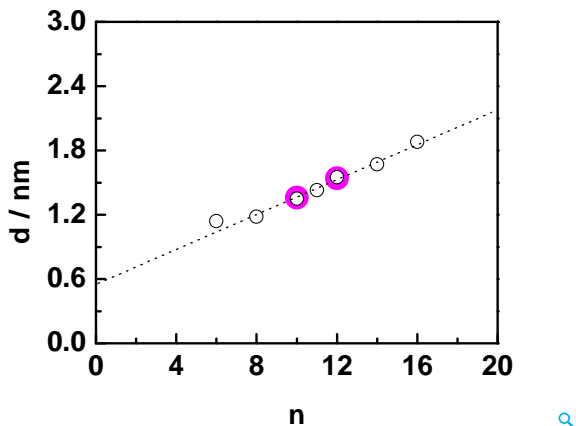
Figure 4.10: Layer spacing d $vs.$ number of carbon atoms per side chain n. d_{100} values for modification B in PPDOT (n=10) and PPDDOT (n=12) samples (full circles) are compared to those reported by Ballauff et al (open circles). [11] The intercept (dotted line) with the y-axis (n=0) corresponds to the thickness of the main chain domains (d_{mc}).

Table 4.3: Unit cell parameters, spacings and crystallographic density for modification B in PPDOT and PPDDOT

Label	n	d_{100}	d_{020}	d_{001}	**a**	**b**	**c**	M_o	ρ
		Å	Å	Å	Å	Å	Å	g/mol	g/cm^3
PPDOT	10	13.7	4.4	11.8	13.6	8.8	11.8	558	1.30
PPDDOT	12	15.4	4.4	11.9	15.4	8.8	11.9	614	1.26

Similar to modification A, an orthorhombic unit cell is describing the scattering pattern of modification B in PPDOT and PPDDOT. The scattering peaks are indexed with lattice parameters (i) **a**: 1.36 nm **b**: 0.88 nm and **c**: 1.18 nm for PPDOT (Figure 4.11.a) and (ii) **a**: 1.54 nm **b**: 0.88 nm and **c**: 1.19 nm for PPDDOT (Figure 4.11.b), respectively. The crystallographic density as calculated from the volume of the unit cell and monomer mass of 558 g/mol and 614 g/mol is 1.30 g/cm^3 and 1.26 g/cm^3 for two monomers per unit cell for 'as-received' PPDOT and PPDDOT, respectively (Table 4.3). In modification B, the reflection corresponding to the $\pi - \pi$ stacking appears at $q \approx 14.3$ nm^{-1} and is observed at lower q values as compared to modification A (Figure 4.5). It seems that the crystalline packing of side chains in modification B causes the backbones to pack differently leading to an 20% increment in the lattice parameter **b**. Note that the scattering peaks for semi-crystalline alkyl side groups often occur at $q \approx 15$ nm^{-1} for comb-like polymers with disordered backbones like atactic poly (n-octadecyl methacrylate) corresponding to the hexagonal packing of the alkyl groups [128]. Such hexagonal packing in the alkyl nanodomain has also been reported
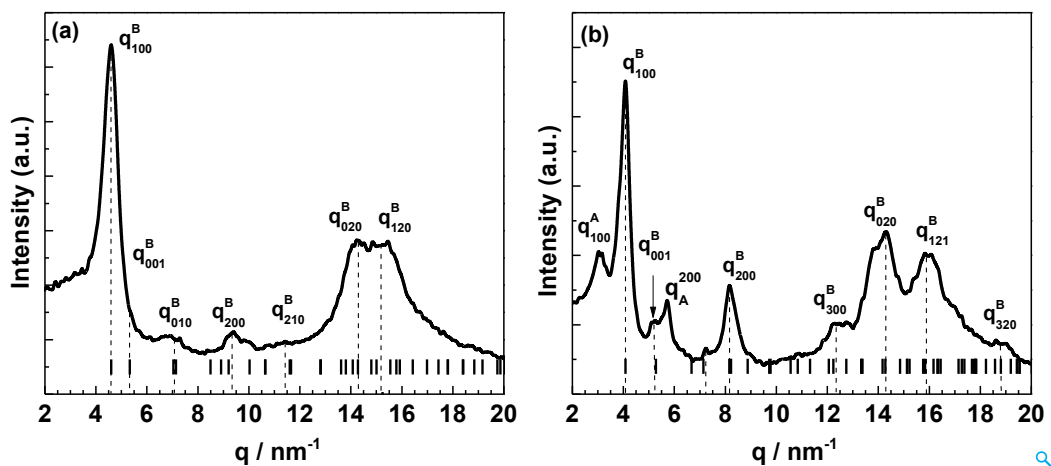
Figure 4.11: Scattering pattern of 'as-received' (a) PPDOT (n=10) and (b) PPDDOT (n=12) samples exhibiting higher fractions of modification B along with peak indexing based on an orthorhombic unit cell.

in the case of polyethyleneimines with short side chains (14 to 18 CH_2 units) [129].

So far modification B is only seen in 'as-received' PPDOT and PPDDOT in which it is transformed to modification A during heating (Figure 4.7). This transition is an irreversible process as modification B cannot be obtained by cooling from melt (Figure 4.1). However, various techniques have been reported in literature for the preparation of modification B. Dammann et al suggested two different routes for the preparation of modification B in PPDDOT ($n = 12$) [130, 131]. According to them modification B of PPDDOT can be achieved from samples containing modification A either by (i) a treatment with methanol and/or (ii) long time storage under ambient conditions. Here both methods were used to study the solid-solid transition from modification A to modification B in PPDOT ($n = 10$) as a representative example. In case of method (i), a PPDOT sample was treated according to the thermal program presented in Figure 4.2 giving a sample containing practically only modification A which is then soaked in a methanol bath for about two weeks at room temperature. Further, samples stored under ambient conditions for different times up to three years according to method (ii) are investigated. Samples prepared by both methods were analyzed using x-ray scattering technique.

X-ray diffraction pattern for differently treated PPDOT samples are shown in Figure 4.12, tiny fraction of modification B indicated by a weak reflection at q_{100}^B is observed for both, the long-time stored sample as well as in the methanol treated sample. This
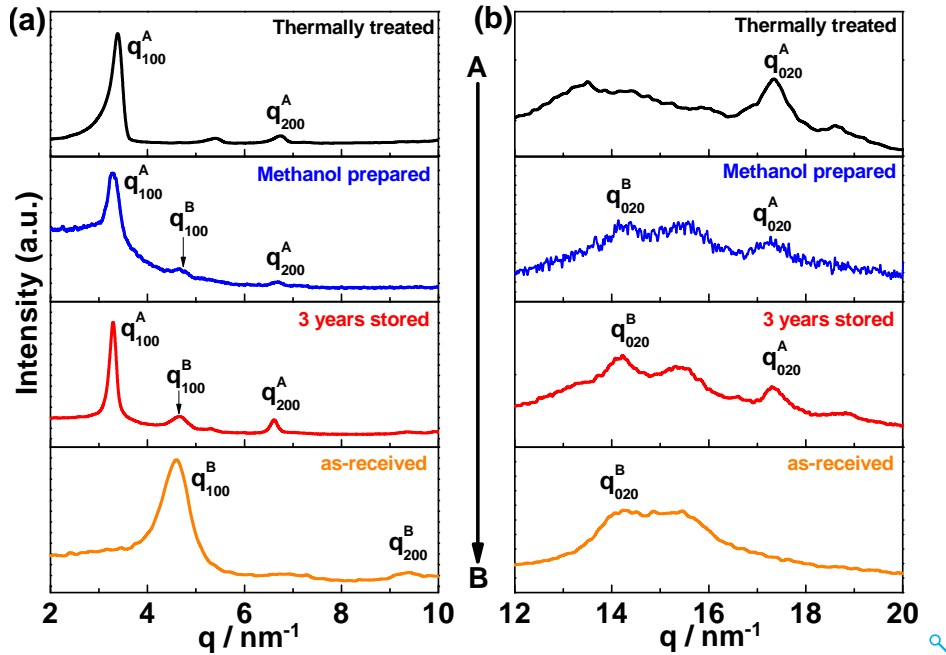
Figure 4.12: Comparison of XRD pattern in the (a) intermediate and (b) wide angle range for PPDOT (n=10) measured after different treatments (from top to bottom: thermally treated according to the program given in Figure 4.2, stored for two weeks in methanol, stored at room temperature for 3 years and as-received. The content of modification B is increasing from the top to the bottom.

evidences, in both the cases, a partial conversion of modification A to modification B. The presence of this minute fraction of modification B suggests that the packing state is at least partially influenced by the solvent or long term storage. The observed transition from modification A to modification B is inline with the idea that the latter modification is thermodynamically preferred under ambient conditions. Most likely, growth of this form is kinetically hindered if a PPAOT melt is relatively fast cooled to room temperature. Hence, the so-called 'mesophase' being modification A seems to form commonly during cooling although it is not the thermodynamically stable modification below a certain solid-solid-transition temperature in the range 30°C to 70°C. On the other hand, in 'as-received' sample a very high fraction of modification B is observed as compared to the MeOH treated and long-time stored modification A samples. This can be attributed to the initial preparation of these polymers where structures will form in the pretense of large amounts of solvent along with the storage time. The scattering patterns in the wide angle range ($12 \ nm^{-1} \leq q \leq 20 \ nm^{-1}$) support in all cases that what has been concluded already from Figure 4.12. In both, MeOH treated sample and long-time stored sample, two scattering peaks are seen the in range $14 \ nm^{-1} \leq q \leq 16 \ nm^{-1}$ in addition to the q_{020}^A reflection of modification A at

$q = 17.4 \ nm^{-1}$. The presence of q_{020}^A reflection in MeOH treated and long-time stored sample corresponds to the $\pi - \pi$ stacking of the main chains as examined in thermally treated modification A, whereas, the two extra peaks are related to modification B as seen in the 'as-received' sample. This scattering pattern clearly highlights the development of modification B from modification A. From the above experiments, it can be concluded that the storage time is a crucial element for the conversion of modification A into modification B which in turn indicates the higher thermodynamic stability of modification B at ambient conditions.

4.1.2   Poly (2,5-n-dialkyloxy-1,4-phenylenevinylene)s

Structure development in AOPPVs.   Temperature-dependent x-ray diffraction data from measurements on all AOPPVs samples under investigation (n = 6 - 12) obtained during stepwise cooling from the melt are shown in Figure 4.13

At the highest temperature (T = 220°C), the scattering pattern for all the AOP-PVs samples exhibit a featureless scattering pattern in the entire scattering range corresponding to a disordered/amorphous state (except HOPPV where this fully amorphous state occurs at T ≈ 230°C). The conventional amorphous halo centered at $q \approx 13 \ nm^{-1}$ to $14 \ nm^{-1}$ and a broad pre-peak at low scattering vectors $q \approx 5 \ nm^{-1}$ are observed in this state without long range ordered structures. Nevertheless, the presence of a pronounced pre-peak indicates nanophase separation of main chain and side chains without long range order like found in many other non-crystalline comb-like polymers. As the AOPPV samples are cooled, sharp Bragg reflections begin to appear corresponding to a long range ordered state. Main features of the scattering patterns are qualitatively similar for all investigated samples independent on side chain lengths. The presence of a reflection at q_{100}^B in the range $2.6 \ nm^{-1}$ to $4.2 \ nm^{-1}$ along with higher orders at q_{200}^B and q_{300}^B evidences the existence a lamellar morphology arising from alternating main and side chain domains like in PPAOTs. The reflection at $q_{020}^B \approx 15.8 \ nm^{-1}$ is due to the $\pi - \pi$ stacking of the aromatic rings within the main chain domains. This has been concluded by Nagamatsu et al. in an earlier paper [18] from studies on an oriented OOPPV (n = 8) sample and will be demonstrated based on own data for oriented DOPPV (n = 10) in more detail below. Interestingly, the q_{020}^B reflection appears during cooling also in the AOPPVs series commonly at a lower temperature as compared to the q_{100}^B reflection. The onset temperatures where both Bragg peaks set in during cooling, $T_{on,100}$ and $T_{on,020}$, are given in Table 4.4.
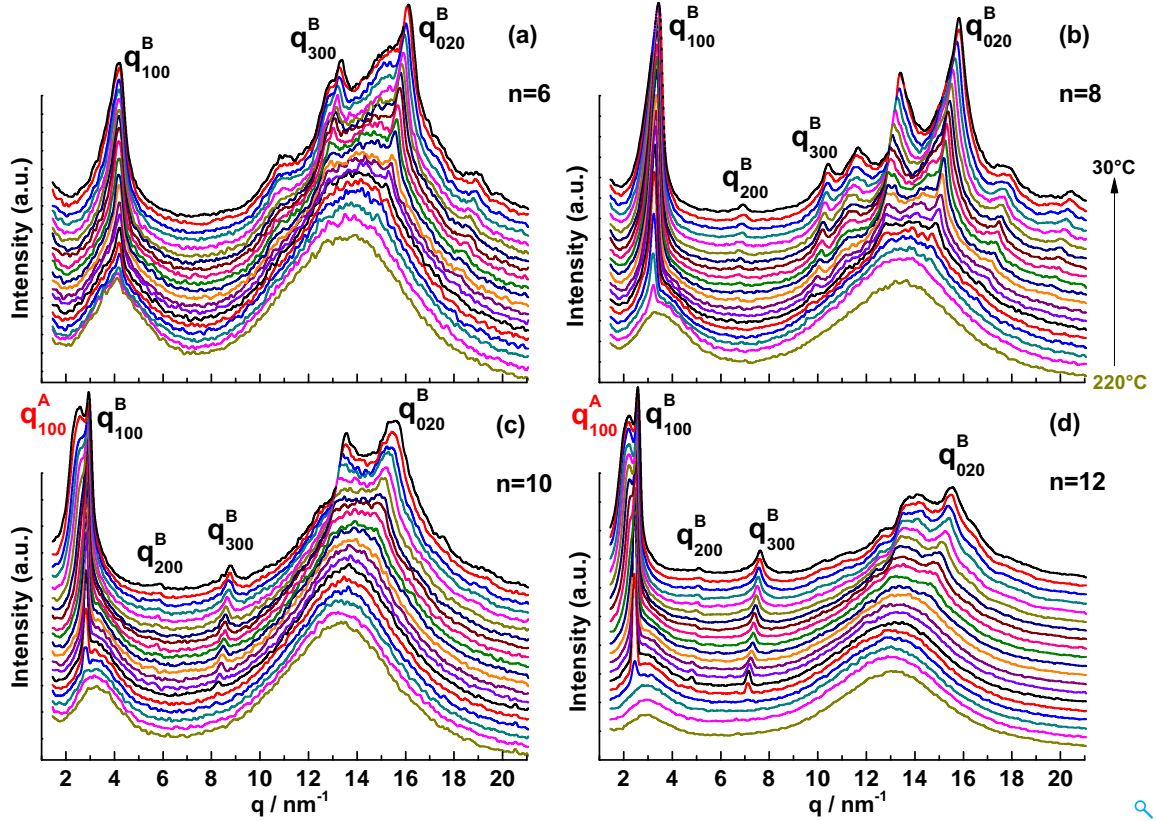
Figure 4.13: Temperature-dependent x-ray diffraction data patterns for (a) HOPPV (n=6), (b) OOPPV (n=8), (c) DOPPV (n=10) and (d) DDOPPV (n=12) measured during the first cooling scan (220°C to 30°C) in steps of 10°C/min. The labels indicate the Miller indicies for the most important scattering peaks.

Table 4.4: Crystallization temperatures for AOPPV samples (* onset temperatures where (100) and (020) reflection peaks start to develop)

Label	n	$T_{on,100*}$	$T_{on,020*}$
		°C	°C
HOPPV	6	220	170
OOPPV	8	210	170
DOPPV	10	190	110
DDOPPV	12	190	110

Like in PPAOTs, the $T_{on,020}$ values are commonly $\approx 40 - 80$°C lower that $T_{on,100}$. This indicates possibly that a liquid-crystalline state without well stacked backbones in the main chain domains exists in AOPPVs between $T_{on,100}$ and $T_{on,020}$. A more detailed overview showing the development of q_{100}^{B} along with its higher orders and q_{020}^{B} is given for the OOPPV ($n = 8$) and DOPPV ($n = 10$) members in Figures 4.14 and

Figure 4.14: X-ray diffraction patterns for OOPPV (n=8) measured during cooling at different temperatures. (a) The reflection at q_{100}^B along with its higher orders at q_{200}^B and q_{300}^B as well as (b) the reflection at q_{020}^B do develop with decreasing temperature.

4.15. The selected curves represent the different intermediate states discussed already above. Note that the higher members of the AOPPVs series -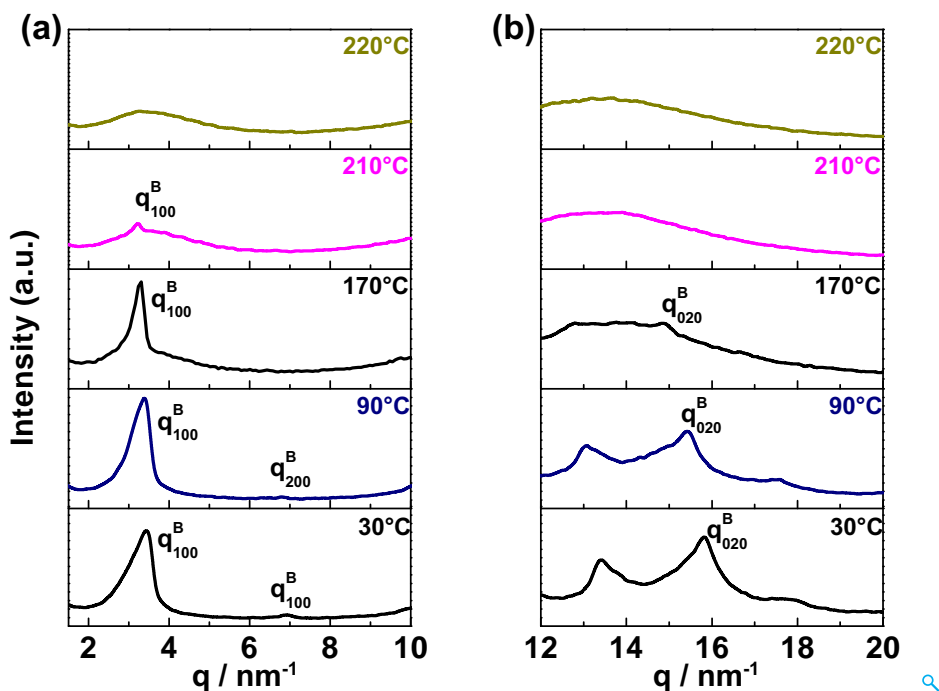 DOPPV ($n = 10$) and DDOPPV ($n = 12$) - exhibit an additional peak at low scattering vectors at about 2.5 nm^{-1} and 2.1 nm^{-1}, respectively (Figure 4.13.c and 4.13.d). This reflection occurs at scattering vectors lower than q_{100}^B and develops at temperatures below 100°C. This Bragg peak indicates the presence of another crystallographic modification in AOPPVs that occurs preferentially at low temperatures and has a lower packing density. This structural feature will be discussed in more detail at the end of this section.

Lattice model for modification B. X-ray diffraction patterns for all investigated AOPPVs measured at room temperature after cooling are compared in Figure 4.16.a. As already discussed above, the main features are related to a layered structure which is called modification B here since it has a high packing density of the side chains in analogy to modification B in PPAOTs as shown in detail below. Higher orders to the narrow main peak at q_{100}^B appearing at q_{200}^B and q_{300}^B are clearly visible and labeled in Figure 4.16.a. A systematic shift of the peak at q_{100}^B to lower scattering vectors q is observed with increasing lengths of the side chains (n) related to an increasing domain
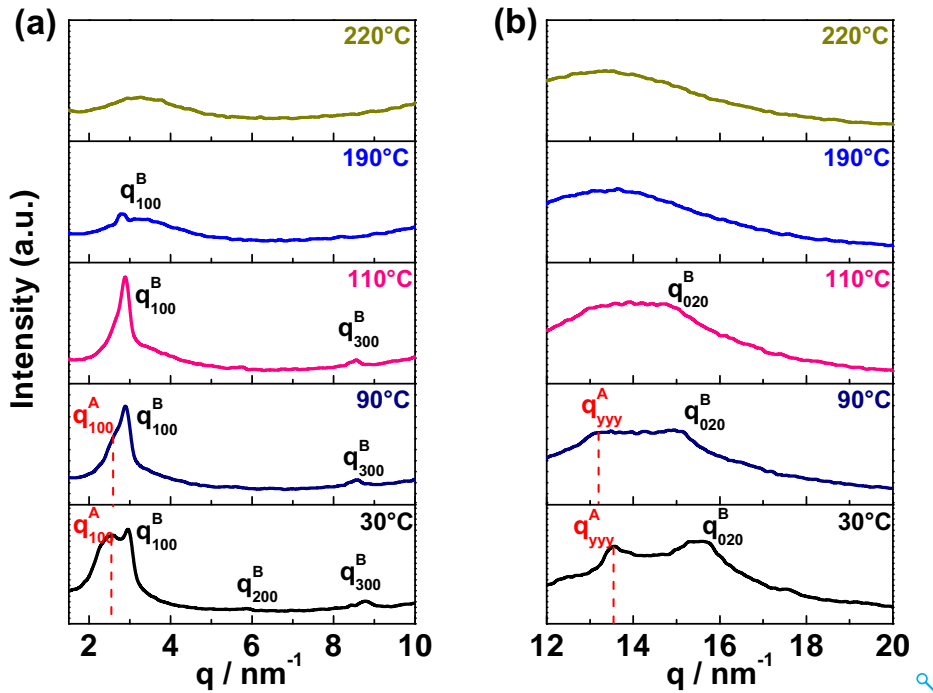
Figure 4.15: X-ray diffraction patterns for DOPPV (n=10) measured during cooling at different temperatures. (a) The reflection at q^B_{100} along with its higher orders at q^B_{200} and q^B_{300} as well as (b) the reflection at q^B_{020} do develop with decreasing temperature. An additional reflection at low q values (q^A_{100}) is observed only for temperatures below T $\approx$ 100°C.

size. The relevant Bragg spacings d^B_{100} corresponding to the lamellar morphology resulting from a periodic arrangement of nanodomains containing aggregated side chains and stacked aromatic rings are plotted in Figure 4.16.b. This plot shows a practically linear increase of d^B_{100} with side chain length n. The slope obtained from a linear fit is about 1.5 Å per additional carbon atom in the side chain. This slope is larger than that what is expected for fully interdigitating side chains in all trans conformation (1.25 Å per additional carbon-atom in the side chain). The extrapolated value at n = 0, which corresponds to the space required for the main chain, is d_{mc} = 5.4 Å. The position of the peak at q^B_{020} is obviously for all samples nearly identical $\approx$ 15.8 nm^{-1} (Figure 4.16), i.e., the $\pi - \pi$ stacking distances is basically independent on side chain lengths. The corresponding Bragg spacings d^B_{020} are in the range of about 4 Å and are listed together with all other relevant spacings (d^B_{100}) in Table 4.5.

Based on the obtained information about d^B_{100} and d^B_{020} as well as literature information about d^B_{001} a lattice model was established. The predictions of different lattice models were compared with the experimentally obtained scattering pattern at room temperature (after cooling from the melt state) in order to refine the unit cell parame-
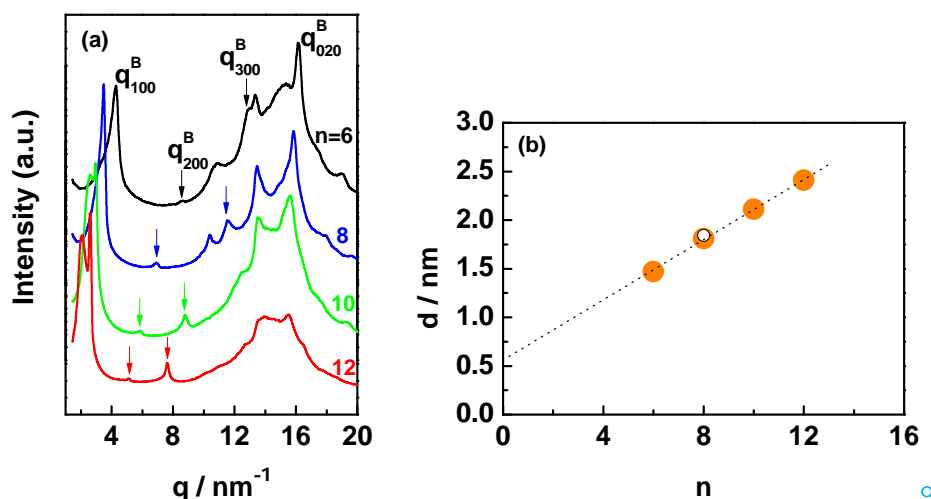
Figure 4.16: (a) X-ray diffraction patterns for HOPPV (n=6), OOPPV (n=8), DOPPV (n=10), and DDOPPV (n=12) of modification B measured at room temperature (after cooling the melt). Position and Miller indicies of the most important scattering peaks are indicted. (b) Layer spacing d_{100}^B vs. number of carbon atoms per side chain n (full circles). The d_{100} value for OOPPV from the literature is given for comparison (open circle). [27] The dotted line is a fit to the experimental data. The extrapolated spacing at n=0 corresponds to the thickness of the main chain domains (d_{mc}).

Table 4.5: Unit cell parameters, spacings and crystallographic density for AOPPVs

Label	n	d_{100}	d_{020}	d_{001}	d_{alkyl}^a	**a**	**b**	**c**	M_o	ρ	γ
		Å	Å	Å	Å	Å	Å	Å	g/mol	g/cm^3	
HOPPV	6	14.7	3.89	6.4	9.3	14.6	7.8	6.4	302	1.36	95°
OOPPV	8	18.1	3.96	6.4	12.7	18.2	7.9	6.4	358	1.29	95°
DOPPV	10	21.2	4.02	6.4	15.7	21.3	8.0	6.4	414	1.26	95°
DDOPPV	12	24.2	4.04	6.4	18.7	24.3	8.1	6.4	470	1.24	95°

^{a} $d_{alkyl} = d_{100} - d_{mc}$

ters. An optimal agreement between lattice model and experimental data for AOPPVs is commonly achieved using a monoclinic unit cell.

Figure 4.17 shows the x-ray diffraction pattern of the octyl member (n=8) of the AOPPV series indexed using a monoclinic unit cell as a representative example. The expected peak positions corresponding to the chosen unit cell are marked by (black) vertical lines and fit the data well. The lattice parameters used are **a** = 1.82 nm, **b** = 0.79 nm, **c** = 0.64 nm and γ = 95°. The crystallographic density, as calculated from the unit cell parameters and the monomer mass, is 1.29 g/cm^3 for 2 monomers per unit cell. For the unit cell fit, the shoulder at $q \approx 9.9$ nm^{-1} is chosen as q_{001}^B reflection is associated with the side chain to side chain distance along the backbone in agreement
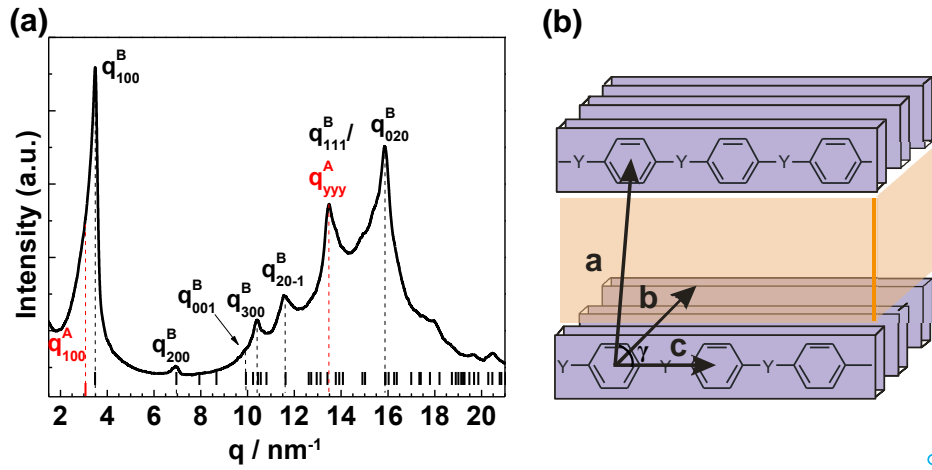
Figure 4.17: (a) Scattering pattern of a OOPPV (n=8) sample with peak indexing using a monoclinic unit cell. (b) A schematic of the monoclinic unit cell. The light orange box denotes the alkyl nanodomain. The lattice parameters **a**, **b** and **c** are labeled.

with the value reported for OOPPV in Ref. [18]. The proposed unit cell structure is schematically shown in Figure 4.17.b.

A similar unit cell was successfully used to fit the scattering pattern for other members of the AOPPV series (Figure 4.18). Obviously, a monoclinic lattice model is applicable independent on side chain length. The obtained unit cell parameters are given together with the monomer masses and crystallographic densities in Table 4.5. The lattice parameters **b**, **c** and γ are similar for all AOPPVs whereas the **a** varies systematically with the side chain length (n). The crystallographic densities (ρ) are comparable with those obtained for modification B of PPAOTs. This is is a first indication for a dense packing of side chains within the alkyl nanodomains. On the other hand, modification B in AOPPVs shows similarities with modification B in PPAOTs regarding the crystallographic densities. This will be discussed in more detail in Section 5.1.

In order to check the proposed lattice model a ram extruded DOPPV ($n = 10$) fiber has been prepared at T = 70°C with a shear rate of 30 mm/min. 2D scattering patterns for the DOPPV fiber measured at room temperature in the intermediate and wide angle scattering range are shown in Figure 4.19. Measurements in a geometry where the x-ray beam is perpendicular to the fiber axis show for the q_{100}^{B} reflection an anisotropic intensity distribution with intensity maxima along the equatorial position. The (100) lattice planes are nearly perpendicular to the (020) lattice planes of modification B
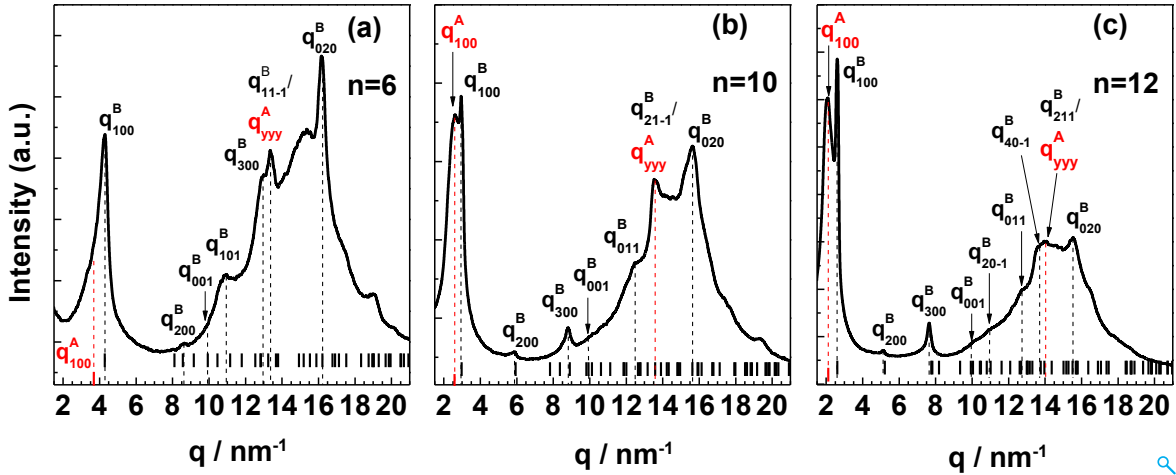
Figure 4.18: Scattering pattern of (a) HOPPV (n=6), (b) DOPPV (n=10) and (c) DDOPPV (n=12) sample exhibiting modification B (black) along with peak indexing based on a monoclinic unit cell. Bragg reflections corresponding to Modification A (q_{100}^A) are shown for comparison.

related to the reflection at $q \approx 15.8 \ nm^{-1}$ showing mainly scattering intensity in meridional direction. This observations fit well to the expected angle of 95° between the surface normals describing $\pi - \pi$ stacking (020) and lamellar morphology (100) in case of modification B. A similar orientation between both reflections was also observed in shear oriented thin films for the octyl member of the AOPPV [18]. This confirms main predictions of the derived monoclinic lattice model. An interesting finding is that the backbones are majorly oriented perpendicular to the fiber axis in case of DOPPV while they are basically parallel to the fiber axis in PPOOT.

Indications for modification A. It has been mentioned earlier that the higher members (DOPPV, $n = 10$ and DDOPPV, $n = 12$) of the investigated AOPPV series show an additional reflection centered at scattering vectors smaller than q_{100}^B. This reflection behaves like a q_{100}^A reflection in case of PPAOTs. Hence, it is assumed that this reflection corresponds to another polymorphic state in higher AOPPVs similar to modification A in PPAOTs. The additional peak at low q values in DOPPV and DDOPPV is therefore associated to a q_{100}^A peak belonging to modification A. This idea is further supported by the fact that the orientation of this peak at q_{100}^A is also identical to that of the (100) reflection belonging to modification B in case of an extruded DOPPVs fiber (Figure 4.19). Although, such a q_{100}^A reflection is not observed for the lower members of the AOPPVs series ($n = 6$ and 8), the asymmetric peak shape may suggests that it is only hidden under the wing of the reflection at q_{100}^B (Figure 4.14). A main difference compared to modification A in PPAOTs is, however, that higher orders
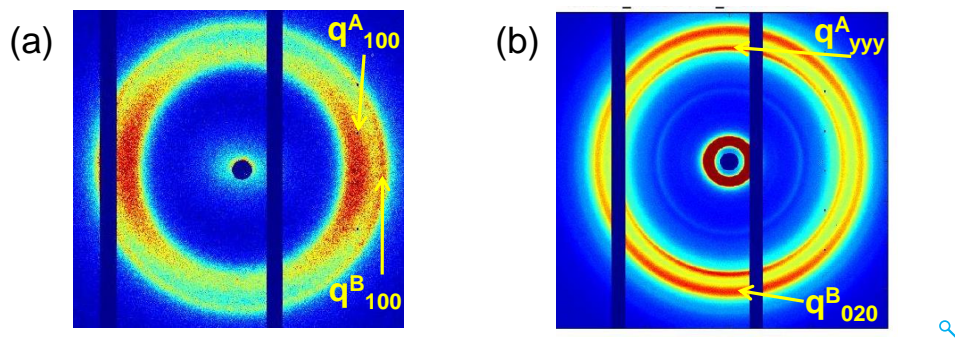
Figure 4.19: 2D x-ray scattering pattern of an extruded DOPPV (n=10) fiber measured in the (a) intermediate and (b) wide angle range. The fiber axis is placed perpendicular to the direction of incoming x-ray beam parallel to the detector plane in vertical direction. The labels indicate the position of the relevant scattering peaks. Vertical dark blue bars are blind area of detector.

to the reflection at q_{100}^A do not appear. Note that the peak at q_{100}^A is a bit broader compared to the (100) reflection of modification B (Figure 4.18) indicating a reduced long range order. The coherence lengths as calculated from the peak width of the peaks at q_{100}^A and q_{100}^B using the Scherrer equation ($d_c = K\lambda/(w.cos\theta_{max})$) are 7.5 nm and 30.5 nm for modification A and modification B of DOPPV, respectively. The corresponding values for DDOPPV are 9.97 nm and 34.7 nm, i.e., the coherence length for modification B is in both cases 3-4 times larger than that of modification A. Another difference compared to PPAOTs is that thermal stability ranges of modification A and modification B are seemingly exchanged. Modification A forms at high temperatures in higher PPAOTs while modification B appears only at low temperatures. The situation is inverted in higher AOPPVs.

Considering that the peak at q_{100}^A indicates the existence of modification A in DOPPV and DDOPPV the question arises whether or not there are additional reflections in the WAXS range belonging to this structure. Potential candidate is here in particular the Bragg peak at ≈ 13.6 nm^{-1} labeled as q_{yyy}^A in Figure 4.18. Speculatively this peak is related to $\pi - \pi$ stacking (q_{020}^A) for modification A. The corresponding Bragg spacing would be then ≈ 4.6 Å. Possible arguments for this interpretation are listed below.

1. The peak at q_{yyy}^A is oriented like the q_{020}^B reflection nearly orthogonal to that at q_{100}^A (Figure 4.19). Note that there are no peaks of modification B close to ≈ 13.6 nm^{-1} where such an orientation would be expected.

2. The commonly larger peak width of the peaks at q_{yyy}^A and q_{100}^A indicating a small

coherence length in both directions (Figure 4.18).

3. The temperature dependence of the peaks at q_{yyy}^A and q_{100}^A is quite similar. Both peaks appear below 100°C, i.e., at lower temperatures compared to other reflections in the WAXS range belonging to modification B (Figure 4.13).

The arguments given above support the assumption that the peak at $q_{yyy}^A \approx 13.6\,nm^{-1}$ can be understood as q_{020}^A reflection in higher AOPPVs. Although it is seems to be clear that a second polymorphic state similar to modification A in PPAOTs is observed in higher AOPPVs, many details are open yet. In particular, the evaluation of the crystallographic structure of this polymorphic state needs further investigations. Very helpful would be oriented samples containing large fractions of modification A without modification B crystals.

4.2 Relaxation spectroscopy of alkyl side chains in rigid main chain polymers

In this section, the results obtained from dynamic shear and broadband dielectric spectroscopy measurements on a series of PPAOTs are presented. Thermally treated PPAOT samples containing a large fraction of modification A, which do not change their structure significantly in the temperature interval of interest, are used. Special focus of the work presented in section is a deeper understanding of the main factors influencing the cooperative side chain dynamics (α_{PE} process) in the self-assembled alkyl nanodomains of long-range ordered PPAOTs.

Dynamic shear measurements. Temperature dependent shear loss modulus G″(T) data for different PPAOTs measured at frequencies ranging from 0.1 to 100 rad/s are shown in Figure 4.20. Two prominent relaxation processes are detected. At low temperatures between -125°C and -30°C, a strong relaxation process appears in all the investigated PPAOTs. This process occurs at temperatures below the conventional α relaxation and takes place in the similar temperature-frequency range where the α_{PE} process (polyethylene-like glass transition) has been found for long-range ordered rreg P3ATs [21] and for other fully amorphous nanophase-separated side chain polymers with $n = 6$ to 12 alkyl carbons in the side chain [15]. This α_{PE} process shifts to higher temperatures with increasing number of CH_2 groups per side chain. The peak maximum for a measurement frequency of 10 rad/s as approximated by Gaussian fits

69
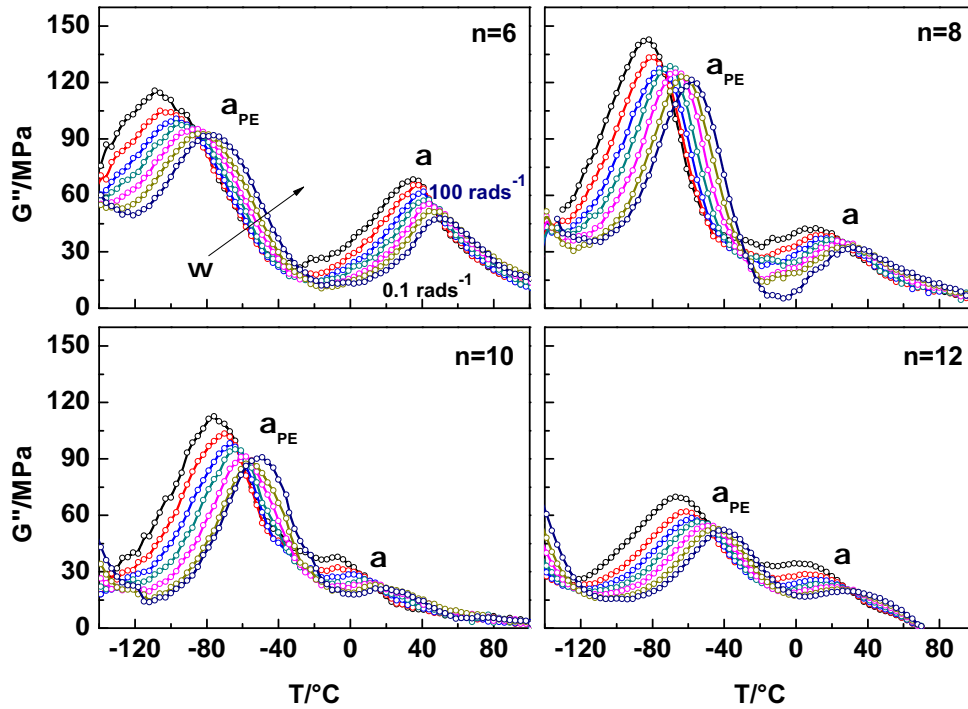
Figure 4.20: Shear loss modulus G″ of PPAOTs *vs.* temperature (T). The two relaxation processes, α and α_{PE}, are indicated. The labels indicate the number of alkyl carbons per side chain (n). The measurement frequency (ω) is 0.1 to 100 rad/s.

appears at about -91°C for PPHOT ($n = 6$) and approaches -50°C for PPDDOT ($n = 12$). Accordingly, the α_{PE} process is interpreted as dynamics of CH$_2$ groups within amorphous alkyl nanodomains [15]. The existence of an α_{PE} process with relatively large intensity supports the idea that the alkyl side groups in the investigated PPAOTs remain disordered although a lamellar long range order exists. However, at higher temperatures (between -10°C and 80°C) the conventional α relaxation process of amorphous PPAOT chain segments is observed which shifts to the lower temperatures with increasing methylene units in the side chains. This relaxation process indicates the cooperative dynamics of entire monomeric units in the amorphous fraction of our PPAOTs. The relaxation strength of the α process is expectedly weak compared to other relaxation processes in the shear curves since a large fraction of the main chains in PPAOTs is incorporated in 'main chain stacks' where the rings are packed in a crystal-like manner. The α peak maximum in G″(T) taken from a Gaussian fit appears at 10 rad/s at about 45°C for PPHOT ($n = 6$) and approaches 11°C for PPDOT ($n = 10$). This decrease in the α relaxation temperature with side chain length is well known for fully amorphous comb-like polymers like poly(n-alkyl methacrylates) and has been
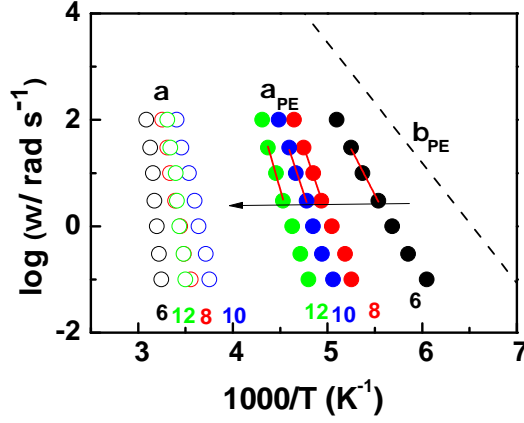
Figure 4.21: Arrhenius plot log ω vs 1000/T for PPHOT (n=6), PPOOT (n=8), PPDOT (n=10) and PPDDOT (n=12). The maxima for α process (open circles) and the α_{PE} relaxation process (full circles) taken from the G″ isochrones measured at different frequencies are given. The dotted line corresponds to the β_{PE} process in poly(n-alkyl acrylates) with very short side chains [15] showing an Arrhenius-like temperature dependence. The slopes used for the determination of $m_{\alpha_{PE}}$ are shown as short solid lines.

discussed as a consequence of internal plasticization effects caused by highly mobile alkyl side groups [12]. Interestingly, this trend is not continued for PPDDOT ($n = 12$) showing no clear decrease of the relaxation temperature but eventually even a slight increase compared to the PPDOT member. Note that very long alkyl groups with $n > 12$ alkyl carbons normally crystallize even in comb-like polymers where the backbones are not able to pack on a regular lattice since they are mobile and flexible enough to crystallize away from the backbones [132]. A similar effect may exist in higher PPAOTs and might be also important for the slight upwards shift of the α relaxation temperature in case of PPDDOT.

Table 4.6: Characteristic parameters for PPAOTs obtained from DMA (* measurement frequency $\omega = 10$ rad/s)

Label	n	T_α*	$T_{\alpha_{PE}}$*	$m_{\alpha_{PE}}$
		°C	°C	
PPHOT	6	45	-91	19.0
PPOOT	8	25	-67	25.6
PPDOT	10	11	-58	25.1
PPDDOT	12	19	-50	27.9

The frequency-dependence of the position of the shear loss peaks in shear loss modulus (G″) isochrones is compared in the Arrhenius plot shown in Figure 4.21. Two

different relaxation processes are shown for PPAOTs: (a) The α relaxation occurring at higher temperatures belonging most likely to cooperative motions in the fully amorphous regions where main chain and side chains are disordered. A strong non-Arrhenius-like temperature dependence is observed which can be quantified with an VFT equation (Eq.2.2). The α process shifts consistently to lower temperatures with increasing side chain length for $n = 6$ to 10 alkyl carbons. This shift is related according to the discussion in the literature to an 'internal plasticization' of the main chains by surrounding alkyl groups as discussed by Heijboer for poly(n-alkyl methacrylates) [12]. The behavior of the PPDDOT ($n = 12$) sample, however, is not in line with this phenomenological interpretation and shows an inverted trend. Similar effects are at least indicated in other homologous series for $n > 12$ and normally discussed as a consequence of crystallization of CH_2 units far away from the backbone. (b) The α_{PE} relaxation process appears at low temperatures and is related to an independent dynamics of CH_2 units within amorphous alkyl nanodomains being obviously relatively independent on the state of the neighbored main chains. The relaxation temperatures of the α_{PE} process shift systematically to higher temperatures if the number of alkyl carbons per side chain n increases like observed for other polymers with comb-like architecture [15, 21, 132]. Additionally, a non-Arrhenius like behavior is observed for all investigated PPAOTs. This is indicated by an increasing deviation from the line representing the Arrhenius-like temperature dependence of the β_{PE} process in Figure 4.21. This deviation from Arrhenius behavior can be also quantified using the steepness index $m_{\alpha_{PE}}$ which can be calculated based on the slope of the α_{PE} trace in the Arrhenius plot taken at $\omega = 10$ rad/s according to [80]

$$m_{\alpha_{PE}} = -dlog\omega/d(T_{\alpha_{PE},10rad/s}/T)|_{T=T_{\alpha_{PE},10rad/s}}. \tag{4.1}$$

The obtained $m_{\alpha_{PE}}$ values for the series increase systematically with the increasing number of methylene units per side chain (with slight variation in $n = 10$) indicating non-Arrhenius like behavior in PPAOTs (Table 4.6). Note that $m_{\alpha_{PE}}$ values larger than 13 indicate non-Arrhenius-like behavior. Values of about 13 are expected for secondary relaxation processes (Johari- Goldstein relaxations [74]) in glass forming materials showing Arrhenius-like temperature dependence. Higher values as obtained for PPAOTs with longer side chains indicate that the underlying motions are cooperative in nature.

Broadband dielectric spectroscopy. Dielectric spectroscopy measurements are used to obtain further information about the relaxation dynamics of poly (1,4-phenylene-
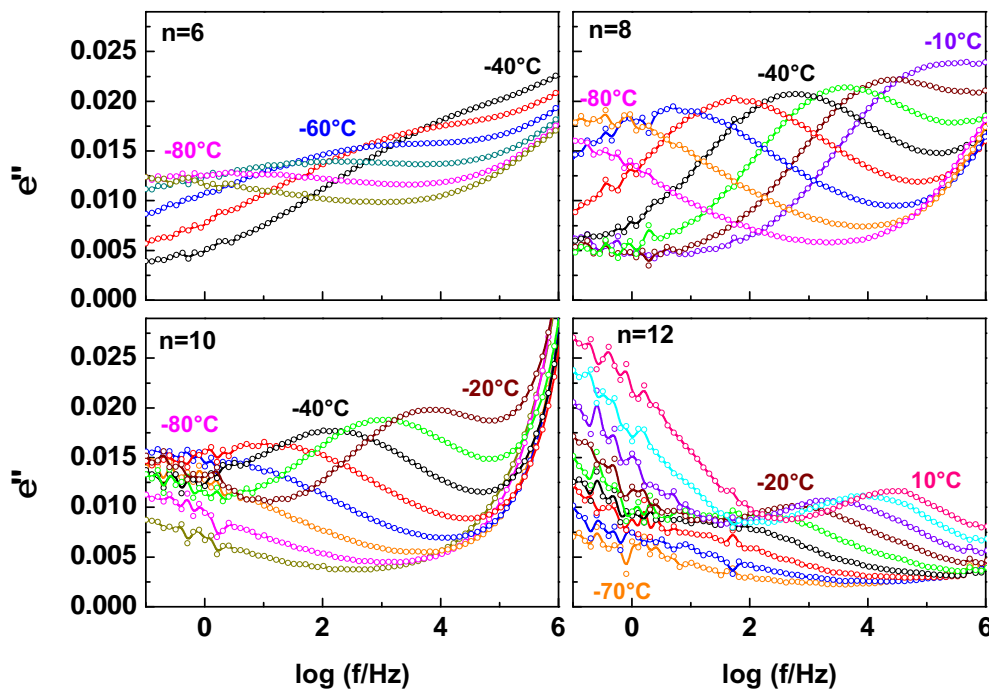
Figure 4.22: Imaginary part of dielectric function ϵ'' *vs.* frequency (log f) for PPAOTs at the measured temperature range from -90°C to 10°C. The entire data corresponds to α_{PE} relaxation process. The number of alkyl carbons per side chain (n) is indicated.

2,5-n-dialkyloxy terephthalate)s in a broad frequency range (0.03Hz to 1MHz). The frequency dependence of imaginary parts of the dielectric function (ϵ'') of PPAOTs from isothermal experiments at different temperatures between -90°C to 10°C is displayed in Figure 4.22.

The peaks appearing in ϵ'' isotherms measured at low temperatures far below the conventional T_g are related to the α_{PE} process. This process is differently pronounced depending on side chain length. In the isotherms for PPHOT ($n = 6$), there is only a weak shoulder indicating the existence of an α_{PE} process while clear peaks are seen for the PPAOTs with longer side chains due to an increasing CH_2 fraction in the samples. In general, the α_{PE} peaks in ϵ''(f) are seemingly symmetric and broad as compared to the conventional α relaxation processes observed in the other polymeric materials [119, 121, 133, 134]. The α_{PE} peak position shifts expectedly with increasing temperature towards the higher frequencies. A strong additional wing at high frequencies seen in the isotherms of PPHOT, PPOOT and PPDOT indicates the existence of an additional γ process. Interestingly, this high frequency wing is missing for PPDDOT where the conventional α process is seen at the low frequencies in the investigated temperature

Figure 4.23: Dielectric loss ϵ'' *vs.* temperature (T) for PPAOTs measured at a frequency of 1 kHz. The two relaxation processe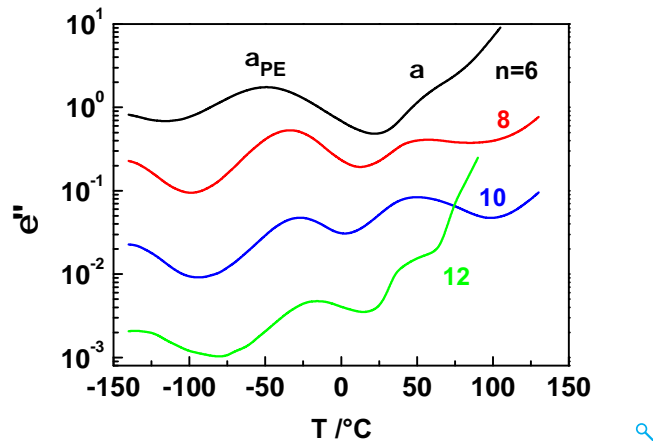s, α and α_{PE}, are indicated. The curves are vertically shifted by 1-3 decades relative to the isochrone for PPHOT (n=6). The labels indicate the number of alkyl carbons per side chain (n).

window. The latter is consistent with the finding from shear data that α and α_{PE} processes come close in PPDDOT. Note that the relaxation strength of the α_{PE} process is small in our measurements, as it is only related to the cooperative dynamics of CH_2 units in alkyl nanodomains which do not have a significant permanent dipole moment.

Beside of the dielectric isotherms, isochrones showing the dielectric loss *vs.* temperature (ϵ'' (T)) at a given frequency (e.g. 1kHz) for different PPAOTs provide additional insights (Figure 4.23). The dependence of the α and α_{PE} peak positions on side chain length is similar to those seen in related curves for the shear loss modulus G''. As expected, the α_{PE} process which is observed at lower temperatures shift towards higher temperatures while the α process seen at higher temperatures move towards lower temperatures with increasing number of methylene units per side chain n. The latter shift is due to the internal plasticization [12] as determined in other comb-like polymers [15]. Moreover, the α_{PE} peak intensity is higher as compared to α process which is qualitatively also in line to the data obtained from dynamic mechanical measurements. Besides these two relaxation processes, at high temperatures conductivity contributions are observed which strongly superimpose with the α relaxation process. In case of PPHOT ($n = 6$) the α relaxation process appears only as a weak shoulder on top of the dominating conductivity wing $\sigma/\epsilon_0\omega$ while a clear α peak is seen in other cases. In addition, at the lowest temperatures the existence of a γ relaxation process is indicated which is related to fast, extremely localized motions of small subunits.
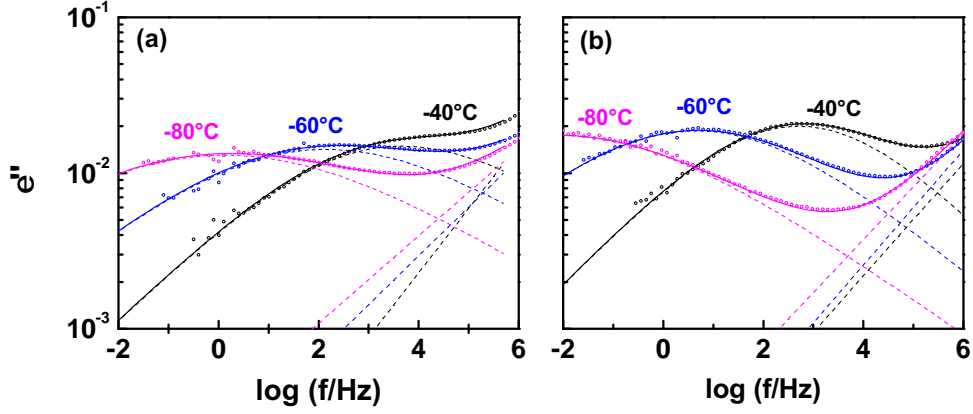
Figure 4.24: Havriliak-Negami function is used to obtain α_{PE} peak maxima (ω_{max}) for (a) PPHOT (n=6) and (b) PPOOT (n=8). Open symbols corresponds to actual data, dotted lines are two individual HN-functions and the solid line is superposition of two HN-functions.

Normally the dielectric relaxation spectroscopy data are analyzed by using model fit functions. Here, the α_{PE} process is parametrized using a fitting procedure based on Havriliak-Negami (HN) functions [121, 133]. Representative examples for such fits are shown in Figure 4.24. Main aim is to extract the α_{PE} peak maxima positions ω_{max} from the measured isotherms. The uncertainties of all HN fit parameters are not negligible as the α_{PE} process in the investigated samples is extremely broad and superimposed with other relaxation processes. A superposition of two HN functions is used to get the average relaxation frequencies (ω_{max}) for the α_{PE} process in dielectric loss isotherms. The corresponding HN fit parameters are given in Table 6.1 in the Appendix. The temperature dependence of the α_{PE} relaxation frequency ω_{max} from HN-fits is compared for all PPAOTs in the Arrhenius plot (log ω $vs.$ 1000/T) shown in Figure 4.25.

The temperature dependence of ω_{max} for the α_{PE} relaxation process are obviously well approximated by the Vogel-Tammann-Fulcher-Hesse (VFTH) equation as seen in Figure 4.21. Clear trends are observed with increasing number of alkyl carbons per side chain n. The α_{PE} relaxation process moves systematically towards higher temperature and a more pronounced non-Arrhenius-like behavior is generally observed. The later trend can be quantified based on the steepness index (or fragility) which is calculated here based on the VFTH parameters using [80,81,83]

$$m_{\alpha_{PE}} = B.T_{\alpha_{PE},10rad/s}/(T_{\alpha_{PE},10rad/s} - T_\infty)^2 \qquad (4.2)$$

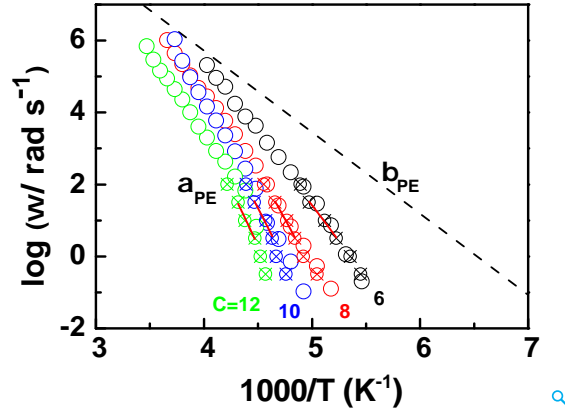where B is the curvature and T_∞ is the Vogel temperature. The obtained fragility

Figure 4.25: Arrhenius plot log ω vs 1000/T for PPHOT (n=6), PPOOT (n=8), PPDOT (n=10) and PPDDOT (n=12). Open circles correspond to α_{PE} relaxation frequencies taken from HN-fits and the open circles with cross are data for the α_{PE} relaxation process taken from isochrones measured at different frequencies ($\omega = 0.3$ - 100 rad/s). The dotted line indicates the Arrhenius-like β_{PE} process in poly(n-alkyl acrylates) with short side chains [15]. The solid lines are VFTH fits used for the determination of $m_{\alpha_{PE}}$ from dielectric data.

values, $m_{\alpha_{PE}}$, are shown in Table 4.7. A systematic increase in $m_{\alpha_{PE}}$ is obviously observed with increasing number of methylene units per side chain n.

Table 4.7: Characteristic parameters for PPAOTs obtained from BDS (* measurement frequency ω = 10 rad/s)

Label	n	$T_{\alpha_{PE}}$	B	T_{∞}	$\log\omega_o$	$m_{\alpha_{PE,VFTH}}$
		°C		°C		
PPHOT	6	-77.7	1630	-202.6	14.01	20.4
PPOOT	8	-63.4	1273	-164.2	13.58	26.2
PPDOT	10	-54.5	1229	-153.8	13.3	27.3
PPDDOT	12	-44.8	1205	-144.9	13.12	27.5

Comparison of relaxation temperatures and fragilities for the α_{PE} ***process.*** The main trends of α_{PE} relaxation processes observed in shear and dielectric measurements on PPOATs samples appearing as modification A are summarized in Figure 4.26. The trends observed in the relaxation temperature $T_{\alpha_{PE}}$ and fragility $m_{\alpha_{PE}}$ depending on side chain length are obviously independent on the experimental method and quite similar to those obtained for other polymers with comb-like architecture [20, 21]. It can be observed that the relaxation temperatures of the α_{PE} process in PPAOTs shift systematically to higher temperatures if the number of alkyl carbons per side chain n increases (Figure 4.26.a). The α_{PE} relaxation process determined from dynamic mechanical analysis at 10 rad/s for PPHOT ($n = 6$) appears at -91°C and
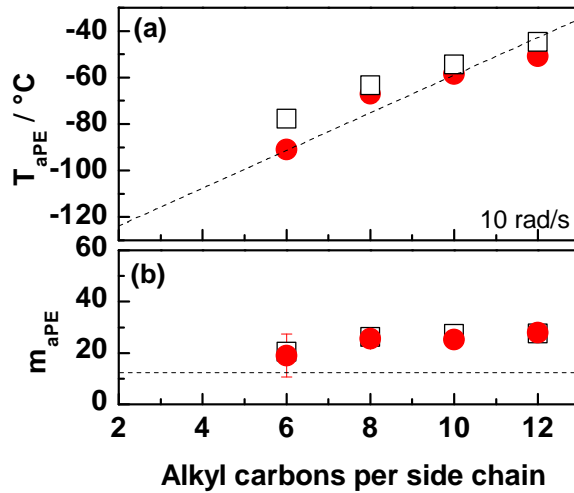
Figure 4.26: (a) Relaxation temperatures $T_{\alpha_{PE}}$ and (b) steepness indicies $m_{\alpha_{PE}}$ of the α_{PE} process of PPAOTs from DMA (full symbols) and dielectric spectroscopy (open symbols). The dotted lines in part (a) indicate the range where $T_{\alpha_{PE}}$ appears for nanophase-separated side-chain polymers [15,21]. The dashed line in part (b) is the $m_{\beta_{PE}}$ limit corresponding to an relaxation process with Arrhenius-like temperature dependence.

is shifted to -50°C for PPDDOT ($n = 12$), whereas it emerges at -78°C for PPHOT and moved to -45°C for PPDDOT when analyzed by dielectric spectroscopy. This difference between the measurements obtained from both techniques is mainly associated to the experimental method and also found in other cases. However, the trends in both cases are clearly similar. $T_{\alpha_{PE}}$ increases with increase in side chain length. The steepness index $m_{\alpha_{PE}}$ of the α_{PE} process in PPAOTs also increases with increasing side chain length as shown in Figure 4.26.b. This corresponds to a transition from Arrhenius to non-Arrhenius behavior as reported previously for P3ATs [21] and other fully amorphous polymers with comb-like architecture [15]. The estimated fragility values for higher PPAOTs correspond to that of strong glasses with a weakly but significantly non-Arrhenius temperature dependence of the relaxation frequency [80,135]. The observed trends will be further discussed and interpreted in the Discussion section (Chapter 5).

Chapter 5

Discussion

5.1 Packing states of alkyl groups in comb-like polymers

The structural analysis of PPAOTs and AOPPVs revealed presence of two different polymorphic states, namely modification A and modification B. Both modifications (modification A and B in PPAOTs and modification B in AOPPVs) are characterized by a lamellar morphology with alternating main chain and alkyl nanodomains along with stacked backbones ($\pi-\pi$ stacking). The resulting long range order within the main chain domains often determines the performance of the materials. However, of major importance for the overall structure, is the packing of the methylene sequences within the alkyl nanodomains which can vary depending on the microstructure of the rigid backbones as well as the conditions under which structure formation occurs [1, 2, 21]. Fundamental questions that arise are for example

1. What is the reason of the occurrence of different polymorphic states in comb-like polymers with rigid backbones?

2. Is the packing state of the side chains within the alkyl nanodomains driving the formation of different polymorphic states?

3. Can the packing state of the side chains be quantified? and

4. What is the influence of the packing of side chains on the packing behavior of main chains?

Various studies on comb-like polymers have been performed to determine the crystallinity and packing behavior of side chains [136–139]. A prominent example is the

discussion about the packing of alkyl groups in the extensively studied organic semi-conductor regio-regular P3HT where various models with different predictions regarding the state of the side chains have been proposed [22–25]. Typically, the crystallographic analysis is often made based on models considering interdigitation and tilting of alkyl side groups assuming that they are in a totally stretched all-trans state [22,23,25]. Whether or not this assumption is really applicable seems to be open and is controversially debated in several cases. In contrast to these often discussed packing models, an alternative approach is considered here where the average volume per CH_2 unit is used to learn more about the packing state of the side chains in different layered states of comb-like polymers. The advantage of this approach lies in the fact that it excludes presumptions of interdigitation, tilting or having the all-trans configuration for predicting the packing state of alkyl side chains.

According to the crystallographic analysis, based on a comparison of the entire X-ray diffraction patterns with appropriate lattice models and parameters for PPAOTs and AOPPVs (Table 4.2, 4.3 and 4.5), the average volume per CH_2 unit for each member of both series can be estimated based on the minimum assumptions using information about the packing of the backbones and alkyl nanodomains size according to

$$V_{CH_2} = \frac{(d_{100} - d_{mc}) \times 2d_{020} \times d_{001}}{(4 \times n)}. \tag{5.1}$$

Note that the methyl end groups (CH_3) are treated in Eq.(5.1) like methylene units (CH_2). Calculations based on Eq.5.1 require not only information about the distance between the points where the side chains are attached to the rigid backbone (d_{001}, d_{020}) but also the thickness of alkyl nanodomains $d_{alkyl} = (d_{100} - d_{mc})$ with d_{mc} being the average thickness of the main chain layers. These d_{mc} values are estimated for both investigated polymer series from a linear extrapolation of the d_{100} values observed for members with different side chain lengths and vary depending on the microstructure of the main chain (Figures 4.3.b, 4.10 and 4.16.b).

A comparison of the V_{CH_2} values calculated from scattering data for different comb-like polymers using Eq.(5.1) is presented in Figure 5.1. It is obvious that there are significant differences between different modifications and polymer series while the scatter in the values depending on side chain length is rather limited. The V_{CH_2} values for modification A of the PPAOTs as well as rreg P3ATs of about 25 to 26 Å^3 seem to be significantly larger than those of methylene units in orthorhombically packed polyethylene
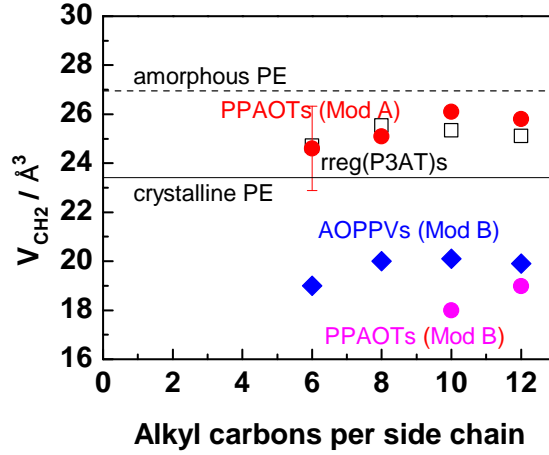
Figure 5.1: Average volume per methylene unit V_{CH_2} dependent on side chain length for rreg P3ATs (black squares) [21], PPAOTs modification A (red circles), PPAOTs modification B (magenta circles) and AOPPVs (blue diamonds). The V_{CH_2} values for amorphous polyethylene (dotted line) [140] and crystalline polyethylene (solid line) [133] are given for comparison. All values are measured under ambient conditions.

of about 23.5 Å^3 [133] and approach the values estimated for amorphous polyethylene in the amorphous state of about 27 Å^3 [140]. The question arises whether or not it is reasonable to assume that such a low density of the alkyl nanodomains is compatible with a crystalline packing of the methylene units. Further it has to be mentioned that non-crystalline side chains are also indicated by the relaxation dynamics of the CH$_2$ units in case of rreg P3ATs [21] as well as information from special 2D NMR studies in case of PPAOTs [54]. Hence, it seems to be reasonable to assume that the alkyl groups are in a more or less disordered state in these samples. Quite different behavior is observed in AOPPVs and PPAOTs for modification B, where average volumes V_{CH_2} of about 18 to 20 Å^3 are obtained for all members of AOPPVs and for $n \geq 10$ for PPAOTs. Seemingly, the packing density of the methylene sequences is significantly higher than in crystalline polyethylene or alkanes showing larger volumina per CH$_2$ unit. This seems to be a strong hint towards crystalline packing of the methylene sequences with a comparatively high density possibly due to a limited distance between neighbored side chains (in AOPPVs) and a strong interaction between neighbored, non-bonded main chains. This comparison of V_{CH_2} values allows a clear classification for different polymorphic states in different comb-like polymers. Note that the differences between the V_{CH_2} values for both modifications is quite large while the scatter depending on side chain length n is rather limited. This hints to a uniform side chain packing state for a given modification. This finding provides strong evidence for the occurrence of signifi-

cantly different packing densities of the methylene sequences in alkyl nano-domains of comb-like polymers with rigid backbones depending on the modification formed.

The occurrence of different modifications can now be successfully explained by different packing densities of the CH_2 units within the alkyl nanodomains, e.g. methylene sequences in the disordered state vs. those in the crystalline state. This approach gives more independence to the subunits - main chains containing rings and the side groups made from CH_2 units - and assumes that their packing tendency is a main driving force for the formation of different layered structures (polymorphic states) in comb-like polymers. Rigid backbones containing ring-like units tend to form $\pi - \pi$ stacks already at very high temperatures while free methylene sequences with limited length ($n \leq 12$) would form only at low temperatures crystals as equilibrium statev [141]. At high temperatures their disordered state is thermodynamically preferred. Hence, the formation of $\pi - \pi$ bonds may drive structure formation during cooling of comb-like polymers first before the formation of crystalline methylene sequences is becoming important. Consequently, the methylene sequence may have problems to achieve their equilibrium state. Otherwise, the thermodynamic driving forces caused by the side chains can be huge under ambient conditions since methylene sequences are characterized by large free energy differences between crystalline and disordered state.

Thus, one can conclude that there are obviously different packing states of long methylene sequences in the side chains of comb-like polymers with rigid backbones showing long-range ordered lamellar morphologies. There might be situations (i) where the alkyl groups are non-crystalline and disordered within their domains as well as (ii) where the methylene sequences are (fully or partially) crystalline within their alkyl nanodomains. This can explain the significant differences regarding the volume V_{CH_2} per methylene unit for comb-like polymers with different rigid backbones. Based on this interpretation different polymorphic states can occur due to differences in the packing of the subunits within their individual nanodomains. This leads us to another fundamental question namely the influence of different packing states of the alkyl side chains on the packing behavior of main chains.

5.2 Interrelations between main and side chain packing in comb-like polymers

Starting from the inferences drawn from the previous section, it can be concluded that two modifications exist in PPAOTs depending on the packing state of side chains (Fig-
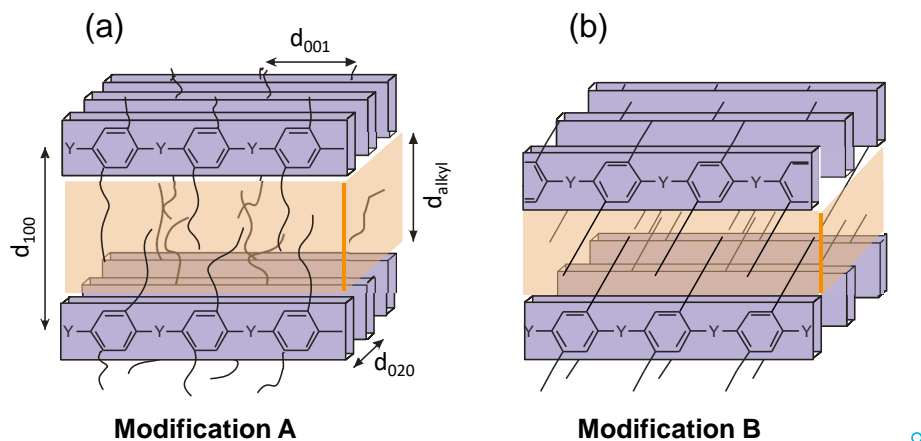
Figure 5.2: Schematic showing two commonly observed modifications: (a) modification A with disorder side chains and (b) modification B with densely packed side chains in the rigid main chains comb-like polymers. Different periodicities are indicated.

ure 5.1). However, an important question that arises is to what extent the packing of side chains is influencing the main chain packing. The indications for such an interrelation are depicted in Figure 5.2 and are mainly observed in the higher members ($n =$ 10 and 12) of the PPAOT series. Based on the results from XRD measurements, while the layer spacing d_{100} of the modification B decreases by 20-30%, an 20% increase in the d_{020} spacings can be observed as compared to the corresponding spacings in modification A. This difference in the d_{020} spacings mainly arises due to the dense packing of alkyl side chains in modification B as compared to disorder in modification A. In terms of functional properties this is a large difference in the $\pi - \pi$ spacing causing usually significant differences in application relevant properties. This is known especially in terms of electronic properties like conductivity since larger stacking distances substantially reduce the overlap of electronic orbitals [23, 24, 142].

The reported packing models suggest that the functional properties of comb-like polymers are to a large extent characterized by the packing state of the side chain since these sub-units strongly influence the packing of the rigid backbones. This statement is obviously true although the functional parameters are majorly determined by the packing state of rigid backbones. Central message is that changes in side chain packing in comb-like polymers will always influence main chain packing and therefore (at least potentially) the performance of functional materials. It is important to consider this in all cases where different polymorphs may occur although they are not so well distinguished in the discussion. An example of this type might be the famous

case of regio-regular poly(3-hexyl thiophenes) [rreg P3HT] where structural states with crystalline side chains seem to exist [25] beside of states where the side chains remain disordered within alkyl nanodomains [22, 125] depending on microstructure and treatment of the samples. The influence of side chain packing on the overall performance has to be also kept in mind if side chains with variable microstructure are attached to identical backbones. This a well known playground for performance optimization. Avoiding crystallization of side chains by introducing "defects" (e.g. ethyl-hexyl instead of n-octyl side chains) like done in many organic semi-conductors with high performance and comb-like architecture [143, 144] can lead to robust functional states but means at the same time that improving the performance by choosing other polymorphic states is no longer possible. Otherwise, the absence of different polymorphic states can avoid problems towards long term stability which go hand in hand with the occurrence of solid-solid transitions in comb-like polymers with crystallizable side chains [21].

As discussed above native packing and thermodynamic equilibrium state of main chains and alkyl groups in comb-like polymers are basically different. This fact seems to be of major importance for the formation of different crystalline modifications and also for the thermodynamically stable state. Based on the experimental results for the PPAOT series, it can be assumed that at high temperatures the rings in the backbones may form in a first step $\pi-\pi$ stacks while the side chain remain disordered since there is no intrinsic driving force in the alkyl nanodomains to crystallize. Despite of that, a long range ordered lamellar morphology can obviously exist due to nanophase-separation of main and side chain domains. The polymorph which exists at this stage is known as modification A. This modification can be considered as the thermodynamically stable state in all investigated PPAOTs at high temperatures. At lower temperatures, in particular close to ambient, modification B with crystalline methylene units in the side chains seems to be thermodynamically stable for higher PPAOTs ($n \geq 10$). This can be concluded from (i) the appearance of modification B in as synthesized PPDOT and PPDDOT samples (crystallized in the presence of solvent, Figure 4.7), (ii) a transition from modification B to modification A during heating at temperatures between 70°C and 120°C (Figure 4.8 and 4.9), and (iii) a slow growth of modification B at room temperature in PPDOT samples which contain initially only modification A (Figure 4.12) [130, 131]. During cooling, the once formed main chain stacks of modification A do probably hinder the crystallization of methylene sequences at lower temperatures preventing the transition to modification B in case of slowly cooled melts. Hence, modification A occurs even at low temperatures where modification B with crystalline

side chains might be thermodynamically stable. Over time, the free energy difference between the amorphous and crystalline state of the methylene sequences acts as a driving force and the system tries to recreate its equilibrium state being modification B under ambient conditions. Note that this can lead to changes in important properties under application-relevant conditions. Whether or not the side chains are really tilted with respect to the main chains and to what extent the side chains are crystallized in modification B is still a question for further investigations e.g. by appropriate NMR methods [54]. Very small V_{CH_2} values point to a high degree of crystallinity. The parallel increase in d_{020} might be due to an optimization of the overall free energy. Further details of the packing states within main and side chain domains might be still interesting targets for in-depth investigations.

Summarizing this section one can conclude that the findings reported in this work clearly highlight the importance of interrelations between side chain packing and main chain packing in comb-like polymers. These interrelations are of major relevance for the optimization of functional polymers since a consequence is that increased solubility and processibility by alkyl side groups can not be reached without changes in the main chain packing determining majorly other performance parameters like conductivity or mechanical strength.

5.3 Factors influencing the relaxation dynamics in nano-confined systems

The structural situation in case of modification A of the PPAOT series with disordered alkyl nanodomains allows systematic studies focusing on the influence of geometrical confinement and other constraints on the cooperative dynamics of CH_2 units. This is an interesting question since the nature of the dynamic glass transition (α) in glass forming materials is still not finally understood [37, 44]. One of the common approaches to understand this phenomenon is based on the assumption that dynamic heterogeneities related to cooperatively rearranging region (CRR) with typical dimensions in the range ξ_α = 10-30 Å do exist in all glass forming materials [45, 46, 48]. Hence, changes in the cooperative dynamics should occur in nanoscopic domains if these CRR dimensions are approached. This is the very basic prediction of the hindered glass transition concept [15, 29, 92]. Consequently, the dynamics of various glass-forming materials has been studied under geometrical confinement, e.g. in nanoporous host systems [29, 33, 137],

in ultra-thin films [32, 40, 145] as well as in small self-assembled domains formed by nanophase separation in comb-like polymers [21, 146]. One major disadvantage of these studies is, however, that beside of purely geometrical confinement effects, other effects have to be expected like interfacial effects [109, 110] or changes of the average density in nanoscopic domains [96].

A major advantage of detailed investigations on modification A of the PPAOT series in this work is that all these influencing factors can be quantified what is unique situation compared to practically all comparable studies which are reported in the corresponding literature. The relaxation spectroscopy experiments on PPAOTs samples where modification A occurs should provide together with the obtained structural information further insights about the relevance of the different influencing factors for systematic changes in the cooperative dynamics under confinement. Starting point for this discussion is the observed influence of side chain length n on the cooperative dynamics of CH_2 units seen as α_{PE} process. A systematic increase of relaxation temperature $T_{\alpha_{PE}}$ and stepness index $m_{\alpha_{PE}}$ is observed in case of modification A of the PPAOT members with $6 \leq n \leq 12$ (cf. Section 4.2) like in other comb-like polymers [15, 21]. Since alkyl nanodomain size (d_{alkyl}), volume per CH_2 unit (V_{CH_2}) and area per side group in the interface between main an side chain domains (A_{IF}) are known (cf. Section 4.1.1 and 5.1), the influence geometrical confinement, density effects and interfacial constrains can be estimated. Hence, the PPAOT series can be understood as an excellent model system to judge the importance of different influencing factors for the obtained changes regarding the α_{PE} dynamics with side chain lengths. The most important conclusions are summarized below.

Geometrical confinement. The variation of side chain length n results for nanophase-separated comb-like polmyers with layered morphology in a systematic change of the thickness of the alkyl nanodomains (Figure 5.3). For modification A of PPAOTs on gets an increase from $d_{alkyl} = 7.2$ Å for PPHOT ($n = 6$) to $d_{alkyl} = 14.3$ Å for PPDDOT ($n = 12$). This effect has been used to explain the increase in $T_{\alpha_{PE}}$ and $m_{\alpha_{PE}}$ in the recent literature [15, 21]. Idea is that geometrical confinement influences the cooperative dynamics of CH_2 units in amorphous alkyl nanodomains. Assuming that d_{alkyl} is smaller than that of the relevant size of cooperative rearranging regions (CRRs) $\xi_{\alpha_{PE}}$ for the polyethylene-like glass transition α_{PE}, one expected according to the hindered glass transition picture geometrical confinement effects. These effects should be stronger for smaller nanodomains. Hence, changes in the cooperative α_{PE} dynamics and a non Arrhenius-to-Arrhenius transition are expected. Since the relevant
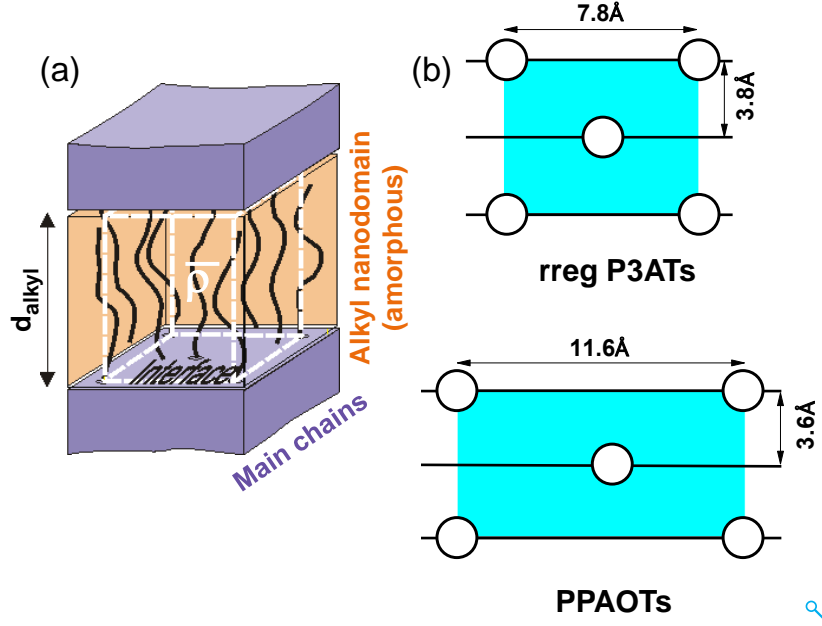
Figure 5.3: (a) Sketch of the alkyl nanodomains in PPAOTs. The alkyl nanodomains (orange) formed by the side chains are surrounded by main chains containing aromatic rings (dark blue). The alkyl nanodomain size $d_{alkyl} = d_{100} - d_{mc}$ is indicated. The white box represents the volume element used to calculate the volume per CH_2 group V_{CH_2} based on Eq.5.1. (b) Position of the side groups (open circles) in the interface between the main chain layers and alkyl nanodomains are indicated in the sketches for rreg P3ATs and PPAOTs. The typical distances are indicated.

CRR size is expected to decrease with increasing temperature [47], deviations from the bulk behavior of $\omega_{\alpha_{PE}}(T)$ should also start at higher temperatures if the alkyl nanodomain size decreases [15]. This provides a qualitative understanding of the changes in the polyethylene-like glass transition α_{PE} depending on side chain length.

Density effects. The influence of the average volume per methylene unit V_{CH_2} in the alkyl domains on the α_{PE} process can be nicely considered in case of the PPAOT series. The average volumes V_{CH_2} for all PPAOT samples are shown in Figure 5.1. An important finding is that there is no systematic change in V_{CH_2} with increasing side chain length for modification A. This result demonstrates that changes in average density are no appropriate explanation for the systematic increase of $T_{\alpha_{PE}}$ and $m_{\alpha_{PE}}$ with increasing side chain length n. A similar conclusion can be drawn based on the results for a series rreg P3ATs reported by S. Pankaj [21] which are also included in Figure 5.1 for comparison.

Interfacial effects. A comparison of the situation at the interface between main and side chain domains in case of modification A of PPAOTs and rreg P3ATs [21]

(Figure 5.3.b) shows clearly that there are significant differences between both series of comb-like polymers. A calculation interfacial area per side group A_{IF} based on these sketches gives about 43.5 Å^2 per chain for PPAOTs and about 29.5 Å^2 per side chain for rreg P3ATs. Despite of this significant difference ($>$50%), the α_{PE} dynamics in the alkyl nanodomains seems to be quite similar in both polymer series. Hence, one can conclude that strong changes in the main chain packing have also no serious consequences for the cooperative dynamics of the CH$_2$ groups in alkyl nanodomains. This is somehow surprising since the local packing at the interface is quite different resulting in significantly different distances between neighbored side chains. Otherwise, this finding is compatible with similar V$_{CH_2}$ values for PPAOTs and rreg P3ATs (Figure 5.1). Obviously, dense packing of the CH$_2$ units is preferred and approached in amorphous alkyl nanodomains independent of constraints incorporated by covalent bonds to the main chain. Consequence is a weak dependence of the cooperative α_{PE} dynamics on main chain packing and interfacial situation in comb-like polymers with disordered alkyl nanodomains.

Main conclusion of this part of the work is that the domain size is indeed the most important parameter influencing the cooperative dynamics of the CH$_2$ units in self-assembled alkyl nanodomains. Other parameters like average volume per CH$_2$ unit or number of side groups per interfacial area do modify the α_{PE} dynamics but only slightly. This finding is in accordance with the general observation that the α_{PE} process in several series of comb-like polymers shows common trends depending on alkyl side chain length although the main chain packing is significantly different. All together, these results support the idea that there is a characteristic length scale $\xi_{\alpha_{PE}}$ in the one nanometer range determining the cooperative dynamics in glass forming materials.

Chapter 6

Conclusions

In the first part of this work, structural features of two series of comb-like polymers with rigid main chains, poly(1,4-phenylene-2,5-n-dialkyloxyterephthalate)s (PPAOTs) and poly (2,5-n-dialkyloxy-1,4-phenylene-vinylene)s (AOPPVs), with $n = 6$ - 12 alkyl carbons per side chain were broadly investigated by X-ray diffraction. A layer morphology with alternating main and side chain domains is found in all investigated systems. The rigid main chains are nicely stacked within their domains and the side chains are aggregated in alkyl nanodomains with typical dimensions in the 10-20 Å range. Lattice models are proposed for both series based on a crystallographic analysis of the X-ray diffraction data. Main goal of these structural investigations was to learn more about the packing state of the alkyl side groups with their alkyl nanodomains as well as a possible influence of the side chain packing state on main chain ordering. Two different polymorphic states, modification A and modification B, are observed for both investigated series, PPAOTs and AOPPVs. The packing state of the side chains is further investigated in more detail based on a comparison of the average volumes per CH_2 unit, V_{CH_2}, in both modifications of the PPAOT series. The results of such an analysis clearly demonstrate that (i) the alkyl groups are non-crystalline and disordered within alkyl nanodomains in case of modification A while (ii) the methylene sequences are probably fully crystalline in case of modification B. The V_{CH_2} values for the standard packing state of AOPPV shows that the long range ordered state in these samples is related to a situation like in modification B of PPAOTs, i.e., the side chains are packed very densely. Note that this approach is able to discriminate between different packing states of the side chains using minimal assumptions, i.e., differences are found based on the unit cell dimensions without additional model. The obtained difference in the packing state of the side chains result in significantly different d_{100} spacings between

modifications A and modification B. From a detailed analysis of X-ray diffraction patterns one can further conclude that changes in side chain packing result in a significant variation ($\approx$ 20%) of the $\pi - \pi$ spacing, i.e., the transition from modification A to modification B in PPAOTs is related to an increase of the distance between neighbored rings within the main chain stacks. This clearly indicates interrelations between main and side chain packing and is a very important finding since the $\pi - \pi$ spacings are of major importance for properties like conductivity and strength in functional polymers with comb-like architecture. Finally, one can conclude that a competition of the individual packing tendencies of main and side chains is probably very important for structure formation processes and thermodynamic stability of different crystallographic modifications in comb-like polymers.

In the second part of this work, the results of relaxation studies by dynamic mechanical analysis and dielectric spectroscopy on modification A of PPAOTs are presented. The influence of different factors affecting the cooperative dynamics of methylene units in alkyl nanodomains seen as α_{PE} process is studied systematically. Quantitative information about (i) alkyl nanodomain size d_{alkyl}, (ii) average volume per CH_2 unit V_{CH_2} and (iii) interfacial area per side chain A_{IF} are used in order to check which parameter is most important. The experimental results clearly show that the cooperative dynamics of the methylene units confined within alkyl nanodomains is mainly affected by the domain size d_{alkyl} as confirmed by the transition from a weak to more pronounced non-Arrhenius character of the α_{PE} process with increasing side chain lengths. At the same time the relaxation temperatures of the α_{PE} process $T_{\alpha_{PE}}$ increase systematically. Both trends in the α_{PE} dynamics can be explained by geometrical confinement effects. Basic idea behind is the so called 'hindered glass transition' picture assuming that the cooperative motions will be affected if the size of nanoscopic domains approaches that of cooperatively rearranging regions (CRRs) in the range 10-30 Å being an intrinsic feature of glass forming materials. This is an interesting finding and can be understood as an indirect evidence for the existence of CRRs. The average density as well as constraints at the interfaces are obviously of minor importance for the overall trends seen for the α_{PE} process in modificantion A of PPAOTs. This is concluded from the fact that the α_{PE} dynamics is strongly changing with side chain lengths n although V_{CH_2} and A_{IF} are nearly constant. The final conclusion of this study is that the domain size is indeed the most important parameter influencing the cooperative dynamics of the CH_2 units in self-assembled alkyl nanodomains. This finding supports and substantiates the conclusions drawn from previous investigations on other series

of comb-like polymers and should contribute to the ongoing discussion about changes in the cooperative α dynamics of glass forming materials confined in pores or domains having typical dimensions of a very few nanometers.

Appendix

A1. Parameters of Havriliak-Negami function for modification A of PPAOTs

As mentioned in section 4.2, under dielectric relaxation spectroscopy, the dielectric relaxation data are analyzed by using Havriliak-Negami function to extract the α_{PE} peak maxima positions ω_{max} from the measured isotherms. The corresponding HN fit parameters used for the fitting of the data for the selected temperatures of all the PPAOT members are given in Table 6.1.

Table 6.1: Parameters of Havriliak-Negami function for modification A of PPAOTs

Label	n	T	log f$_{max}$	$\Delta\epsilon$	b	g
		°C	Hz			
PPHOT	6	-40	3.9	0.14	0.31	0.89
		-60	2.5	0.15	0.25	0.89
		-80	0.79	0.17	0.21	0.89
PPOOT	8	-40	2.7	0.15	0.33	0.97
		-60	0.66	0.17	0.27	0.97
		-80	-2.1	0.19	0.23	0.97
PPDOT	10	-40	2.1	0.15	0.38	0.49
		-60	-0.51	0.17	0.30	0.49
		-80	-4.2	0.21	0.25	0.49
PPDDOT	12	0	4.7	0.038	0.34	0.94
		-20	3.4	0.036	0.33	0.94
		-40	2.1	0.033	0.32	0.94

Bibliography

[1] N. A. Platé and V. P. Shibaev, "Comb-like polymers - structure and properties," *Macromolecular Reviews Part D-Journal of Polymer Science*, vol. 8, pp. 117–253, 1974.

[2] H. F. Shi, Y. Zhao, X. Dong, Y. Zhou, and D. J. Wang, "Frustrated crystallisation and hierarchical self-assembly behaviour of comb-like polymers," *Chemical Society Reviews*, vol. 42, no. 5, pp. 2075–2099, 2013.

[3] M. Beiner, "Relaxation in poly(alkyl methacrylate)s: Crossover region and nanophase separation," *Macromolecular Rapid Communications*, vol. 22, pp. 869–895, 2001.

[4] B. S. Ong, Y. L. Wu, P. Liu, and S. Gardner, "High-performance semiconducting polythiophenes for organic thin-film transistors," *Journal of the American Chemical Society*, vol. 126, no. 11, pp. 3378–3379, 2004.

[5] H. N. Tsao, D. Cho, J. W. Andreasen, A. Rouhanipour, D. W. Breiby, W. Pisula, and K. Mullen, "The influence of morphology on high-performance polymer field-effect transistors," *Advanced Materials*, vol. 21, no. 2, pp. 209–212, 2009.

[6] Y. J. Cheng, S. H. Yang, and C. S. Hsu, "Synthesis of conjugated polymers for organic solar cell applications," *Chemical Reviews*, vol. 109, no. 11, pp. 5868–5923, 2009.

[7] P. W. M. Blom and M. C. J. M. Vissenberg, "Charge transport in poly(p-phenylene vinylene) light-emitting diodes," *Materials Science & Engineering R-reports*, vol. 27, no. 3-4, pp. 53–94, 2000.

[8] M. Ballauff, "Stiff-chain polymers - structure, phase-behavior, and properties," *Angewandte Chemie-International Edition In English*, vol. 28, no. 3, pp. 253–267, 1989.

[9] J. Majnusz, J. Catala, and R. W. Lenz, "Liquid-crystal polymers .11. structure property relationships in a series of thermotropic poly(2-normal-alkyl-1,4-phenylene terephthalates)," *European Polymer Journal*, vol. 19, no. 10-1, pp. 1043–1046, 1983.

[10] W. R. Krigbaum, H. Hakemi, and R. Kotek, "Nematogenic polymers having rigid chains. 1. substituted poly(p-phenylene terephthalates)," *Macromolecules*, vol. 18, no. 5, pp. 965–973, 1985.

[11] M. Ballauff and G. F. Schmidt, "Rigid rod polymers having flexible side-chains .3. structural investigations on a novel layered mesophase formed by thermotropic poly(1,4-phenylene-2,5-dialkoxy terephthalate)s," *Molecular Crystals and Liquid Crystals*, vol. 147, pp. 163–177, 1987.

[12] J. Heijboer, *Physics of Non-Crystalline Solids*. Prins, J. A., Ed.; North Holland: Amsterdam, 1965.

[13] M. Ballauff, "Phase-equilibria in rodlike systems with flexible side-chains," *Macromolecules*, vol. 19, no. 5, pp. 1366–1374, 1986.

[14] M. Ballauff, "Rigid rod polymers having flexible side-chains .1. thermotropic poly(1,4-phenylene 2,5-dialkoxyterephthalate)s," *Makromolekulare Chemie-rapid Communications*, vol. 7, no. 6, pp. 407–414, 1986.

[15] M. Beiner and H. Huth, "Nanophase separation and hindered glass transition in side-chain polymers," *Nature Materials*, vol. 2, no. 9, pp. 595–599, 2003.

[16] T. Babur, G. Gupta, and M. Beiner, "About different packing states of alkyl groups in comb-like polymers with rigid backbones," *Soft Matter*, vol. 12, no. 39, pp. 8093–8097, 2016.

[17] M. Muthukumar, C. K. Ober, and E. L. Thomas, "Competing interactions and levels of ordering in self-organizing polymeric materials," *Science*, vol. 277, no. 5330, pp. 1225–1232, 1997.

[18] S. Nagamatsu, M. Misaki, M. Chikamatsu, T. Kimura, Y. Yoshida, R. Azumi, N. Tanigaki, and K. Yase, "Crystal structure of friction-transferred poly(2,5-dioctyloxy-1,4-phenylenevinylene)," *Journal of Physical Chemistry B*, vol. 111, no. 17, pp. 4349–4354, 2007.

[19] S. Nagamatsu, M. Misaki, T. Kimura, Y. Yoshida, R. Azum, N. Tanigaki, and K. Yasez, "Side-chain effects on friction-transferred polymer orientation," *Polymer Journal*, vol. 39, no. 12, pp. 1300–1305, 2007.

[20] M. Beiner, K. Schröter, E. Hempel, S. Reissig, and E. Donth, "Multiple glass transition and nanophase separation in poly(n-alkyl methacrylate) homopolymers," *Macromolecules*, vol. 32, no. 19, pp. 6278–6282, 1999.

[21] S. Pankaj and M. Beiner, "Confined dynamics and crystallization in self-assembled alkyl nanodomains," *Journal of Physical Chemistry B*, vol. 114, no. 47, pp. 15459–15465, 2010.

[22] T. J. Prosa, M. J. Winokur, J. Moulton, P. Smith, and A. J. Heeger, "X-ray structural studies of poly(3-alkylthiophenes): an example of an inverse comb," *Macromolecules,*, vol. 25, no. 17, pp. 4364–4372, 1992.

[23] T. J. Prosa, M. J. Winokur, and R. D. McCullough, "Evidence of a novel side chain structure in regioregular poly(3-alkylthiophenes)," *Macromolecules*, vol. 29, no. 10, pp. 3654–3656, 1996.

[24] R. J. Kline, D. M. DeLongchamp, D. A. Fischer, E. K. Lin, L. J. Richter, M. L. Chabinyc, M. F. Toney, M. Heeney, and I. McCulloch, "Critical role of side-chain attachment density on the order and device performance of polythiophenes," *Macromolecules*, vol. 40, no. 22, p. 7960–7965, 2007.

[25] Z. Y. Wu, A. Petzold, T. Henze, T. Thurn-Albrecht, R. H. Lohwasser, M. Sommer, and M. Thelakkat, "Temperature and molecular weight dependent hierarchical equilibrium structures in semiconducting poly(3-hexylthiophene)," *Macromolecules*, vol. 43, no. 10, pp. 4646–4653, 2010.

[26] L. Červinka and M. Ballauff, "Rigid-rod polymers with flexible side-chains .9. wide-angle x-ray-analysis of side-chain ordering in poly(1,4-phenylene-2,5-di-n-hexadecyloxyterephthalate)," *Colloid and Polymer Science*, vol. 270, no. 9, pp. 859–872, 1992.

[27] S. H. Chen, A. C. Su, S. R. Han, S. A. Chen, and Y. Z. Lee, "Molecular aggregation and luminescence properties of bulk poly(2,5-di-n-octyloxy-1,4-phenylenevinylene)," *Macromolecules*, vol. 37, no. 1, pp. 181–186, 2004.

[28] E. Thorn-Csanyi and P. Kraxner, "All-trans oligomers of 2,5-dialkyl-1,4-phenylenevinylenes - metathesis preparation and characterization," *Macromolecular Chemistry and Physics*, vol. 198, no. 12, pp. 3827–3843, 1997.

[29] M. Arndt, R. Stannarius, H. Groothues, E. Hempel, and F. Kremer, "Length scale of cooperativity in the dynamic glass transition," *Physical Review Letters*, vol. 79, no. 11, pp. 2077–2080, 1997.

[30] G. Barut, P. Pissis, R. Pelster, and G. Nimtz, "Glass transition in liquids: Two versus three-dimensional confinement," *Physical Review Letters*, vol. 80, no. 16, pp. 3543–3546, 1998.

[31] F. Kremer, A. Huwe, M. Arndt, P. Behrens, and W. Schwieger, "How many molecules form a liquid?," *Journal of Physics-Condensed Matter*, vol. 11, no. 10A, pp. A175–A188, 1999.

[32] A. Serghei, H. Huth, C. Schick, and F. Kremer, "Glassy dynamics in thin polymer layers having a free upper interface," *Macromolecules*, vol. 41, no. 10, pp. 3636–3639, 2008.

[33] A. Schönhals, H. Goering, C. Schick, B. Frick, and R. Zorn, "Glassy dynamics of polymers confined to nanoporous glasses revealed by relaxational and scattering experiments," *European Physical Journal E*, vol. 12, no. 1, pp. 173–178, 2003.

[34] K. Binder, A. Milchev, and J. Baschnagel, "Simulation studies on the dynamics of polymers at interfaces," *Annual Review of Materials Science*, vol. 26, pp. 107–134, 1996.

[35] L. Yelash, P. Virnau, K. Binder, and W. Paul, "Slow process in confined polymer melts: Layer exchange dynamics at a polymer solid interface," *Physical Review E*, vol. 82, no. 5, p. 050801, 2010.

[36] K. Paeng, S. F. Swallen, and M. D. Ediger, "Direct measurement of molecular motion in freestanding polystyrene thin films," *Journal of the American Chemical Society*, vol. 133, no. 22, pp. 8444–8447, 2011.

[37] M. D. Ediger and J. A. Forrest, "Dynamics near free surfaces and the glass transition in thin polymer films: A view to the future," *Macromolecules*, vol. 47, no. 2, pp. 471–478, 2014.

[38] C. L. Jackson and G. B. McKenna, "The glass-transition of organic liquids confined to small pores," *Journal of Non-crystalline Solids*, vol. 131, pp. 221–224, 1991.

[39] C. Schick and E. Donth, "Characteristic length of glass-transition - experimental-evidence," *Physica Scripta*, vol. 43, no. 4, pp. 423–429, 1991.

[40] J. A. Forrest and K. Dalnoki-Veress, "The glass transition in thin polymer films," *Advances In Colloid and Interface Science*, vol. 94, no. 1-3, pp. 167–196, 2001.

[41] A. Serghei and F. Kremer, "Metastable states of glassy dynamics, possibly mimicking confinement-effects in thin polymer films," *Macromolecular Chemistry and Physics*, vol. 209, no. 8, pp. 810–817, 2008.

[42] C. J. Ellison and J. M. Torkelson, "Sensing the glass transition in thin and ultrathin polymer films via fluorescence probes and labels," *Journal of Polymer Science Part B-Polymer Physics*, vol. 40, no. 24, pp. 2745–2758, 2002.

[43] H. J. Yin, S. Napolitano, and A. Schönhals, "Molecular mobility and glass transition of thin films of poly(bisphenol a carbonate)," *Macromolecules*, vol. 45, no. 3, pp. 1652–1662, 2012.

[44] S. Napolitano and M. Wübbenhorst, "The lifetime of the deviations from bulk behaviour in polymers confined at the nanoscale," *Nature Communications*, vol. 2, p. 260, 2011.

[45] G. Adam and J. H. Gibbs, "On temperature dependence of cooperative relaxation properties in glass-forming liquids," *Journal of Chemical Physics*, vol. 43, no. 1, pp. 139–146, 1965.

[46] E. Donth, "The size of cooperatively rearranging regions at the glass-transition," *Journal of Non-crystalline Solids*, vol. 53, no. 3, pp. 325–330, 1982.

[47] E. Donth, H. Huth, and M. Beiner, "Characteristic length of the glass transition," *Journal of Physics-condensed Matter*, vol. 13, no. 22, pp. L451–L462, 2001.

[48] L. Berthier, G. Biroli, J. P. Bouchaud, L. Cipelletti, D. El Masri, D. L'Hote, F. Ladieu, and M. Pierno, "Direct experimental evidence of a growing length scale accompanying the glass transition," *Science*, vol. 310, no. 5755, pp. 1797–1800, 2005.

[49] H. Huth, M. Beiner, and E. Donth, "Temperature dependence of glass-transition cooperativity from heat-capacity spectroscopy: Two post-adam-gibbs variants," *Physical Review B*, vol. 61, no. 22, pp. 15092–15101, 2000.

[50] J. M. Rodriguez-Parada, R. Duran, and G. Wegner, "A comparative study of mesophase formation in rigid-chain polyesters with flexible side chains," *Macromolecules*, vol. 22, no. 5, p. 2507–2516, 1989.

[51] U. Falk and H. W. Spiess, "Phase behaviour and macroscopic alignment of rigid chain polyesters with short flexible side chains," *Die Makromolekulare Chemie, Rapid Communications*, vol. 10, no. 4, pp. 149–155, 1989.

[52] M. Ballauff and G. F. Schmidt, "Rigid rod polymers with flexible side chains, 2. observation of a novel type of layered mesophase," *Die Makromolekulare Chemie, Rapid Communications*, vol. 8, no. 2, pp. 93–97, 1987.

[53] A. Adam and H. W. Spiess, "On the packing behaviour of alkoxy-substituted stiff macromolecules," *Die Makromolekulare Chemie, Rapid Communications*, vol. 11, no. 6, pp. 249–259, 1990.

[54] J. Clauss, K. Schmidt-Rohr, A. Adam, C. Boeffel, and H. W. Spiess, "Stiff macromolecules with aliphatic side chains: side-chain mobility, conformation, and organization from 2d solid-state nmr spectroscopy," *Macromolecules*, vol. 25, p. 5208–5214, 1992.

[55] K. Tashiro, K. Ono, Y. Minagawa, M. Kobayashi, T. Kawai, and K. Yoshino, "Structure and thermochromic solid-state phase-transition of poly(3-alkylthiophene)," *Journal of Polymer Science Part B-polymer Physics*, vol. 29, no. 10, pp. 1223–1233, 1991.

[56] T. Kawai, M. Nakazono, R. Sugimoto, and K. Yoshino, "Crystal structure of poly(3-alkylthiophene) and its doping effect," *Journal of the Physical Society of Japan*, vol. 61, no. 9, pp. 3400–3406, 1992.

[57] R. McCullough, "The chemistry of conducting polythiophenes," *Advanced Materials*, vol. 10, no. 2, pp. 93–116, 1998.

[58] K. E. Mena-Osteritz, A. Meyer, B. M. W. Langeveld-Voss, R. A. J. Janssen, E. W. Meijer, and P. Baürele, "Two-dimensional crystals of poly(3-alkyl- thiophene)s:

Direct visualization of polymer folds in submolecular resolution," *Angewandte Chemie-International Edition In English*, vol. 39, no. 15, p. 2679–2684, 2000.

[59] S. T. Salammal, S. Dai, U. Pietsch, S. Grigorian, N. Koenen, U. Scherf, N. Kayunkid, and M. Brinkmann, "Influence of alkyl side chain length on the in-plane stacking of room temperature and low temperature cast poly(3-alkylthiophene) thin films," *European Polymer Journal*, vol. 67, pp. 199–212, 2015.

[60] R. Loewe, P. Ewbank, J. Liu, L. Zhai, and R. McCullough, "Regioregular, head-to- tail coupled poly(3-alkylthiophenes) made easy by the grim method: Investigation of the reaction and the origin of regioselectivity," *Macromolecules*, vol. 34, pp. 4324–4333, 2001.

[61] R. Loewe, M. Khersonsky, and R. McCullough, "A simple method to prepare head-to-tail coupled, regioregular poly(3-alkylthiophenes) using grignard metathesis," *Advanvced Materials*, vol. 11, pp. 250–253, 1999.

[62] H. Shirakawa, E. J. Louis, A. G. MacDiarmid, C. C. K., and H. A. J., "Synthesis of electrically conducting organic polymers: halogen derivatives of polyacetylene, (ch)x," *Journal of the Chemical Society, Chemical Communications*, vol. 16, pp. 578–580, 1977.

[63] T. J. Prosa, M. J. Winokur, J. Moulton, P. Smith, and A. J. Heeger, "X-ray-diffraction studies of the three-dimensional structure within iodine-intercalated poly(3-octylthiophene)," *Physcial Review B*, vol. 51, no. 1, pp. 159–168, 1995.

[64] K. Tashiro, M. Kobayashi, T. Kawai, and K. Yoshino, "Crystal structural change in poly(3-alkyl thiophene)s induced by iodine doping as studied by an organized combination of x-ray diffraction, infrared/raman spectroscopy and computer simulation techniques," *Polymer*, vol. 38, no. 12, pp. 2867–2879, 1997.

[65] A. Bolognesi, W. Porzio, F. Provasoli, and T. Ezquerra, "The thermal behaviour of low-molecular-weight poly(3-decylthiophene)," *Die Makromolekulare Chemie*, vol. 194, no. 3, pp. 817–827, 1993.

[66] S. Pankaj, *Confined dynamics, side-chain crystallization and long term behavior of nanophase separated poly(3-alkyl thiophenes)*. PhD thesis, Institut für Physik der Naturwissenschaftlichen Fakultät II - Chemie, Physik und Mathematik der Martin-Luther-Universität Halle-Wittenberg, 2011.

[67] K. Yazawa, Y. Inoue, T. Shimizu, M. Tansho, and N. Asakawa, "Molecular dynamics of regioregular poly(3-hexylthiophene) investigated by nmr relaxation and an interpretation of temperature dependent optical absorption," *Journal of Physical Chemistry B*, vol. 114, pp. 1241–1248, 2010.

[68] J. D. Ferry, *Viscoelastic Properties of Polymers*. JohnWiley and sons, USA, 3rd. edition ed., 1980.

[69] E. Donth, *The Glass Transition: Relaxation Dynamics in Liquids and Disordered Materials*. Springer, Berlin-Heidelberg, 2001.

[70] P. Heydemann and H. D. Guicking, "Specific volume of polymers as a function of temperature and pressure," *Kolloid-Zeitschrift und Zeitschrift für Polymere*, vol. 193, no. 1, pp. 16–25, 1963.

[71] R. J. Seyler, ed., *Assignment of the Glass Transition*. ASTM, Philadelphia, 1994.

[72] D. I. Bower, *An Introduction to Polymer Physics*. Cambridge University Press, 2002.

[73] G. Höhne, W. Hemminger, and H.-J. Flammersheim, *Differential Scanning Calorimetry: An Introduction for Practitioners*. Springer, Berlin, 1996.

[74] G. P. Johari and M. Goldstein, "Viscous liquids and glass transition .2. secondary relaxations in glasses of rigid molecules," *Journal of Chemical Physics*, vol. 53, no. 6, pp. 2372–2388, 1970.

[75] M. Zajac, H. Kahl, B. Schade, T. Rödel, M. Dionisio, and M. Beiner, "Relaxation behavior of polyurethane networks with different composition and crosslinking density," *Polymer*, vol. 111, pp. 83–90, 2017.

[76] H. Vogel, "The law of the relationship between viscosity of liquids and the temperature," *Physikalische Zeitschrift*, vol. 22, pp. 645–646, 1921.

[77] G. S. Fulcher, "Analysis of recent measurements of the viscosity of glasses," *Journal of the American Ceramic Society*, vol. 8, no. 6, p. 339–355, 1925.

[78] G. Tamman and G. Hesse, "Die abhängigkeit der viscosität von der temperatur bie unterkühlten flüssigkeiten," *Zeitschrift für Anorganische und Allgemeine Chemie*, vol. 156, p. 245–257, 1926.

[79] C. A. Angell, "Formation of glasses from liquids and biopolymers," *Science*, vol. 267, no. 5206, pp. 1924–1935, 1995.

[80] R. Böhmer, K. L. Ngai, C. A. Angell, and D. J. Plazek, "Nonexponential relaxations in strong and fragile glass formers," *Journal of Chemical Physics*, vol. 99, no. 5, pp. 4201–4209, 1993.

[81] D. H. Huang and G. B. McKenna, "New insights into the fragility dilemma in liquids," *Journal of Chemical Physics*, vol. 114, no. 13, pp. 5621–5630, 2001.

[82] P. Debenedetti and F. Stillinger, "Supercooled liquids and the glass transition," *Nature*, vol. 410, pp. 259–267, 2001.

[83] TRB committee AFK10-General Issues in Asphalt Technology for 84th TRB Annual Meeting, *Low Temperature Property Evaluation and Fragility of Asphalt Binders Using NonArrhenius Viscosity Temperature Dependency*, 2004.

[84] M. Beiner, H. Huth, and K. Schröter, "Crossover region of dynamic glass transition: general trends and individual aspects," *Journal of Non-Crystalline Solids*, vol. 279, pp. 126–135, 2001.

[85] A. K. Doolittle, "Studies in newtonian flow. i. the dependence of the viscosity of liquids on temperature," *Journal of Applied Physics*, vol. 22, no. 8, p. 1031–1035, 1951.

[86] E. Donth, E. Hempel, and C. Schick, "Does temperature fluctuate? indirect proof by dynamic glass transition in confined geometries," *Journal of Physics: Condensed Matter*, vol. 12, no. 16, p. L281–L286, 2000.

[87] J. Korus, E. Hempel, M. Beiner, S. Kahle, and E. Donth, "Temperature dependence of α glass transition cooperativity," *Acta Polymerica*, vol. 48, pp. 369–378, 1997.

[88] A. Saiter, J.-M. Saiter, R. Golovchak, M. Shpotyuk, and O. Shpotyuk, "Cooperative rearranging region size and free volume in as–se glasses," *Journal of Physics: Condensed Matter*, vol. 21, no. 7, p. 075105, 2009.

[89] E. Hempel, G. Hempel, A. Hensel, C. Schick, and E. Donth, "Characteristic length of dynamic glass transition near tg for a wide assortment of glass-forming substances," *Journal of Physical Chemistry B*, vol. 104, no. 11, pp. 2460–2466, 2000.

[90] M. Beiner, S. Kahle, E. Hempel, K. Schroter, and E. Donth, "Crossover region of dynamic glass transition in poly(n-hexyl methacrylate) by heat capacity spectroscopy," *Macromolecules*, vol. 31, no. 25, pp. 8973–8980, 1998.

[91] H. Huth, M. Beiner, S. Weyer, M. Merzlyakov, and E. Schick, C.and Donth, "Glass transition cooperativity from heat capacity spectroscopy — temperature dependence and experimental uncertainties," *Thermochimica Acta*, vol. 337, no. 1-2, pp. 113–124, 2001.

[92] E. Donth, *Glasübergang.* Akademie-Verlag, 1980.

[93] J. A. Forrest, K. Dalnoki-Veress, J. R. Stevens, and J. R. Dutcher, "Effect of free surfaces on the glass transition temperature of thin polymer films," *Physical Review Letters*, vol. 77, no. 10, pp. 2002–2005, 1996.

[94] A. Schönhals, H. Goering, C. Schick, B. Frick, and R. Zorn, "Glass transition of polymers confined to nanoporous glasses," *Colloid and Polymer Science*, vol. 282, no. 8, pp. 882–891, 2004.

[95] M. Alcoutlabi and G. B. McKenna, "Effects of confinement on material behaviour at the nanometre size scale," *Journal of Physics: Condensed Matter*, vol. 17, no. 15, pp. R461–R524, 2005.

[96] C. Alba-Simionesco, B. Coasne, G. Dosseh, G. Dudziak, K. E. Gubbins, R. Radhakrishnan, and M. Sliwinska-Bartkowiak, "Effects of confinement on freezing and melting," *Journal of Physics: Condensed Matter*, vol. 18, no. 6, pp. R15–R68, 2006.

[97] W. Zheng and S. L. Simon, "Confinement effects on the glass transition of hydrogen bonded liquids," *The Journal of Chemical Physics*, vol. 127, no. 19, pp. 194501–11, 2007.

[98] M. Erber, M. Tress, E. U. Mapesa, A. Serghei, K. J. Eichhorn, B. Voit, and F. Kremer, "Glassy dynamics and glass transition in thin polymer layers of pmma deposited on different substrates," *Macromolecules*, vol. 43, no. 18, pp. 7729–7733, 2010.

[99] J. D. McCoy and J. G. Curro, "Conjectures on the glass transition of polymers in confined geometries," *Journal of Chemical Physics*, vol. 116, no. 21, pp. 9154–9157, 2002.

[100] D. Morineau, Y. D. Xia, and C. Alba-Simionesco, "Finite-size and surface effects on the glass transition of liquid toluene confined in cylindrical mesopores," *Journal of Chemical Physics*, vol. 117, no. 19, pp. 8966–8972, 2002.

[101] J. H. Gibbs and E. A. DiMarzio, "Nature of the glass transition and the glassy state," *The Journal of Chemical Physics*, vol. 28, pp. 373–383, 1958.

[102] G. B. McKenna, *Glass formation and glassy behavior in Comprehensive Polymer Science*, vol. 2. Oxford, 1989.

[103] G. Reiter, "Mobility of polymers in films-thinner than their unperturbed size," *Europhysics Letters*, vol. 23, no. 8, pp. 579–584, 1993.

[104] W. E. Wallace, N. C. B. Tan, W. L. Wu, and S. Satija, "Mass density of polystyrene thin films measured by twin neutron reflectivity," *The Journal of Chemical Physics*, vol. 108, pp. 3798–3804, 1998.

[105] M. Arndt, R. Stannarius, W. Gorbatschow, and F. Kremer, "Dielectric investigations of the dynamic glass transition in nanopores," *Physical Review E*, vol. 54, no. 5, pp. 5377–5390, 1996.

[106] P. Pissis, A. Kyritsis, D. Daoukaki, G. Barut, R. Pelster, and G. Nimtz, "Dielectric studies of glass transition in confined propylene glycol," *Journal of Physics-condensed Matter*, vol. 10, no. 28, pp. 6205–6227, 1998.

[107] Q. X. Li and S. L. Simon, "Surface chemistry effects on the reactivity and properties of nanoconfined bisphenol m dicyanate ester in controlled pore glass," *Macromolecules*, vol. 40, no. 10, pp. 3573–3579, 2009.

[108] R. Richert and M. Yang, "Surface induced glass transition in a confined molecular liquid," *Journal of Physical Chemistry B*, vol. 107, no. 4, pp. 895–898, 2003.

[109] C. J. Ellison and J. M. Torkelson, "The distribution of glass-transition temperatures in nanoscopically confined glass formers," *Nature Materials*, vol. 2, no. 10, pp. 695–700, 2003.

[110] C. J. Ellison, M. K. Mundra, and J. M. Torkelson, "Impacts of polystyrene molecular weight and modification to the repeat unit structure on the glass transition-nanoconfinement effect and the cooperativity length scale," *Macromolecules*, vol. 38, no. 5, pp. 1767–1778, 2005.

[111] D. A. M. Egbe, B. Cornelia, J. Nowotny, W. Günther, and E. Klemm, "Investigation of the photophysical and electrochemical properties of alkoxy-substituted arylene ethynylene/arylene vinylene hybrid polymers," *Macromolecules*, vol. 36, no. 15, pp. 5459–5469, 2003.

[112] D. A. M. Egbe, R. Stockmann, and M. Hotzel, "Third-order nonlinear optical behaviour of hybrid phenylene–ethynylene/phenylene–vinylene polymers," *Journal of Optics: A Pure and Applied Optics*, vol. 6, no. 8, pp. 791–797, 2004.

[113] A. Wild, D. A. M. Egbe, E. Birckner, V. Cimrovă, R. Baumann, U. Grummt, and U. S. Schubert, "Anthracene- and thiophene-containing meh-ppe-ppvs: Synthesis and study of the effect of the aromatic ring position on the photophysical and electrochemical properties," *Journal of Polymer Science Part A: Polymer Chemistry*, vol. 47, pp. 2243–2261, 2009.

[114] D. A. M. Egbe, S. Türk, S. Rathgeber, F. Kühnlenz, R. Jadhav, A. Wild, E. Birckner, G. Adam, A. Pivrikas, V. Cimrovă, G. Knör, N. S. Sariciftci, and H. Hoppe, "Anthracene based conjugated polymers: Correlation between $\pi - \pi$ stacking ability, photophysical properties, charge carrier mobility, and photovoltaic performance," *Macromolecules*, vol. 43, no. 3, pp. 1261–1269, 2010.

[115] C. Rauwendaal, *Polymer Extrusion*. Carl Hanser Verlag, Munich, 4th ed., 2001.

[116] G. K. Gupta, *Structural investigations on semiconducting donor-acceptor block copolymers and related model systems for organic photovoltaics*. PhD thesis, Institut für Physik der Naturwissenschaftlichen Fakultät II - Chemie, Physik und Mathematik der Martin-Luther-Universität Halle-Wittenberg, 2014.

[117] J. E. Mark, B. Erman, and F. R. Eirich, *Science and Technology of Rubber*. Academic Press, Inc., San Diego, 1994.

[118] *http://www.tainstruments.com/pdf/brochure/BROCH-ARESG2-2014-EN.pdf*.

[119] N. G. McCrum, B. E. Read, and G. Williams, *Anelastic and Dielectric Effects in Polymeric Solids*. Dover Publication, New York, 1991.

[120] P. Hedvig, *Dielectric Spectroscopy of Polymers*. AkadémiaiKiadó, Budapest, 1977.

[121] F. Kremer and A. Schönhals, *Broadband Dielectric Spectroscopy*. Springer-Verlag, Berlin Heidelberg, 2003.

[122] K. S. Cole and R. Cole, "Dispersion and absorption in dielectrics i. alternating current characteristics," *The Journal of Chemical Physics*, vol. 9, no. 4, pp. 341–351, 1941.

[123] D. W. Davidson and R. H. Cole, "Dielectric relaxation in glycerine," *Journal of Chemical Physics*, vol. 18, no. 10, pp. 1417–1417, 1950.

[124] Havriliak.S and S. Negami, "A complex plane analysis of alpha-dispersions in some polymer systems," *Journal of Polymer Science Part C-polymer Symposium*, no. 14PC, pp. 99–117, 1966.

[125] S. Pankaj, E. Hempel, and M. Beiner, "Side-chain dynamics and crystallization in a series of regiorandom poly(3-alkylthiophenes)," *Macromolecules*, vol. 42, no. 3, pp. 716–724, 2009.

[126] S. B. Damman and G. J. Vroege, "Liquid-crystalline main-chain polymers with a poly(p-phenylene terephthalate) backbone .4. x-ray-diffraction of the polyester with dodecyloxy side-chains," *Polymer*, vol. 34, no. 13, pp. 2732–2739, 1993.

[127] V. Danke, "Influence of shear processing conditions on the lamellar morphology and orientation of poly(1,4-phenylene 2,5-n-dialkyloxy terephthalate)s," Master's thesis, MLU Halle-Wittenberg, 2016.

[128] M. Beiner, "Nanoconfinement as a tool to study early stages of polymer crystallization," *Journal of Polymer Science Part B-Polymer Physics*, vol. 46, p. 1556–1561, 2008.

[129] H. F. Shi, Y. Zhao, S. C. Jiang, J. H. Xin, J. Rottstegge, D. F. Xu, and D. J. Wang, "Order-disorder transition in eicosylated polyethyleneimine comblike polymers," *Polymer*, vol. 48, p. 2762–2767, 2007.

[130] S. B. Damman and F. P. M. Mercx, "Liquid-crystalline main-chain polymers with a poly(p-phenyleneterephthalate) backbone .2. fiber spinning and mechanical-properties of polyesters with alkoxy side-chains," *Journal of Polymer Science Part B-Polymer Physics*, vol. 31, no. 12, pp. 1759–1767, 1993.

[131] S. B. Damman, F. P. M. Mercx, and P. J. Lemstra, "Liquid-crystalline main-chain polymers with a poly(p-phenylene terephthalate) backbone .3. drawing, structure development and ultimate mechanical-properties of films of the polyester with dodecyloxy side-chains," *Polymer*, vol. 34, no. 13, pp. 2726–2731, 1993.

[132] E. Hempel, H. Budde, S. Horing, and M. Beiner, "On the crystallization behavior of frustrated alkyl groups in poly(n-octadecyl methacrylate)," *Journal of Non-crystalline Solids*, vol. 352, no. 42-49, pp. 5013–5020, 2006.

[133] G. Strobl, *The Physics of Polymers*. Springer, Berlin, 1997.

[134] A. Jonscher, *Dielectric Relaxation in Solids*. Chelsea Dielectrics Press, London, 1983.

[135] K. Ngai, *Relaxation and diffusion in complex systems*. Springer,New York, 2011.

[136] J. Watanabe, H. Ono, I. Uematsu, and A. Abe, "Thermotropic polypeptides. 2. molecular packing and thermotropic behavior of poly(l-glutamates) with long n-alkyl side chains," *Macromolecules*, vol. 18, no. 11, pp. 2141–2148, 1985.

[137] W. Zheng, K. Levon, J. Laakso, and J. Oesterholm, "Characterization and solid-state properties of processable n-alkylated polyanilines in the neutral state," *Macromolecules*, vol. 27, no. 26, pp. 7754–7768, 1994.

[138] H. Shi, Y. Zhaoa, X. Zhanga, Y. Zhoua, Y. Xub, S. Zhoua, D. Wanga, C. Hana, and D. Xu, "Packing mode and conformational transition of alkyl side chains in n-alkylated poly(p-benzamide) comb-like polymer," *Polymer*, vol. 45, pp. 6299–6307, 2004.

[139] H. R. Kricheldorf and A. Domschke, "Layer structure.1.poly(phenylene-terephthalamide)s derived from mono-, di-, and tetrakis(alkylthio)terephthalic acids," *Macromolecules*, vol. 27, no. 6, pp. 1509–1516, 1994.

[140] G. Ungar, X. B. Zeng, G. M. Brooke, and S. Mohammed, "Structure and formation of noninteger and integer folded-chain crystals of linear and branched monodisperse ethylene oligomers," *Macromolecules*, vol. 31, p. 1875–1879, 1998.

[141] G. Höhne, "Another approach to the gibbs–thomson equation and the melting point of polymers and oligomers," *Polymer*, vol. 43, no. 17, pp. 4689 – 4698, 2002.

[142] A. Crotty, A. N. Gizzi, H. Rivera-Jacquez, A. Masunov, Z. Hu, J. Geldmeier, and A. Gesquiere, "Molecular packing in organic solar cell materials: Insights from the emission line shapes of p3ht/pcbm polymer blend nanoparticles," *Journal of Physical Chemistry C*, vol. 118, pp. 19975–19984, 2014.

[143] V. Ho, B. W. Boudouris, and R. A. Segalman, "Tuning polythiophene crystallization through systematic side chain functionalization," *Macromolecules*, vol. 43, p. 7895–7899, 2010.

[144] B. Burkhart, P. P. Khlyabich, and B. C. Thompson, "Influence of the ethyl-hexyl side-chain content on the open-circuit voltage in rr-poly(3-hexylthiophene-co-3-(2-ethylhexyl)thiophene) copolymers," *Macromolecules*, vol. 45, no. 9, p. 3740–3748, 2012.

[145] J. L. Keddie, R. A. L. Jones, and R. A. Cory, "Size-dependent depression of the glass transition temperature in polymer films," *Europhysics Letters*, vol. 27, no. 1, pp. 59–64, 1994.

[146] T. Babur, J. Balko, H. Budde, and M. Beiner, "Confined relaxation dynamics in long range ordered polyesters with comb-like architecture," *Polymer*, vol. 55, no. 26, pp. 6844–6852, 2014.

Acknowledgement

I would like to express my gratitude to all the people who helped and supported me during my Ph.D studies.

First of all, I am indebted to my supervisor, Prof. Dr. Mario Beiner for giving me an opportunity to work in his work group as a Ph.D student. The regular scientific discussion with him, his ideas, suggestions, guidance and encouragement significantly contributed to the successful completion of this study. I would also like to thank SFB-Transregio 102 for providing the financial support.

I am specially thankful to Prof. Dr. Thomas Thurn-Albrecht for providing me the work space in his group as well as the facility for the X-ray measurements for my work.

My sincere gratitude goes towards Dr. Klaus Schröter for his help and advice for DMA measurements.

Sincere thanks to my colleagues both in the university and Frauhofer IWMS. Dr. Nasir Mahmood, Dr. Anas Mujtaba, Dr. Gaurav Kumar Gupta, Varun Danke, Brain Lin and former colleagues of group, Nicole Sonnenberger, Cecilia Aguiar da Silva, Talha Ahmad and Arqam Anjum, for providing me a cordial and friendly environment besides their scientific assistance in some form or the other. Specially I would like to thank Dr. Gaurav Kumar Gupta for providing me great help during my thesis writing and data interpretation for x-ray measurements. I am also thankful to Jens Balko for assisting me throughout the x-ray measurements.

Many thanks to all my Pakistani friends who made my stay pleasant and enjoyable in Halle (Saale) for their help and support during the entire Ph.D period.

Words fail to express my appreciation to my parents, my brothers and sisters for their enormous support and being always with me and taking care of me.

Eidesstattliche Erklärung

Hiermit erkläre ich an Eides statt, dass ich die vorliegende Arbeit selbständig und ohne fremde Hilfe verfasst, andere als die angegebenen Quellen und Hilfsmittel nicht benutzt und die aus anderen Quellen entnommenen Stellen als solche gekennzeichnet habe. Ferner habe ich nicht versucht, anderweitig mit oder ohne Erfolg eine Dissertation einzureichen oder mich einer Doktorprüfung zu unterziehen.

Tamoor Babur

Halle (Saale), March 13, 2017

Curriculum vitae

First Name	Tamoor
Family Name	Babur
Date of Birth	March 17, 1987
Place of Birth	Lahore, Pakistan
Nationality	Pakistani
E-mail	tamoor.babur@yahoo.com

EDUCATION

Sep. 2004 - Aug. 2006	Bachelor of Science Government College University, Lahore Lahore, Pakistan
Sep. 2006 - Aug. 2008	Master of Science: Industrial Chemistry Government College University, Lahore Lahore, Pakistan
Oct. 2009 - Jun. 2012	Master of Science: Polymer Materials Science Martin-Luther-Universität Halle-Wittenberg Halle(Saale), Germany
Since January. 2013	**Ph.D** student at the Faculty of Natural Sciences II, Martin-Luther-Universität Halle-Wittenberg (Supervised by Prof. Mario Beiner)

Publications

1. G. Gupta, V. Danke, T. Babur, M. Beiner, 'Interrelations between side chain and main chain packing in different crystal modifications of alkoxylated polyesters' The Journal of Physical Chemistry B, 2017, 121(17), 4583-4591.

2. T. Babur, G. Gupta, M. Beiner, 'About different packing states of alkyl groups in comb-like polymers with rigid backbones' Soft Matter, 2016, 12(39), 8093-8097.

3. T. Babur, J. Balko, H. Budde, M. Beiner, 'Confined relaxation dynamics in long range ordered polyesters with comb-like architecture' Polymer, 2014, 55(26), 6844-6852.

4. N. Mahmood, A. M. Anton, G. Gupta, T. Babur, K. Knoll, T. Thurn-Albrecht, F. Kremer, M. Beiner, R. Weidisch, 'Influence of shear processing on morphology orientation and mechanical properties of styrene butadiene triblock copolymers' Polymer, 2014, 55(16), 3782-3791.